

**I. Chemical-Scale Studies of Ligand-Gated Ion Channels, and
II. Novel Methods for Phosphonate Synthesis**

Thesis by

Sean M. A. Kedrowski

In Partial Fulfillment of the Requirements
for the Degree of Doctor of Philosophy



California Institute of Technology

Pasadena, California

2012

(Defended 25 August 2011)

© 2011

Sean M. A. Kedrowski

All Rights Reserved

Acknowledgements

In this work and as a scientist, I am indebted to a great many people. This list starts with Professor Dennis Dougherty, who truly defines what it means to be a mentor. He is extremely humble and empathetic: on occasions when I have offered poor hypotheses or made incorrect claims, he has guided me towards self-correction, ensuring that I learn, while going out of his way to avoid making me feel stupid. In choosing and conducting research, he is empowering and flexible. I cannot imagine another advisor allowing me to develop new synthetic methodologies for phosphonate synthesis, given that the original project was to make and incorporate nonhydrolyzable phosphorylated amino acid mimics. For all this, I am extremely grateful.

In addition to Dennis, I am also indebted to Professor Henry Lester, Professor Sarah Lummis, and all members of the Dougherty lab for their support, help, advice, and stimulating conversations. In particular, this work would not have been possible without Kiowa Bower and Kristin Rule Gleitsman. Kiowa collaborated with me on the 1-OT project (Chapter 2), and his work with the D2 receptor inspired the fluorinated dopamine project (Chapter 8). Kristin collaborated with me on the Sah project (Chapter 4), which grew out of her project exploring the peptide backbone flexibility of the nAChR binding site residues. I am especially grateful to Kristin for being my first mentor in the lab: teaching me various molecular biology protocols and whole-cell voltage clamp techniques.

I am also grateful to the members of my thesis committee: Professor Brian Stoltz, Professor Bil Clemons, and Professor Bob Grubbs for their helpful comments and feedback during my time at Caltech. I am particularly indebted to Brian for his welcoming me into his group's weekly meetings, providing a forum for me to focus on synthetic chemistry and enabling me to benefit from his and his students' synthetic insight and expertise. Brian's intensity and depth of synthetic knowledge (as showcased in his introductory synthetic chemistry course) have been an important part of my development as a synthetic chemist. I also thank Professor Dave MacMillan, my advisor of four months, whose creativity, intensity, and passion for chemistry are inspirational and infectious. My thanks also go to the many members of the Stoltz and MacMillan labs

for their tips, advice, and helpful conversations. I am especially grateful to Rob Knowles, who was a mentor for my first several months in the MacMillan lab; his lab routine is an aspirational model, and he taught me many synthetic techniques and tricks.

In the NMR facility where I was a GLA for three years, I am grateful to Tom Dunn, Scott Ross, and Dave VanderVelde for helping me learn and troubleshoot Hg₃, while also providing help with the occasional more complicated experiment. I am grateful to Mona Shahgholi and Naseem Torian in the MS facility, who have collected spectra for this thesis and helped me develop new MS methods (Appendix 1). I would also like to thank Scott Virgil in the catalysis center, whose advice and equipment were helpful in methodology development (Chapters 5 & 6).

My Ph.D. journey began before coming to Caltech, so I would be remiss in failing to acknowledge those who led me onto this path. I would first like to thank my high school chemistry teacher, Peter Melcher, who is quite possibly the best damn science teacher ever. I would also like to thank Professor Stephen Craig, whom I was fortunate enough to have as advisor for four years in college. I have yet to meet another professor so passionate about getting undergraduates involved in scientific research. Within the Craig lab, I am particularly indebted to Chris Bender, who was very generous with his time and patience in teaching me synthetic lab techniques for the first time. The last individual I would like to thank is Professor Steven Baldwin, who taught me several classes in college and helped to get me started doing research.

Finally, I would like to thank Caltech and the NIH, without whom this would not have been possible.

Abstract

Section 1: Chemical-Scale Studies of Ligand-Gated Ion Channels

Ligand-gated ion channels are amazing molecular machines that respond to specific small-molecule agonists by opening a central pore to enable ions to flow through them. In the aggregate, they transduce chemical signals into electrical currents, and they have numerous critical physiological functions. The tools of pharmacology and unnatural amino acid (and hydroxy acid) mutagenesis enable us to study these receptors on an atomic level. Two such projects are presented here. First, the synthesis of a new 5-HT₃ receptor agonist helps to map the receptor's binding site. Second, mutant cycle analysis in the nicotinic acetylcholine receptor with the novel unnatural residue α -hydroxyserine (Sah) enables the identification of a crucial hydrogen bond whose formation is part of the pathway leading from acetylcholine binding to pore opening.

Section 2: Novel Methods for Phosphonate Synthesis

Phosphonates are a key functional group in both organic synthesis and biological chemistry. The Arbuzov reaction stands as dominant method available for synthesizing this important class of compounds. Two new methods for phosphonate synthesis are presented here. The first method enables room-temperature phosphonate synthesis from carboxylic acids, taking advantage of a novel Wolff-Kishner-type reductive deoxygenation of an intermediate acyl phosphonate. The second method enables phosphonate synthesis through the reductive coupling of ketones/aldehydes with dialkyl phosphites, mediated by a tosylhydrazone derivative. The latter method requires only mild heating (60 °C) and enables access to phosphonates containing azides, benzyl halides, and other functional groups poorly tolerated by the Arbuzov conditions.

Table of Contents

Acknowledgements	iii
Abstract	v
Table of Contents	vi
List of Schemes	vii
List of Figures	viii
List of Tables	ix
Introduction	
Chapter 1: Chemical Synthesis as a Tool for Probing Large, Membrane-Bound Receptor Proteins	1
Section 1: Chemical-Scale Studies of Ligand-Gated Ion Channels	
Chapter 2: The Synthesis of 1-oxo-5-hydroxytryptamine to Probe Ligand-Receptor Interactions in the 5-HT ₃ Receptor	17
Chapter 3: The Synthesis of α -Hydroxy Acids to Probe Hydrogen Bonding	29
Chapter 4: Probing a Key Hydrogen Bond in the Nicotinic Acetylcholine Receptor through Mutant Cycle Analysis	48
Section 2: Novel Methods for Phosphonate Synthesis	
Chapter 5: The Room Temperature Wolff-Kishner-Type Reductive Deoxygenation of Acyl Phosphonates: The One-Pot Transformation of Carboxylic Acids into Alkyl Phosphonates	63
Chapter 6: The Reductive Coupling Aldehydes/Ketones with Dialkyl Phosphites: A Mild and Orthogonal Alternative to the Arbuzov Reaction	84
Section 3: Miscellaneous Experiments	
Chapter 7: Investigations into the Role of Nitrosylation of Cysteine Residues as a Posttranslational Protein Modification	107
Chapter 8: Synthetic Efforts Towards Fluorinated Dopamine Analogs	120
Appendix 1: The Development of a New MALDI-TOF MS Method for the Analysis of Amino Acid-dCA Esters	130
Appendix 2: Exploration of the Feasibility of an Organocatalytic LUMO/Friedel-Crafts-SOMO Cascade	132

List of Schemes

Scheme 2.1:	1-oxo-5-hydroxytryptamine retrosynthesis	18
Scheme 2.2:	1-oxo-5-hydroxytryptamine synthesis	19
Scheme 3.1:	Attempted Nah-dCA synthesis (#1)	30
Scheme 3.2:	Attempted Nah-dCA synthesis (#2)	31
Scheme 3.3:	Nah-dCA synthesis (#3)	32
Scheme 3.4:	Attempted Asn-dCA synthesis	33
Scheme 3.5:	Sah-dCA synthesis	34
Scheme 5.1:	Arbuzov reaction	63
Scheme 5.2:	Retrosynthesis of phosphonates from carboxylic acids	64
Scheme 5.3:	Phosphonate stabilizes the Wolff-Kishner intermediate	65
Scheme 5.4:	Acyl phosphonate hydrazone formation is pH-dependent	65
Scheme 6.1:	1-diazenoalkyl phosphonate retrosynthesis	85
Scheme 6.2:	Inokawa reaction for the conversion of ketones into phosphonates	85
Scheme 6.3:	Conversion of pivaldehyde to a neopentyl phosphonate	93
Scheme 7.1:	Fluorescence quenching by nitrosylation for a thiol-tethered dansyl fluorophore	109
Scheme 7.2:	Chemical double-mutant cycle for measuring the nitrosothiol- π interaction	110
Scheme 7.3:	Attempted synthesis of the chemical double-mutant cycle system	111
Scheme 8.1:	α,α -difluorodopamine and its possible decomposition via quionone methide	122
Scheme 8.2:	Attempted α,α -difluorodopamine synthesis	123
Scheme 8.3:	4-(1,1-difluoroethyl)-catechol acetamide synthesis	124
Scheme A2.1:	Proposed one-pot organocatalytic cascade	132

List of Figures

Figure 1.1:	Chemical synapse	2
Figure 1.2:	Nicotinic acetylcholine receptor (nAChR)	3
Figure 1.3:	Aromatic-lined binding site of the nAChR	4
Figure 1.4:	Leucine 9' gate of the nAChR	4
Figure 1.5:	G protein-couple receptors (GPCRs)	5
Figure 1.6:	Two-electrode voltage clamp on a <i>Xenopus</i> oocyte and sample current traces	5
Figure 1.7:	Dose-response curve (EC_{50} plot)	6
Figure 1.8:	Unnatural amino acid and hydroxy acid mutagenesis by nonsense suppression	7
Figure 1.9:	Fluorinated tryptophans	8
Figure 1.10:	Elimination of a backbone hydrogen bond by introduction of an ester through α -hydroxy acid incorporation	9
Figure 1.11:	Amino acid phosphorylation and phosphonate analogs	10
Figure 1.12:	Cysteine nitrosylation	11
Figure 2.1:	5-Hydroxytryptamine and 1-oxo-5-hydroxytryptamine	17
Figure 2.2:	5-HT ₃ receptor pharmacology	20
Figure 3.1:	Elimination of a backbone hydrogen bond by introduction of an ester through α -hydroxy acid incorporation	29
Figure 3.2:	α -hydroxy asparagine and α -hydroxy serine	30
Figure 4.1:	Acetylcholine binding protein, hydrogen bond between loop C and loop F	49
Figure 4.2:	Mutations in nAChR	50
Figure 4.3:	Double mutant-cycle analysis in nAChR	53
Figure 4.4:	Double mutant-cycle coupling energies in nAChR	53
Figure 6.1:	Product inhibition in the aldehyde-to-phosphonate reaction	92
Figure 7.1:	N-methyl-D-aspartate (NMDA) receptor	108
Figure 7.2:	Possible phenol-nitrothiol interaction geometry	112
Figure 8.1:	Dopamine	120
Figure 8.2:	Binding site aromatic residue fluorination plots for various ligand-gated ion channels	121
Figure 8.3:	Possible interaction geometries for dopamine and D2R Trp6.48	122

List of Tables

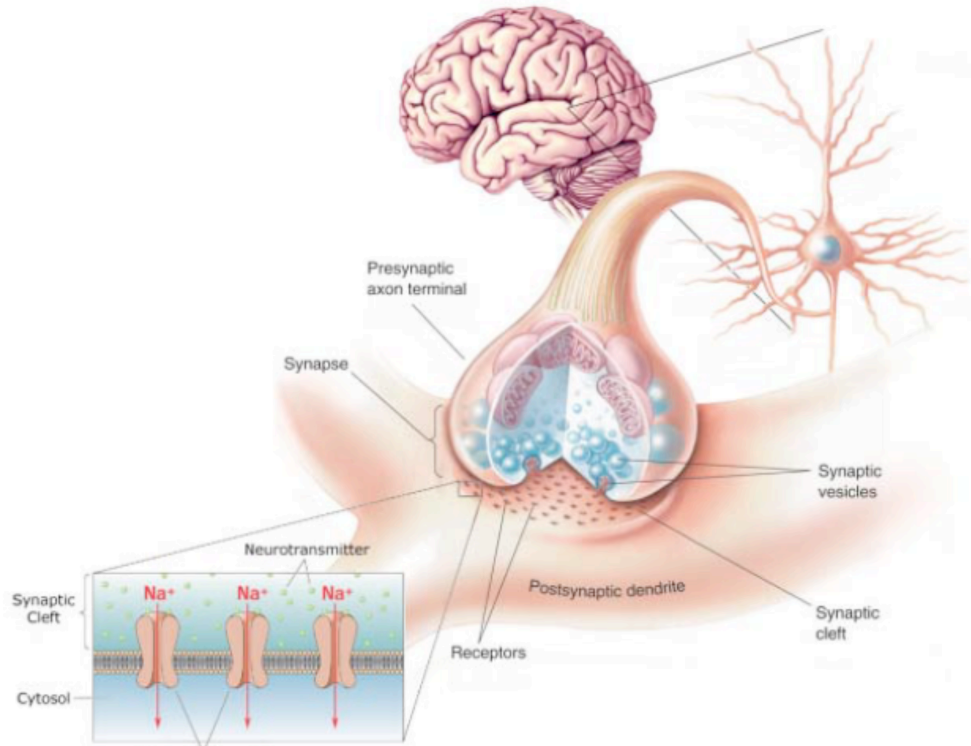
Table 3.1:	Screen of amide protecting groups for α -hydroxy asparagine	32
Table 4.1:	EC ₅₀ data for nAChR mutants	51
Table 5.1:	Acid-to-phosphonate reaction scope	68
Table 6.1:	Screen of reaction conditions for direct ketone-to-phosphonate conversion	86
Table 6.2:	Benzaldehyde-to-phosphonate reaction scope	88
Table 6.3:	Screen of additives for pyridyl substrates in the aldehyde-to-phosphonate reaction	90
Table 6.S1:	Data underlying Figure 6.1	103

Introduction: Chapter 1

Introduction: Chemical Synthesis as a Tool for Probing Large, Membrane-Bound Proteins

In the past decades, neuroscience has grown to be one of the most active areas of research in science today.¹ As it has grown, it has become truly interdisciplinary, gaining from the contributions of researchers initially trained in biology, physics, and chemistry. The action potential—one of the key phenomena of neuroscience—exemplifies this multidisciplinary nature: an electric current travels down a cell, and the signal is relayed to the next cell by diffusion of a small-molecule neurotransmitter across the synaptic cleft.² The neurotransmitters then bind to transmembrane proteins in the postsynaptic neuron that respond by changing conformation to form a pore through which ions can enter the postsynaptic neuron to regenerate the action potential (Figure 1.1).

These integral membrane proteins are known as ligand-gated ion channels (LGICs), and they are one of the two classes of proteins studied in the Dougherty lab. The other class is G protein-coupled receptors (GPCRs), many of which also bind small-molecule neurotransmitters. In contrast, GPCRs initiate signaling pathways within the cell by activating cytosolic proteins. These two classes of proteins are of great physiological and medicinal interest. They are amongst the molecules of learning, memory, and sensory perception. They are believed to be the molecular target of many drugs of abuse, and their dysfunction has been implicated in a variety of cognitive disorders and diseases, including Alzheimer's, Parkinson's, schizophrenia, and mood



Ligand-Gated Ion Channels

Figure 1.1. A chemical synapse. An action potential triggers the release of small-molecule neurotransmitters, which flow across the synapse to activate large transmembrane receptors on the postsynaptic neuron.

disorders.³ As such, these receptors are known to be the targets of many commercial pharmaceuticals.⁴

In the human nervous system, the Cys-loop superfamily is the most prevalent class of LGICs, with its members including the γ -aminobutyric acid type A (GABA_A) receptor, the serotonin type 3 (5-HT₃) receptor, the glycine receptor, and the nicotinic acetylcholine (nACh) receptors.⁵ Of these, the nicotinic acetylcholine receptor (nAChR) is the most studied. These receptors are pentameric in structure, with all five subunits arranged radially about a central pore (Figure 1.2). Each subunit is similar in structure and size, though they are often not all identical. The subunits themselves are quite large—roughly 400 amino acid residues and 60 kDa each—and contain large

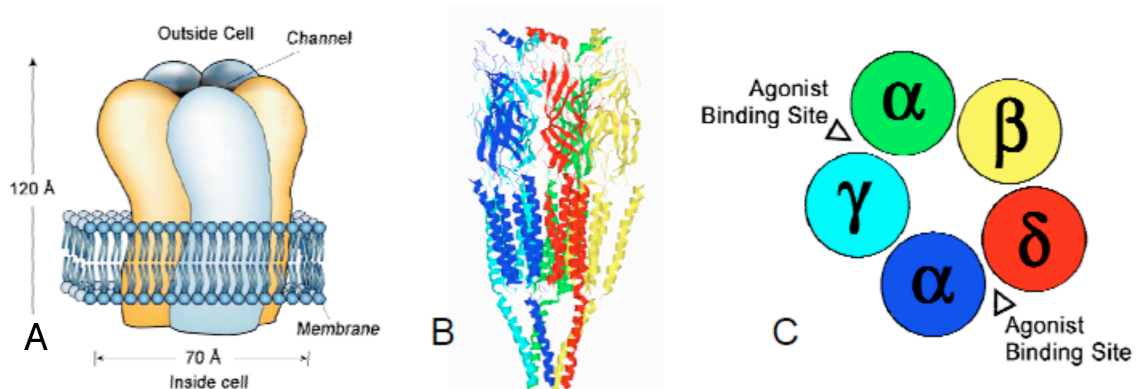


Figure 1.2. The nicotinic acetylcholine receptor (nAChR) is a member of the Cys-loop family of ligand-gated ion channel. Cartoon (a) and ribbon (b) representations of nAChR. There are four unique (five total) subunits and two binding sites (c).

extracellular domains in addition to their four transmembrane helices. Mouse muscle nAChR, the family member used in this study, contains four distinct subunits: α (two subunits), β , γ , and δ . The two nonequivalent binding sites are located at the subunit interfaces $\alpha:\gamma$ and $\alpha:\delta$. Neurotransmitter binding to both sites is typically necessary to open the pore, but monoliganded openings are known, particularly for certain mutants.⁶ The binding sites are defined by an ‘aromatic binding box;’ these aromatic residues, particularly α Trp149, have been shown to bind acetylcholine through the cation- π effect (Figure 1.3).⁷

Also of note is β Leu251 (commonly called β Leu9’, where the 9’ designates its position on the transmembrane helix #2), which, along with α Leu9’, γ Leu9’, and δ Leu9’, is believed to form the gate of the channel pore. When the leucine side chains are pointed into the pore, the channel is closed. Binding of acetylcholine molecules in the two extracellular binding sites initiates a conformational change that swings the leucine residues to the side, opening the pore and allowing ions to flow through it and across the cell membrane (Figure 1.4). It has been demonstrated that mutations at the 9’ sites can

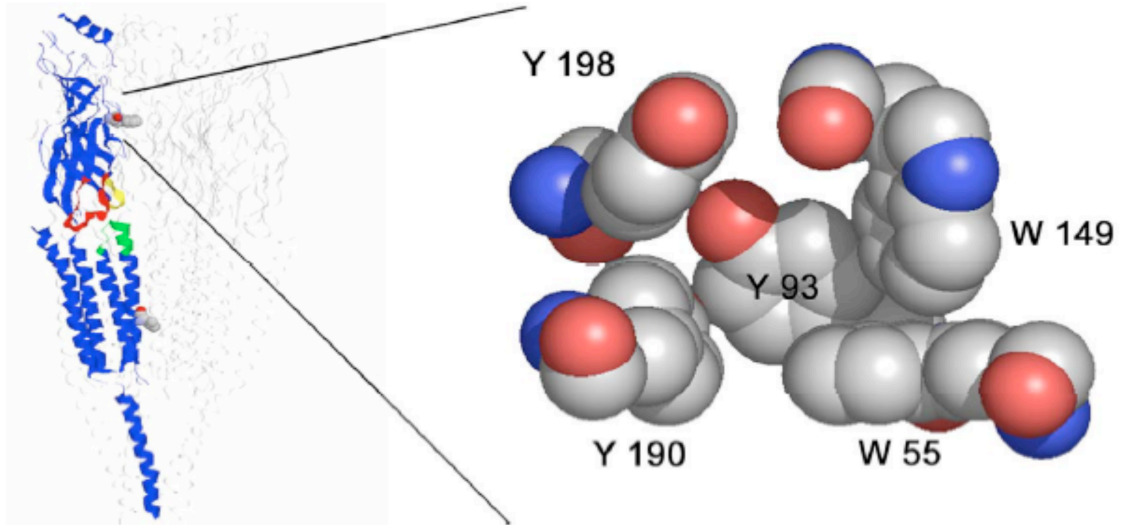


Figure 1.3. Five aromatic residues form the binding site of the nAChR.

have dramatic effects upon the pore's propensity to open. In particular, the mutation β L9'S is known to alter the pore's propensity to open by a constant increment over wild-type. This increment remains constant in the presence of other mutations (it is quantified as a 40-fold shift in EC_{50} , see below), which makes it helpful in the study of other mutations that would otherwise require a high drug concentration to activate.⁸

GPCRs are structurally quite different from LGICs (Figure 1.5).⁹ They have seven

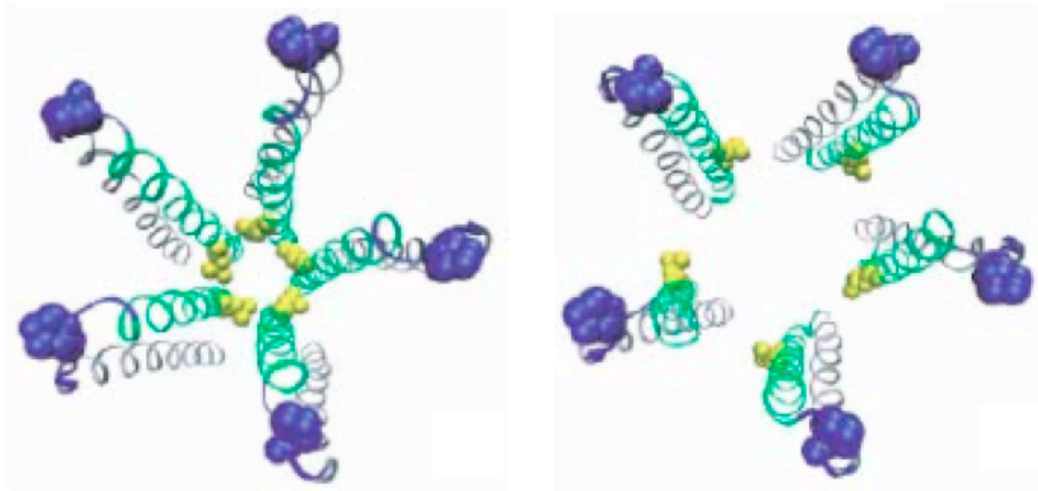


Figure 1.4. The β L9' residues (yellow) form the gate of the nAChR.

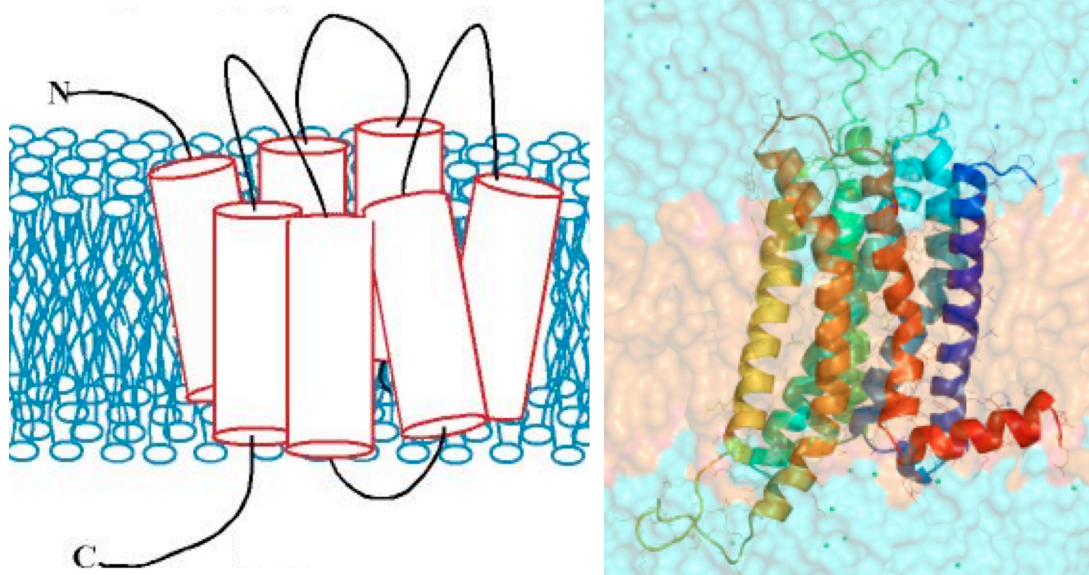


Figure 1.5. Pictorial representations of a G protein-coupled receptor (GPCR).

transmembrane helices, and the agonist binding site is between several of the helices, set deep within the transmembrane region, in contrast to the LGIC binding sites, which are in the extracellular portion. Ligand binding activates the G protein, but there are multiple intracellular pathways through which the signal might be transduced. There are also a wide range of GPCR ligands, including acetylcholine and dopamine.

In the Dougherty lab, we typically study these proteins through structure-function experiments, and one of the most common tools for assaying function is

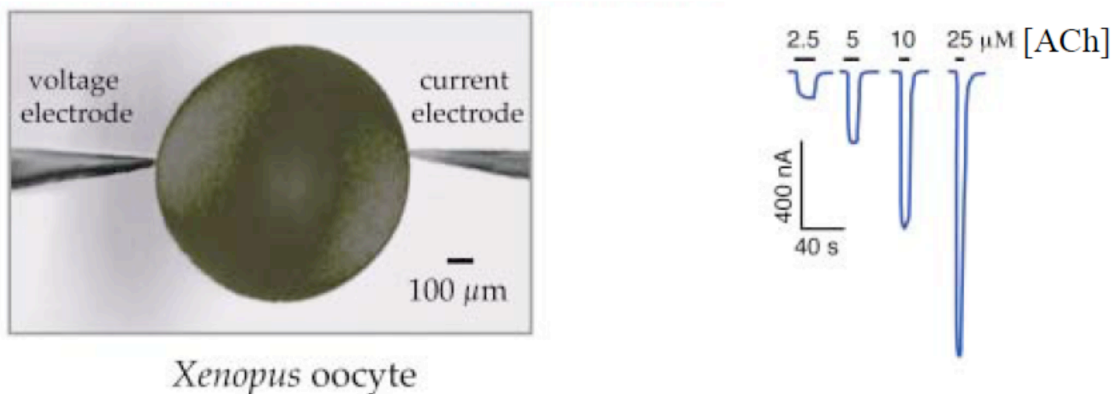


Figure 1.6. Two-electrode voltage clamp on a *Xenopus* oocyte. This technique produces the current traces shown.

electrophysiology. There are a variety of electrophysiological techniques and experiments available, but we use two-electrode whole-cell voltage clamp for the projects described here (Figure 1.6).¹⁰ Starting with a cell that expresses the LGIC of interest on its surface, a constant potential (voltage clamp) is imposed upon the membrane. This is done using two

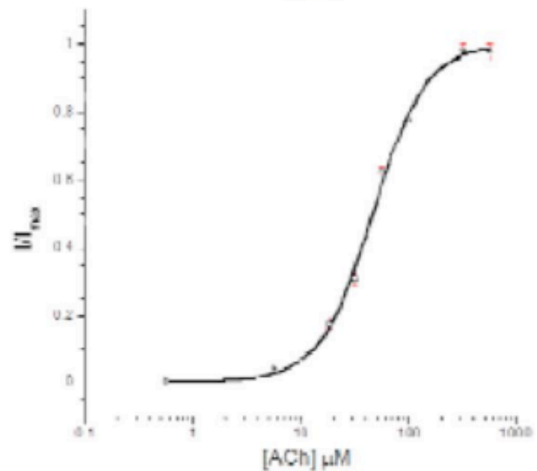


Figure 1.7. The current traces from a series of dose-response experiments are combined to produce an EC₅₀ plot.

electrodes to measure the transmembrane potential and a third electrode to traffic current as needed to maintain the specified potential. When the cell is bathed in an agonist, the LGICs respond by allowing current to flow across the membrane; the current electrode traffics an equal but opposite current to compensate and maintain the specified potential. This current can then be correlated to the concentration of agonist applied. When multiple concentrations are applied, a dose-current response plot can be constructed to illustrate the sensitivity of channel opening to neurotransmitter application (Figure 1.7). The data can then be fit to the Hill equation to determine an EC₅₀ value, which represents the agonist concentration necessary to produce a half-maximal current response.¹¹ The EC₅₀ value is thus a powerful metric in assessing receptor function. GPCRs can be assayed in a similar way by exploiting a G protein pathway that couples GPCR activation to the opening of G protein-coupled inwardly-rectifying potassium channels (GIRKs).¹²

With such a powerful tool for assaying function, the question becomes how to probe structure. One strategy is pharmacology: altering the structure of the small-

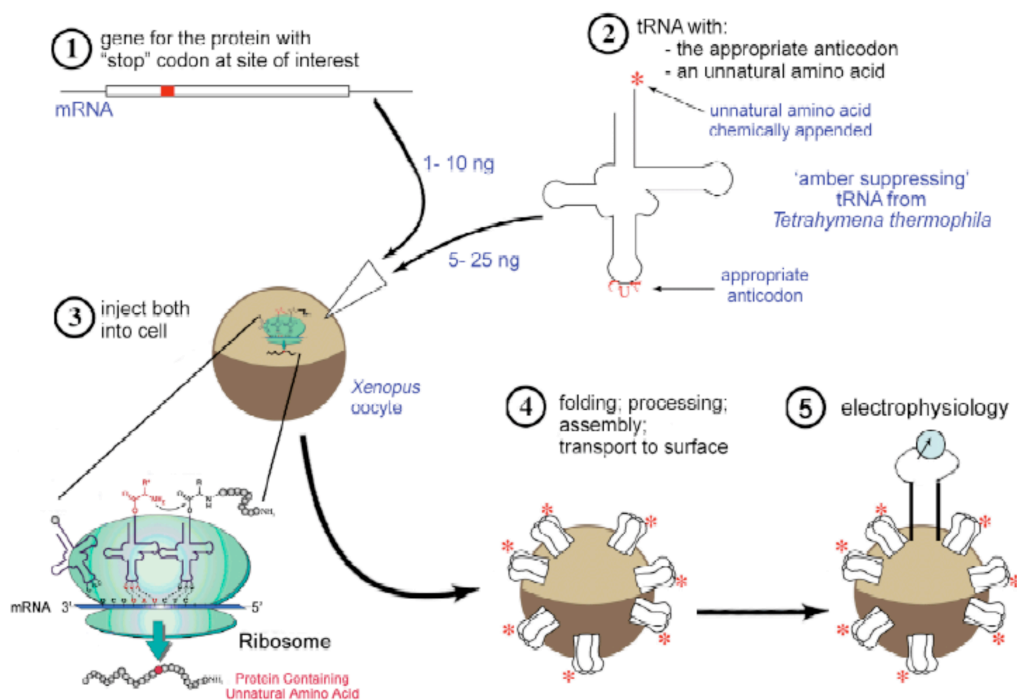


Figure 1.8. Amino acid/hydroxy acid incorporation through nonsense suppression.

molecule agonist, which can be done through synthetic chemistry. This strategy is used by many other researchers, though our ability to perform both the chemical synthesis and the electrophysiology in-house offers us some advantages. Two pharmacological projects are outlined in Chapters 2 and 8.

Another common strategy is to vary the structure of the receptor through mutagenesis. This typically requires the use of PCR to create genetic material encoding a mutant version of the receptor where one or more amino acids have been changed to another of the 20 amino acids, thus ablating or altering a peptide sidechain believed to have an important functional role. This genetic material must be expressed in a system that can be electrophysiologically assayed—in our case, we manually inject mRNA into an oocyte of the frog *Xenopus laevis*, which (usually) will synthesize, fold, and transport the protein to the membrane for assaying.

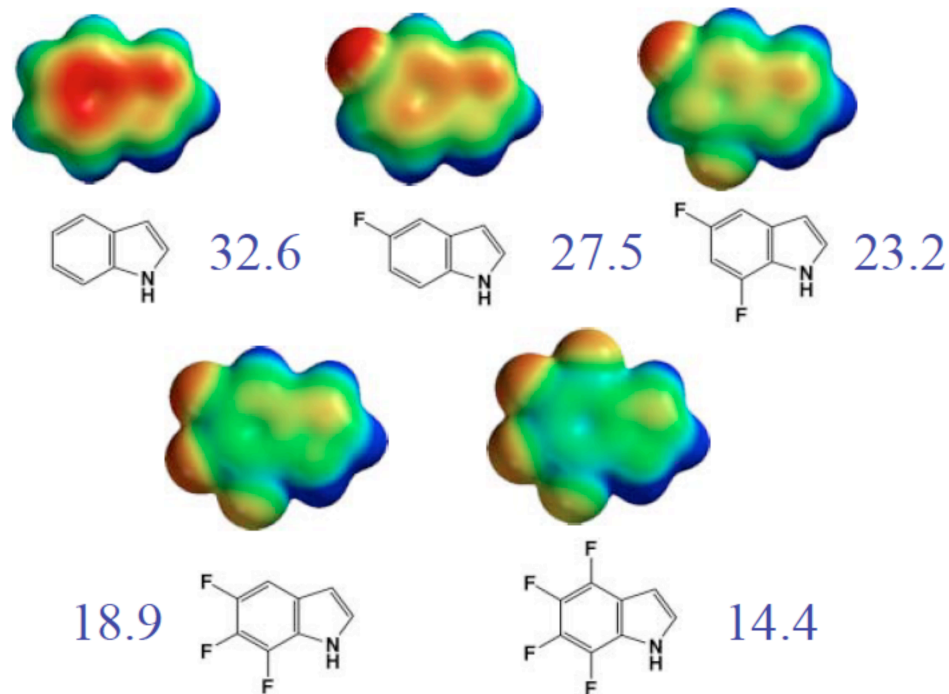


Figure 1.9. Unnatural fluorinated tryptophan-derived amino acids allow the side-chain's electronics to be varied without perturbing sterics. Illustrations show electrostatic potential surfaces. Numbers represent the calculated gas-phase binding energy of the face of each indole with a sodium ion.

However, conventional mutagenesis is a very common strategy that is implemented by many other laboratories. In the Dougherty group, we have developed a mutagenesis protocol enabling the incorporation of unnatural amino acids and hydroxy acids (Figure 1.8).¹³ This method greatly expands the structural alterations that can be accomplished by mutagenesis, and it enables more specific and targeted questions to be asked of the receptors being studied. For example, when studying the role of a tryptophan residue, the electronics of the side chain can be altered through the incorporation of ring-fluorinated analogs without perturbing the side-chain sterics (Figure 1.9). Using conventional mutagenesis, the subtlest mutation possible would be to exchange the tryptophan for a phenylalanine, which is a pretty significant steric and electronic change. This methodology also allows the role of backbone amides to be probed by the

incorporation of hydroxy acids, something that is not possible using conventional mutagenesis (Figure 1.10).

The incorporation of a hydroxy acid in place of an amino acid mutates a backbone amide to an ester, eliminating one hydrogen bond-donor and weakening

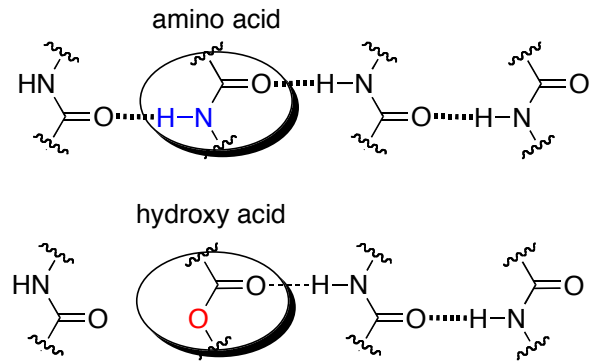


Figure 1.10. Incorporation of an α -hydroxy acid eliminates a hydrogen bond donor

one hydrogen bond-acceptor in a precisely targeted manner.

Unnatural amino acid and hydroxy acid mutagenesis is accomplished by nonsense suppression (Figure 1.8).¹⁴ In this method mutant mRNA encoding the desired protein is made in which the codon of the residue targeted for mutation is mutated to the amber stop codon (UAG). In parallel, a chemically synthesized α -amino acid or α -hydroxy acid is ligated to an amber-suppressor tRNA (CUA). Those two macromolecules are then manually injected into a *Xenopus* oocyte, which then expresses the mutant receptor of interest.

Although the many steps of this method have been extensively optimized by the Dougherty group and the Schultz group, there is still significant variation from mutant to mutant, and a variety of control experiments must always be performed. One concern is that the translational machinery of the oocyte is able to bypass the amber stop codon in reading the mutant mRNA—either by jumping over that codon or mismatching it with a natural tRNA-amino acid couple—a phenomenon known as ‘read-through’. Injection of a set of oocytes with mutant mRNA only should give functional receptors only if read-through is an issue (without read-through or suppressor tRNA, the amber stop codon

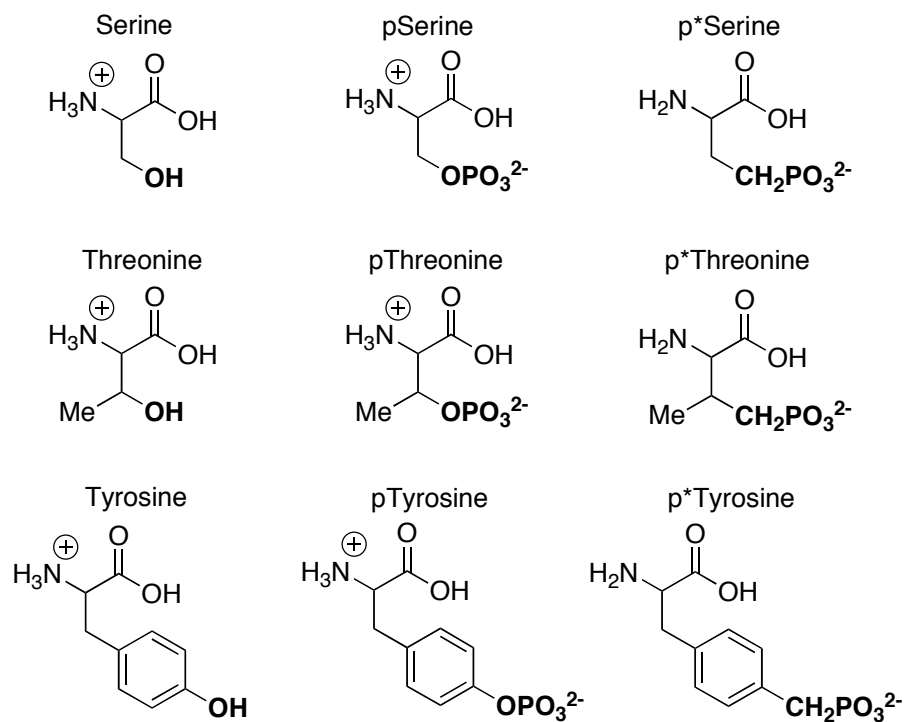


Figure 1.11. Serine, threonine, and tyrosine, their phosphorylated derivatives, and the phosphonate-based analogs that serve as nonhydrolyzable phosphate ester mimics

should break off translation before a functional peptide has been made). A second problem that can occur is the aminoacylation of the amber suppressor tRNA by a naturally occurring aminoacyl tRNA-synthetase after the tRNA's cargo has been incorporated into a polypeptide or hydrolytically lost. This misaminoacylated tRNA can then be recycled to incorporate an undesired natural amino acid into the protein. Injection of mutant mRNA along with unacylated amber-suppressor tRNA can be done to control for this potential problem. Finally, mutant mRNA can be co-injected with amber-suppressor tRNA that is coupled to the naturally occurring amino acid for the mutated site. This control should produce wild-type protein. Projects using this unnatural mutagenesis technique are described in Chapters 3, 4, and 7.

One interesting biochemical phenomenon that can theoretically be studied using this unnatural mutagenesis technique is protein phosphorylation (Figure 1.11). In phosphorylation, serine, threonine, and tyrosine residues enzymatically have a phosphate group appended to them, altering the behavior, structure, and/or function of the protein. This posttranslational modification is a key regulatory mechanism governing most proteins, and LGICs and GPCRs are no exceptions. The Dougherty lab has previously reported on the incorporation of photocaged tyrosine, as well as photocaged phosphoserine, phosphothreonine, and phosphotyrosine as tools for studying the effects of phosphorylation of specific sites.¹⁵ Unfortunately, this strategy is not very useful when the proteins are expressed in live cells because native phosphatases are capable of cleaving the phosphate esters of the mutant proteins.¹⁶ In this case, caged phosphonates may be useful as nonhydrolyzable phosphate ester mimics.¹⁷ In pursuing the syntheses of phosphoserine, phosphothreonine, and phosphotyrosine derivatives, new methods for phosphonate synthesis were explored and developed, and these are presented in Chapters 5 and 6.

In Chapter 7, a less common type of protein posttranslational modification was considered: cysteine nitrosylation (Figure 1.12).¹⁸ The modification is much more poorly understood than phosphorylation, though it has

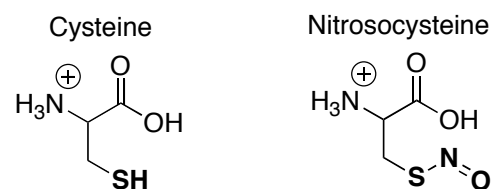


Figure 1.12. Cysteine nitrosylation is a posttranslational modification.

been identified as physiologically relevant for hemoglobin and several glutamate receptors. Even relatively basic questions about the timescale of the modification are

unanswered, and we try to understand it through the use of unnatural amino acids and a small molecule model system.

References

- ¹ (a) *Neuroscience*. Purves, D., et. al. Sinauer Associates. **2001**. (b) *Nicotinic acetylcholine receptors of muscles and nerves—Comparison of their structures, functional roles, and vulnerability to pathology in Myasthenia Gravis and Related Disorders*. Lindstrom, J. 2003. (c) Physical Organic Chemistry on the Brain. Dougherty DA. *J. Org. Chem.* **2008**, *73*, 3667–3673.
- ² (a) Membrane action potentials from the squid giant axon. Curtis, HJ, and Cole, KS. *Journal of Cellular and Comparative Physiology*. *15*, **1940**, 147-157. (b) Membrane potential of the squid giant axon during current flow. Cole, KS, and Curtis, HJ. *Journal of General Physiology*. *24*, **1941**, 551-563. (c) Membrane resting and action potentials from the squid giant axon. Curtis, HJ, and Cole, KS. *Journal of Cellular and Comparative Physiology*. *19*, **1942**, 135-144.
- ³ (a) Corringier, P. J., Le Novere, N., and Changeux, J. P. *Annu. Rev. Pharmacol. Toxicol.*, **2000**, *40*, 431–458. (b) Grutter, T., and Changeux, J. P., **2001**, *Trends Biochem. Sci.* *26*, 459–463. (c) Karlin, A. *Nat. Rev. Neurosci.*, **2002**, *3*, 102–114.
- ⁴ (a) The druggable genome. Hopkins AL, Groom CR. *Nat. Rev. Drug Discov.*, **2002**, *1*, 727–730. (b) Drug design strategies for targeting G-protein-coupled receptors. Klabunde, T., Hessler, G. *Chembiochem.*, **2002**, *3*, 928–944.
- ⁵ (a) Sequence and Functional Expression of the Gaba-a Receptor Shows a Ligand-Gated Receptor Super-Family. Schofield, P.R., Darlison, M.G., Fujita, N., Burt, D.R., Stephenson, F.A., Rodriguez, H., Rhee, L.M., Ramachandran, J., Reale, V., Glencorse, T.A., Seeburg, P.H. and Barnard, E.A. *Nature*. *328*, **1987**, 221-227. (b) Emerging structure of the nicotinic acetylcholine receptors. Karlin, A. *Nature Reviews Neuroscience*. *3*, **2002**, 102-114. (c) Refined structure of the nicotinic acetylcholine receptor at 4 angstrom resolution. Unwin, N. *Journal of Molecular Biology*. *346*, **2005**, 967-989.
- ⁶ (a) Short openings in high resolution single channel recordings of mouse nicotinic receptors. Hallermann, S., Heckmann, S., Dudel, J., and Heckmann, M. *Journal of Physiology-London*. *563*, **2005**, 645-662. (b) A human congenital myasthenia-causing mutation (epsilon L78P) of the muscle nicotinic acetylcholine receptor with unusual

single channel properties. Shelley, C., and Colquhoun, D. *Journal of Physiology—London*. 564, **2005**, 377-396.

⁷ From ab initio quantum mechanics to molecular neurobiology: A cation- π binding site in the nicotinic receptor. Zhong, W.G., Gallivan, J.P., Zhang, Y.O., Li, L.T., Lester, H.A. and Dougherty, D.A. *PNAS*. 95, **1998**, 12088-12093.

⁸ Agonist binding site of the nicotinic acetylcholine receptor: Tests with novel side chains and with several agonists. Kearney, P.C., Nowak, M.W., Zhong, W., Silverman, S.K., Lester, H.A. and Dougherty, D.A. *Molecular Pharmacology*. 50, **1996**, 1401-1412.

⁹ (a) Structural diversity of G protein-coupled receptors and significance for drug discovery. Lagerstrom MC, Schioth HB. *Nat. Rev. Drug Discov.*, **2008**, 7, 339–357; erratum 542. (b) GPCR engineering yields high-resolution structural insights into 2-adrenergic receptor function. Rosenbaum DM, et al. *Science.*, **2007**, 318, 1266–1273. (c) Crystal structure of the human beta2 adrenergic G protein-coupled receptor. Rasmussen SGF, et al. *Nature.*, **2007**, 450, 383–387. (d) Crystal structure of rhodopsin: A Gprotein-coupled receptor. Palczewski K, et al. *Science.*, **2000**, 289, 739–745.

¹⁰ *The Axon Guide*. Sherman-Gold, R., et. al. Axon Instruments, **1993**.

¹¹ (a) The combinations of haemoglobin with oxygen and with carbon monoxide. I. Hill, A.V. *Biochemical Journal*. 7, **1913**, 471-480. (b) The Hill equation revisited: uses and misuses. Weiss, J.N. *Faseb Journal*. 11, **1997**, 835-841.

¹² Probing the Role of the Cation- π Interaction in the Binding Sites of GPCRs Using Unnatural Amino Acids, M. M. Torrice, K. S. Bower, H. A. Lester, D. A. Dougherty, *Proc. Natl. Acad. Sci.*, **2009**, 106, 11919-11924 and references therein.

¹³ (a) Nicotinic Receptor Binding Site Probed with Unnatural Amino-Acid Incorporation in Intact Cells. M. W. Nowak, P. C. Kearney, J. R. Sampson, M. E. Saks, C. G. Labarca, S. K. Silverman, W. Zhong, J. Thorson, J. N. Abelson, N. Davidson, P. G. Schultz, D. A. Dougherty, and H. A. Lester, *Science*, **1995**, 268, 439-442. (b) In Vivo Incorporation of Unnatural Amino Acids into Ion Channels in a *Xenopus* Oocyte Expression System. M. W. Nowak, J. P. Gallivan, S. K. Silverman, C. G. Labarca, D. A. Dougherty, and H. A. Lester, in *Methods in Enzymology*, **1998**, 293, *Ion Channels, Part B*, E. P. Conn, Ed., Academic Press: San Diego, pp. 504-529. (c) Incorporation of Esters into Proteins:

Improved Synthesis of Hydroxyacyl tRNAs. P. M. England, H. A. Lester, D. A. Dougherty, *Tetrahedron Lett.* **1999**, *40*, 6189-6192.

¹⁴ see reference 13

¹⁵ (a) Flash Decaging of Tyrosine Sidechains in an Ion Channel. J. C. Miller, S. K. Silverman, P. M. England, D. A. Dougherty, and H. A. Lester, *Neuron*, **1998**, *20*, 619-624. (b) Tyrosine Decaging Leads to Substantial Membrane Trafficking during Modulation of an Inward Rectifier Potassium Channel. Y. Tong, G. S. Brandt, M. Li, G. Shapovalov, E. Slimko, A. Karschin, D. A. Dougherty, and H. A. Lester, *J. Gen. Phys.* **2001**, *117*, 103-118. (c) Caged Phosphoproteins Deborah M. Rothman, E. James Petersson, M. Eugenio Vázquez, Gabriel S. Brandt, Dennis A. Dougherty, Barbara Imperiali *J. Am. Chem. Soc.*, **2005**, *127*, 846-847.

¹⁶ (a) Protein phosphatase activities *in vivo* in *Xenopus laevis* oocyte: Inhibition by okadaic acid Cormier, P.; Mulner-Lorillon, O.; Ozon, R.; Bellé, R. *Biology of the Cell.* **1990**, *69*, 233-236. (b) Cardiac calcium channels expressed in *Xenopus* oocytes are modulated by dephosphorylation but not by cAMP-dependent phosphorylation. Singer-Lahat D, Lotan I, Biel M, Flockerzi V, Hofmann F, Dascal N. *Receptors Channels.* **1994**, *2*(3), 215-26.

¹⁷ (a) Brandt, G. S. Ph.D. Dissertation, California Institute of Technology, Pasadena, CA, **2003**. (b) Chen, L.; Wu, L.; Otaka, A.; Smyth, M. S.; Roller, P. P.; Burke, T. R.; Denhertog, J.; Zhang, Z. Y. *Biochem. Biophys. Res. Commun.* **1995**, *216*, 976. (c) Engel, R. *Chem. Rev.* **1977**, *77*, 349. (d) Nieschalk, J.; Ohagan, D. *J. Chem. Soc., Chem. Commun.* **1995**, 719. (e) Oleksyszyn, J.; Powers, J. C. *In Proteolytic Enzymes: Serine and Cysteine Peptidases*; Academic Press Inc: San Diego, **1994**; *244*, 423. (f) Panigrahi, K.; Eggen, M.; Maeng, J. H.; Shen, Q. R.; Berkowitz, D. B. *Chem. Biol.* **2009**, *16*, 928 (g) Petersson, E. J. Ph.D Dissertation, California Institute of Technology, Pasadena, CA, **2005**. (h) Zheng, W. P.; Schwarzer, D.; LeBeau, A.; Weller, J. L.; Klein, D. C.; Cole, P. A. *J. Biol. Chem.* **2005**, *280*, 10462. (i) Zheng, W. P.; Zhang, Z. S.; Ganguly, S.; Weller, J. L.; Klein, D. C.; Cole, P. A. *Nat. Struct. Biol.* **2003**, *10*, 1054.

¹⁸ (a) Protein S-nitrosylation: Purview and Parameters. Hess, D. T.; Matsumoto, A.; Kim, S.-O.; Marshall, H. E.; Stamler, J. S. *Nature Reviews.* **2005**, *6*, 150-166. (b) Crystal

Structure of the S-Nitroso Form of Liganded Human Hemoglobin. Chan, N.-L.; Rogers, P. H.; Arnone, A. *Biochemistry*. **1998**, *37*, 16459-16464.

Section 1: Chapter 2

The Synthesis of 1-oxo-5-hydroxytryptamine to Probe Ligand-Receptor Interactions in the 5-HT₃ Receptor¹

Abstract: *A novel synthetic route to 1-oxo-5-hydroxytryptamine, the benzofuran analog of serotonin, has been developed. The new synthesis proceeds via the [3+2] cycloaddition of p-benzoquinone and 2,3-dihydrofuran, followed by a Lewis acid-catalyzed isomerization. This molecule proves to be a competent agonist (equipotent to serotonin) of the 5-HT₃ receptor, demonstrating that the indolic proton of serotonin is not essential to its activation of the receptor.*

As part of the Dougherty group's efforts towards better understanding the Cys-loop ligand-gated ion channels, Kiowa Bower in the lab has been mapping out the binding site of the 5-HT₃ receptor, a homopentameric member of the superfamily that responds to 5-hydroxytryptamine (a.k.a. serotonin, **1**).^{2,3} In the course of this work, he identified a tyrosine residue that might accept a hydrogen bond from the indole nitrogen of 5-HT, but the data were ambiguous. We therefore proposed that an analog of the native agonist—one in which the indole nitrogen is replaced by an oxygen—would elucidate this question. This proposed molecule is 3-(2-aminoethyl)benzofuran-5-ol, which we refer to as 1-OT (1-oxo-5-hydroxytryptamine, **2**), for consistency with 5-HT and related compounds (Figure 2.1).

1-OT has been synthesized once before,⁴ but it has never been explicitly tested on the 5-HT₃ receptor. In fact,

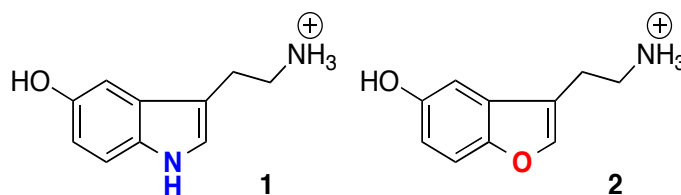
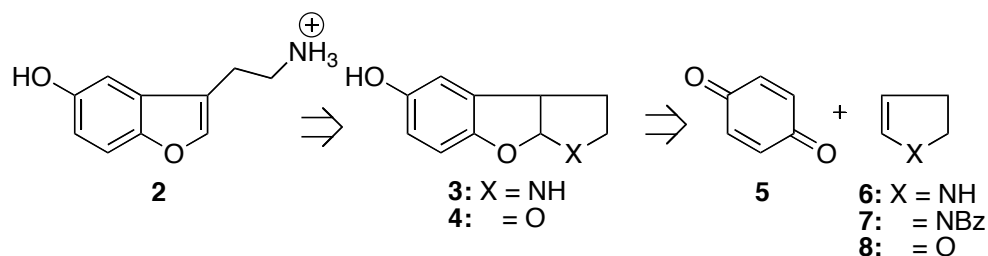


Figure 2.1. 5-hydroxytryptamine (**1**) and its analog 1-oxo-5-hydroxytryptamine (**2**)

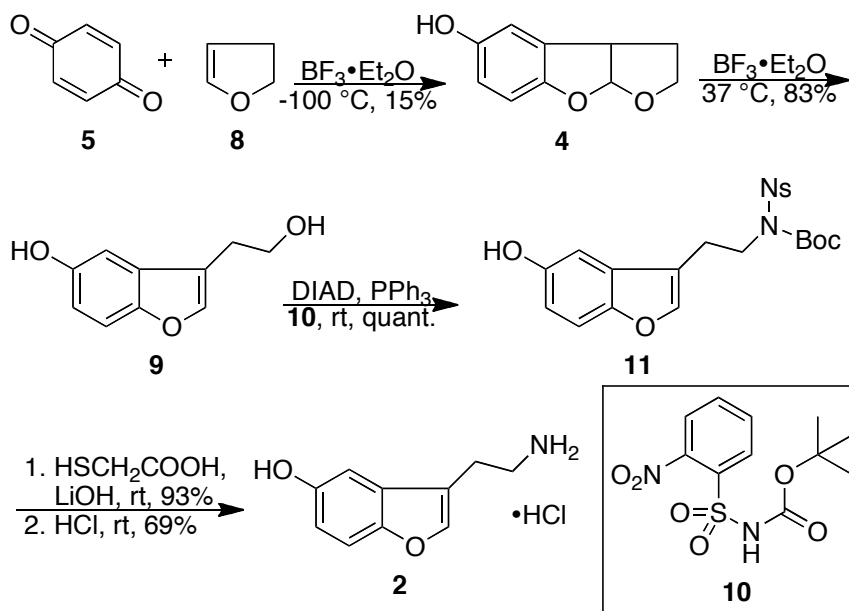
Scheme 2.1. 1-OT retrosynthesis

the only prior study on this molecule was one in which the rate of muscular contraction of surgically removed rat fundus strips was measured following drug application.⁵ The published synthesis (10 steps and < 3% yield) was cumbersome, prompting the pursuit of a novel synthetic strategy that could provide more ready access to **2**. Identification of the quinone synthon within the target molecule suggested a synthetic route utilizing a [3+2] cycloaddition between *p*-benzoquinone and an electron-rich olefin, yielding the benzofuran core in a single step (Scheme 2.1).

Initial attempts focused on the cycloaddition of **5** with enamine **6**, which, when subjected to acidic workup conditions, was expected to give ring-opened product, 1-OT **2**. However, consistent with previous reports, pyrroline (**6**) proved very difficult to work with due to its high reactivity (pyrroline reacts with itself to form a readily oxidizable trimer, which must be broken up by heat immediately prior to reaction).⁶ No desired products could be isolated from the reaction mixture, which formed a black tar, even at cryogenic temperatures. Protection of pyrroline with a carbamate or amide was then considered to reduce its nucleophilic reactivity. However, the *N*-benzoyl pyrroline (**7**) failed to react with *p*-benzoquinone, even at elevated temperatures.

A strategy involving the installation of the primary amine subsequent to formation of the heterocyclic framework was then considered (Scheme 2.2). The tricycle **4** is a known compound that can be synthesized enantioselectively from **5** and 2,3-dihydrofuran

Scheme 2.2. Synthesis of 1-OT



(8) using a Lewis acid catalyst developed by Corey.⁷ Circumventing the multistep synthesis of the Corey catalyst, we discovered that the same transformation can be accomplished racemically by $\text{BF}_3 \cdot \text{Et}_2\text{O}$, albeit in much poorer yield. The reaction was messy, even at $-100\text{ }^\circ\text{C}$, but poor (10-20%) yields of the desired tricycle **4** could be isolated. A screen of other Lewis acids failed to produce markedly better results.

The postulated ring-opening reaction was then explored. Refluxing HCl or HBr failed to yield the desired alcohol **9** or the corresponding alkyl halide. However, treatment of **4** with $\text{BF}_3 \cdot \text{Et}_2\text{O}$ at slightly elevated temperatures produced **9** in good yield. The similarity of these conditions to those of the cycloaddition step, suggested that a one-pot cascade synthesis of **9** from benzoquinone and 2,3-dihydrofuran might be possible. This route was investigated but was not realized. **9** could not be isolated from the reaction of **5** with **8**, even when subjected to longer reaction times, elevated catalyst loadings, and/or elevated temperatures. Using the crude cyclization product **4** in the ring-opening reaction led to no alcohol **9**, but did result in the consumption of **4**. Starting materials or

side products from the cycloaddition step may interfere with the ring opening (for example, p-benzoquinone may be capable of oxidation of tricycle **4** or alcohol **9** at faster rates than ring-opening).⁸ In the previously reported synthesis of tricycle **4**, p-benzoquinone gave significantly poorer yields than more electron rich benzoquinones. A screen of other Lewis acids (e.g., AlCl₃, InCl₃, MgBr₂, etc.) in the desired cascade synthesis also failed. These observations suggest that—if a catalyst exists for this sequence—it is likely to be sterically bulky and quite Lewis acidic, as is the case with the Corey catalyst.

Primary alcohol **9** was then converted to protected amine **11** using Fukuyama's modified Mitsunobu protocol in quantitative yield.⁹ Removal of the nosyl group according to Fukuyama likewise proceeded in quantitative yield, giving Boc-protected 1-OT **11b**. After some experimentation with the reaction conditions, it was discovered that

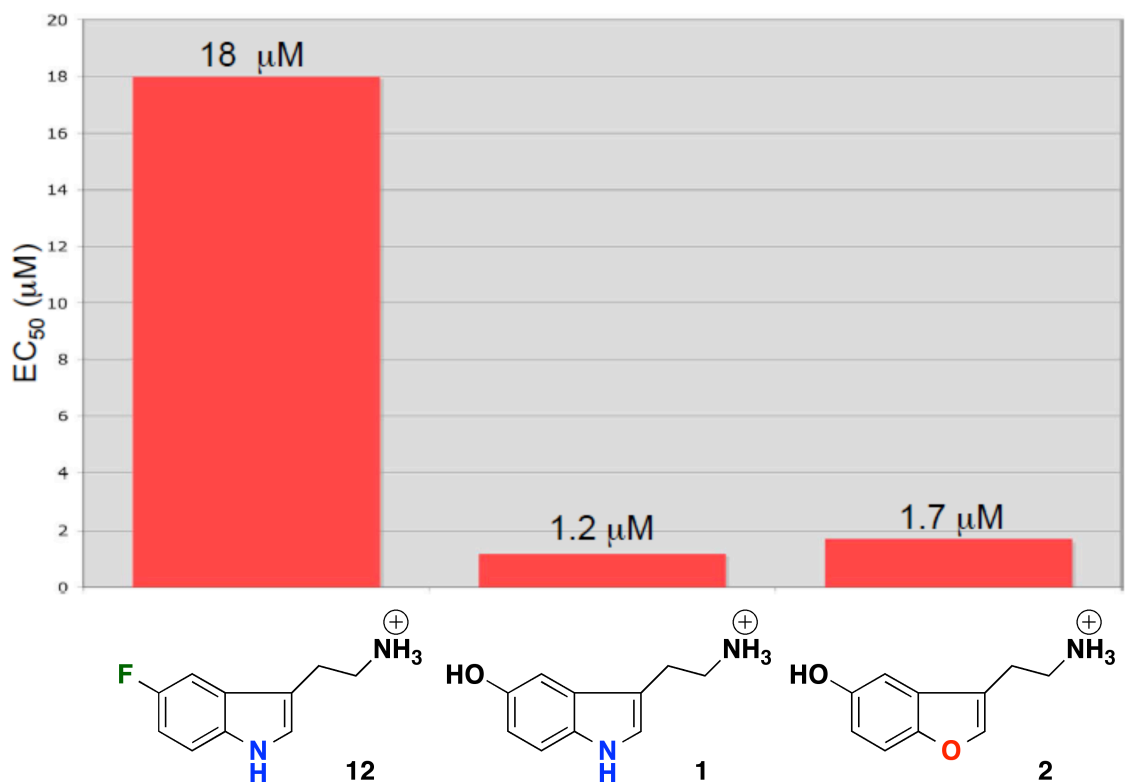


Figure 2.2. Pharmacology of 5-FT, 5-HT, and 1-OT on the 5-HT₃ receptor.

the crystalline hydrochloride salt of 1-OT (**2**) could be isolated in high purity and good yield via deprotection of **11b** using HCl in chloroform/methanol, followed by crystallization from anhydrous ether.

The pharmacology of **2** on the 5-HT₃ receptor proved very interesting, with an EC₅₀ value nearly identical to that of the native agonist (1.7±0.06 vs. 1.2±0.03 μM, respectively; Figure 2.2). Furthermore, **2** is essentially a full agonist, with an efficacy that is 94±4% of **1**. These data strongly indicate that the indole NH of **1** is not important for receptor activation. Comparison of 1-OT to 5-fluorotryptamine (5-FT, **12**, EC₅₀ = 18 μM)—an agonist that likewise differs from serotonin by the elimination of one hydrogen bond donor—emphasizes how well 1-OT mimics serotonin in the 5-HT₃ receptor.

In conclusion, an efficient new route to 1-oxo-5-hydroxytryptamine, the benzofuran analog of serotonin, has been established. This molecule is a competent agonist of the 5-HT₃ receptor, suggesting that the indole nitrogen of **1** does not donate a hydrogen bond to the receptor. The increased availability of **2** afforded by the synthetic route described here will enable similar studies to elucidate agonist binding in the other six classes of 5-HT receptors, perhaps providing a class-specific agonist. In addition, this route should be easily modifiable (through the use of substituted benzoquinones and dihydrofurans) to synthesize more substituted 1-OT derivatives for further elucidation of 5-HT receptor binding sites.

Chemistry—General

All reactions were performed under argon using solvents that were dried and purified according to the method of Grubbs.¹⁰ All flasks and vials were oven dried at 122 °C and cooled in a desiccator box containing anhydrous calcium sulfate. Commercial reagents were purified according to the methods compiled by Armengo and Perrin.¹¹ Hydrogen chloride gas was generated in situ by dropwise addition of concentrated HCl into stirred concentrated H₂SO₄. Reactions were monitored by thin-layer chromatography on Merck Siligel 60-F₂₅₄. Compounds were visualized with UV lamp (254 nm) and stained with ceric ammonium molybdate solution. Column chromatography was carried out in accordance with the methods of Still¹² using EMD-Merck silica gel 60, 230-400 mesh ASTM or Aldrich Brockmann I alumina, 150 mesh (for acid-sensitive compounds such as pyrroline). ¹H and ¹³C NMR spectra were acquired on a Varian Mercury 300 MHz spectrometer. High-resolution mass spectrometry was performed on a JEOL JMS-600H HRMS using an Electrospray Ion Source. Copies of NMR spectra of the synthesized compounds can be found in the supporting information section of our submission of this work to *Organic Letters*.¹

Chemistry—Synthesis

(4). Boron trifluoride-diethyl etherate (0.6 mL, 5 mmol) was added to a mixture of acetonitrile (10 mL) and dichloromethane (30 mL) in a 100 mL round-bottomed flask and

cooled to $-78\text{ }^{\circ}\text{C}$. A solution of *p*-benzoquinone (540 mg, 5 mmol) and 2,3-dihydrofuran (2,3-DHF, 0.6 mL, 7.5 mmol) in acetonitrile (10 mL) was then added to the stirred BF_3 solution at $-78\text{ }^{\circ}\text{C}$ by syringe pump over 2 h. After 5 total hours, additional 2,3-DHF (0.6 mL, 7.5 mmol) was added dropwise over 10 minutes. After 8 total hours, the reaction temperature was allowed to slowly rise to room temperature over the following hour, at which point methanol (10 mL) and 1 N HCl (10 mL) were added. The product was extracted with 4 x 30 mL dichloromethane, washed with 1 x 30 mL brine, dried on magnesium sulfate, and reduced *in vacuo*. The residue was then filtered through a silica plug with ethyl acetate, then purified by flash chromatography on silica (25% EtOAc in hexanes). The product fraction could be purified further by recrystallization from 3 mL toluene to yield flaky, white crystals; 160 mg (18%) **4**. ^1H NMR (300 MHz, CDCl_3) δ 6.59-6.70 (m, 3H), 6.27 (d, 1H, $J = 6\text{ Hz}$), 4.66 (s, 1H, OH), 4.05 (t, 1H, $J = 8\text{ Hz}$), 3.95 (t, 1H, $J = 7\text{ Hz}$), 3.58-3.64 (m, 1H), 2.22-2.29 (m, 1H), 2.03 (dd, 1H, $J = 12, 4.5\text{ Hz}$); ^{13}C NMR (75 MHz, CDCl_3) δ 153.6, 150.5, 128.9, 115.5, 112.1, 111.3, 109.6, 67.5, 47.2, 33.6; HRMS (EI^+) calculated for $[\text{C}_{10}\text{H}_{10}\text{O}_3]$ ($[\text{M}]^+$) 178.0630, found 178.0638. The characterization data matched reported values for this compound synthesized using the Corey oxazaborolidine catalyst.⁷

(9). **4** (89 mg, 0.50 mmol) was measured into a 2 dram vial, and acetonitrile (5 mL) was added to dissolve it. Boron trifluoride-diethyl etherate (140 μL , 1.1 mmol) was then added. The vial was then shaken at $37\text{ }^{\circ}\text{C}$ for 22 h. Aqueous HCl (4 mL, 1 N) was then added, and the product was extracted with 5 x 8 mL dichloromethane, dried on sodium sulfate, and reduced *in vacuo*. The residue was then purified by flash chromatography on

silica (50% EtOAc in hexanes) to yield 74.1 mg (83%) **9**. ^1H NMR (300 MHz, acetone- d_6) δ 8.03 (s, 1H), 7.58 (s, 1H), 7.27 (d, 1H, $J = 9$ Hz), 7.01 (d, 1H, $J = 3$ Hz), 6.81 (dd, 1H, $J = 9, 3$ Hz), 3.99 (s, 1H), 3.82 (t, 2H, $J = 6$ Hz), 2.82 (t, 2H, $J = 6$ Hz); ^{13}C NMR (75 MHz, acetone- d_6) δ 153.9, 150.0, 143.8, 129.8, 118.0, 113.5, 112.0, 104.9, 61.6, 27.5; HRMS (EI^+) calculated for $[\text{C}_{10}\text{H}_{10}\text{O}_3]$ ($[\text{M}]^+$) 178.0630, found 178.0628.

(**11**). **9** (193 mg, 1.1 mmol), triphenylphosphine (341 mg, 1.3 mmol), and N-Boc-*o*-nitrobenzenesulfonamide (393 mg, 1.3 mmol) were measured into a 2 dram vial. THF (5 mL) was added. Diisopropyl azodicarboxylate (256 μL , 1.3 mmol) was added to the stirred solution by a syringe over a 10 minute period. After an additional 20 minutes stirring at room temperature, the reaction was reduced *in vacuo*, and the residue was triturated with toluene (5 mL) to give 372.7 mg of a white solid. Additional product could be recovered by flash chromatography of the filtrate on silica (30% EtOAc in hexanes), followed by trituration of the product fraction to give a total yield of 483.0 mg (96 %) **11**. ^1H NMR. (300 MHz, acetone- d_6) δ 8.28-8.31 (m, 1H), 7.95-8.02 (m, 3H), 7.70 (s, 1H), 7.32 (d, 1H, $J = 9$ Hz), 7.14 (d, 1H, $J = 2$ Hz), 6.86 (dd, 1H, $J = 9, 2$ Hz), 4.03 (t, 2H, 7 Hz), 3.08 (t, 2H, 7 Hz), 1.27 (s, 9H); ^{13}C NMR (75 MHz, acetone- d_6) δ 153.7, 150.4, 150.0, 143.6, 135.3, 133.0, 132.6, 132.5, 128.9, 124.9, 116.6, 113.4, 111.7, 104.5, 85.0, 47.2, 27.1, 21.6; HRMS (EI^+) calculated for $[\text{C}_{21}\text{H}_{22}\text{N}_2\text{O}_8\text{S}]$ ($[\text{M}]^+$) 462.1097, found 462.1100.

1-oxa-5-hydroxytryptamine hydrochloride (2). **11** (445 mg, 0.96 mmol) was measured into a 25 mL round-bottomed flask. DMF (9.6 mL), followed by lithium hydroxide

monohydrate (162 mg, 3.85 mmol) and mercaptoacetic acid (134 μ L, 1.93 mmol), were then added. After 6 h room temperature stirring, the reaction was poured onto 60 mL aqueous sodium bicarbonate, and the product was extracted with 5 x 20 mL EtOAc, washed with 1 x 20 mL brine, reduced *in vacuo*, and filtered through a silica plug (30% EtOAc in hexanes) to yield 247 mg, which was transferred into a 50 mL 3-neck flask appended with an HCl purge. Chloroform (20 mL) and methanol (2 mL) were added, and HCl was purged through the stirring solution for 30 minutes. The reaction was then reduced *in vacuo*, and the residue was redissolved in acetone (5 mL). This acetone solution was then added dropwise to a stirring beaker of ether (20 mL); the resultant white crystals were then isolated by filtration to yield 130 mg (64%, 2 steps) 1-oxa-5-hydroxytryptamine hydrochloride. ^1H NMR (300 MHz, DMSO- d_6) δ 9.31 (s, 1H, OH), 8.13 (s, 3H, NH), 7.78 (s, 1H), 7.34 (d, 1H, $J = 8$ Hz), 6.95 (d, 1H, $J = 2$ Hz), 6.78 (dd, 1H, $J = 9, 2$ Hz), 3.06 (t, 2H, $J = 8$ Hz), 2.91 (t, 2H, $J = 8$ Hz); ^{13}C NMR (75 MHz, DMSO- d_6) δ 154.0, 149.4, 144.1, 128.7, 116.1, 113.9, 112.3, 104.7, 38.7, 22.0; HRMS (EI^+) calculated for $[\text{C}_{10}\text{H}_{11}\text{NO}_2]$ ($[\text{M}]^+$) 177.0790, found 177.0794.

Molecular Biology and Electrophysiology

The measurement of EC_{50} and efficacy values for 5-HT, 1-OT, and 5-HT₃ was carried out by Kiowa Bower using methods described previously.¹³ Briefly, the 5-HT₃ receptor was expressed in *Xenopus laevis* oocytes by manual injection of the corresponding mRNA. Following 1-3 days incubation at 18 °C, transmembrane current in response to drug

application was measured using a two-electrode whole-cell voltage clamp. From these data a dose-response curve was created for each drug and was fit to the Hill equation.

References

¹ We have published this work previously: 1-Oxo-5-hydroxytryptamine: A Surprisingly Potent Agonist of the 5-HT₃ (Serotonin) Receptor. S. M. A. Kedrowski, K. S. Bower, D. A. Dougherty, *Org. Lett.*, **2007**, 9, 3205-3207.

² (a) Meltzer, H. Y.; Li, Z.; Kaneda, Y. *Prog. Neuro-Psychopharmacol. Biol. Psychiatry*, **2003**, 27, 1159-1172. (b) Barnes, N. M.; Sharp, T. *Neuropharmacology* **1999**, 38, 1083. (c) Pucadyil, T. J.; Kalipatnapu, S.; Chattopadhyay, A. *Cell Mol. Neurobiol.* **2005**, 25, 553. (d) Leopoldo, A. *Curr. Med. Chem.* **2004**, 11, 629. (e) Bishop, M. J.; Nilsson, B. M. *Expert Opin. Ther. Pat.* **2003**, 13, 1691. (f) Poissonet, G.; Parmentier, J. G.; Boutin, J. A. *Expert Opin. Ther. Pat.* **2004**, 4, 325. (g) Thomas, D. R. *Pharmacol. Therapeut.* **2006**, 111, 707. (h) Thompson, A. J.; Lummis, S. C. R. *Curr. Pharm. Des.* **2006**, 12, 3615. (i) Reeves, D. C.; Lummis, S. C. R. *Mol. Memb. Biol.* **2002**, 19, 11. (j) Maricq, A. V.; Peterson, A. S.; Brake, A. J.; Myers, R. M.; Julius, D. *Science* **1991**, 254, 432-437.

³ (a) Beene, D. L.; Price, K. L.; Lester, H. A.; Dougherty, D. A.; Lummis, S. C. R. *J. Neurosci.* **2004**, 24, 9097-9104. (b) 5-Fluorotryptamine is a partial agonist at 5-HT₃ receptors, and reveals that size and electronegativity at the 5 position of tryptamine are critical for efficient receptor function. K. S. Bower, K. L. Price, L. E. Sturdee, D. A. Dougherty, S. C. R. Lummis, *Eur. J. Pharm.*, **2008**, 580, 291-297, (c) A hydrogen bond in Loop A is critical for binding and function of the 5-HT₃ receptor. K. L. Price, K. S. Bower, A. J. Thompson, H. A. Lester, D. A. Dougherty, and S. C. R. Lummis, *Biochemistry*, **2008**, 47, 6370-6377.

⁴ Hallmann, G.; Hagele, K. *Leibigs. Ann. Chem.* **1963**, 662, 147.

⁵ Pinder, R. M.; Green, D. M.; Thompson, P. B. *J. Med. Chem.* **1971**, 14, 626-628.

⁶ (a) Nomura, Y.; Ogawa, K.; Takeuchi, Y.; Tomoda, S. *Chem. Lett.* **1977**, 693-696. (b) Kraus, G. A.; Neuenschwander, K. *J. Org. Chem.* **1981**, 46, 4791-4792. (c) Marais, W.; Holzappel, C. W.; *Synth. Commun.* **1998**, 28, 3681-3691.

⁷ Zhou, G.; Corey, E. J.; *J. Am. Chem. Soc.* **2005**, 127, 11958-11959.

⁸ 1,4-Benzoquinone. Yang, T.-K.; Shen, C.-Y. *e-EROS Encyclopedia of Reagents for Organic Synthesis*, **2001**. and references therein.

⁹ Kan, T.; Fukuyama, T. *Chem. Commun.* **2004**, 353-359.

-
- ¹⁰ Pangborn, A. B.; Giardello, M. A.; Grubbs, R. H.; Rosen, R. K.; Timmers, F. J. *Organometallics* **1996**, *15*, 1518-1520.
- ¹¹ Perrin, D. D.; Armarego, W. L. F. *Purification of Laboratory Chemicals*. 3rd Edition. Pergamon Press: Oxford, **1988**.
- ¹² Still, W. C.; Kahn, M.; Mitra, a. *Journal of Organic Chemistry* **1978**, *43*, 2923-2925.
- ¹³ Beene, D. L.; Price, K. L.; Lester, H. A.; Dougherty, D. A.; Lummis, S. C. R. *Journal of Neuroscience* **2004**, *24*, 9097-9104.

Section 1: Chapter 3

The Synthesis of α -Hydroxy Acids to Probe Hydrogen Bonding¹

Abstract: *To study the role of specific hydrogen bonds involving the polypeptide backbone of the nicotinic acetylcholine receptor, the α -hydroxy acid derivatives of serine (Sah) and of asparagine (Nah) were prepared. The asparagine derivative offered a significant challenge in its propensity to cyclize into a succinimide, which could be overcome by the covalent attachment of a steric blocking group to the amide.*

Elimination of a main-chain amide proton from a large integral membrane protein without perturbing the structure in other ways is no simple task. In the Dougherty lab, we use α -hydroxy acid mutagenesis by nonsense suppression to accomplish this, a strategy that requires the chemical synthesis of the ester of the desired α -hydroxy acid and the dinucleotide dCA.² Incorporation of this α -hydroxy acid yields a protein with a single, specific hydrogen bond donor eliminated, though there is a secondary effect of decreasing the hydrogen bond-accepting ability of the adjacent carbonyl (Figure 3.1).³

For this study, the backbone hydrogen bond donors of interest were adjacent to asparagine and serine residues, requiring the synthesis of α -hydroxy asparagine-dCA (Nah-dCA; **1**) and α -hydroxy serine-dCA (Sah-dCA; **2**; Figure 3.2). The synthesis of Nah-dCA

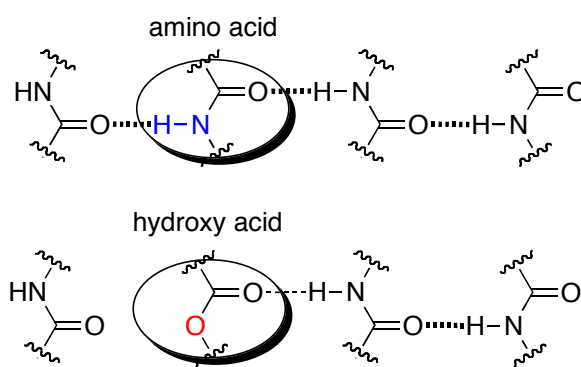


Figure 3.1. Incorporation of an α -hydroxy acid eliminates a hydrogen bond donor

proved to be a challenging task. A search of the literature indicated that it had not been made before; however, an early Schultz paper showed that they had attempted to make at

least one Asn-dCA analog, but could never get the final step (dCA ester formation) to work and ultimately gave up.⁴ Similarly, at least three members of the Dougherty group have attempted to

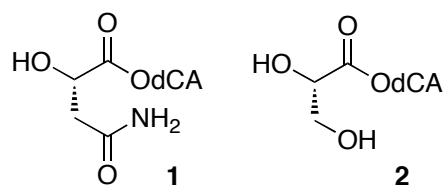
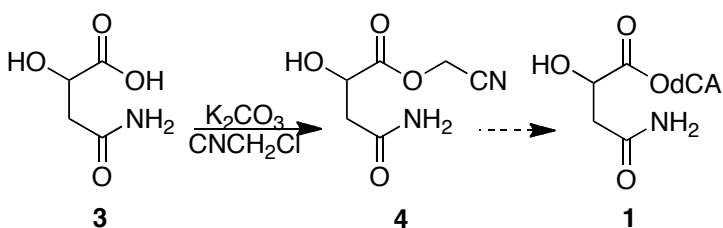


Figure 3.2. Nah-dCA (**1**) and Sah-dCA (**2**).

synthesize Asn-dCA analogues, also with no success. It has been posited that cyclization of the terminal amide into the acid/ester group to form a succinimide was the source of the difficulty, but this had not been demonstrated, in part because the isolation of these highly polar molecules is itself a challenge.

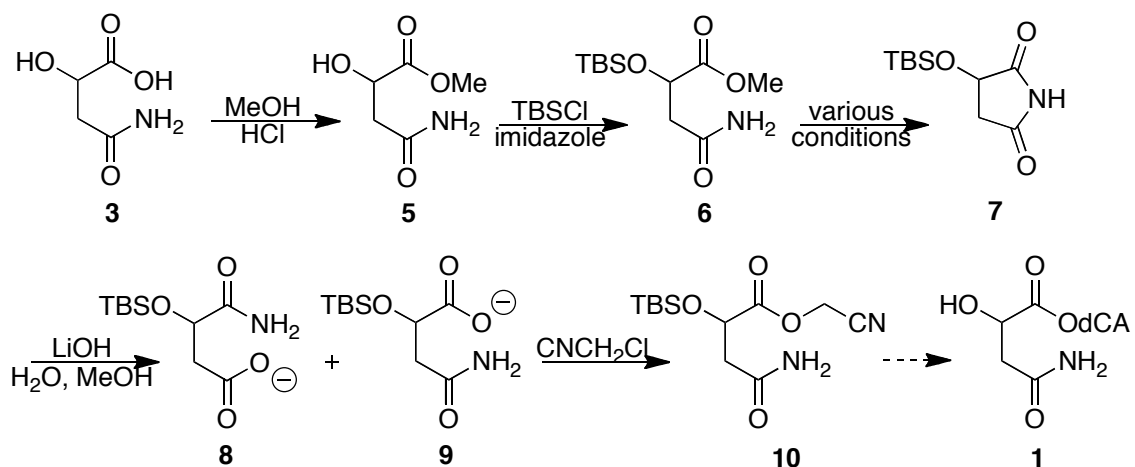
The synthetic route first attempted followed standard protocols for the preparation of α -hydroxy-dCA esters (Scheme 3.1).⁵ α -

Scheme 3.1. Nah-dCA synthesis, route #1 (failed).



Hydroxy asparagine (**3**) was prepared from asparagine using aqueous sodium nitrite.⁶ Cyanomethyl esterification of **3** using triethylamine only gave trace product. A screen of different bases revealed that dry Potassium carbonate was able to give **4** in poor (10-20%) yields. Attempts at coupling **4** to dCA using the well-established procedure of combining the cyanomethyl ester with basic dCA•2.4 TBA in DMF at room temperature gave a disheartening result: even if the reaction had worked (which seemed unlikely), the reactants could not be separated by HPLC.

Therefore a second route, in which a ‘greasy’ protecting group was attached to **3** to improve HPLC separation, was attempted (Scheme 3.2). This strategy had been successfully employed once before in the synthesis of α -hydroxy alanine-dCA (Aah-

Scheme 3.2. Nah-dCA synthesis, route #2 (failed).

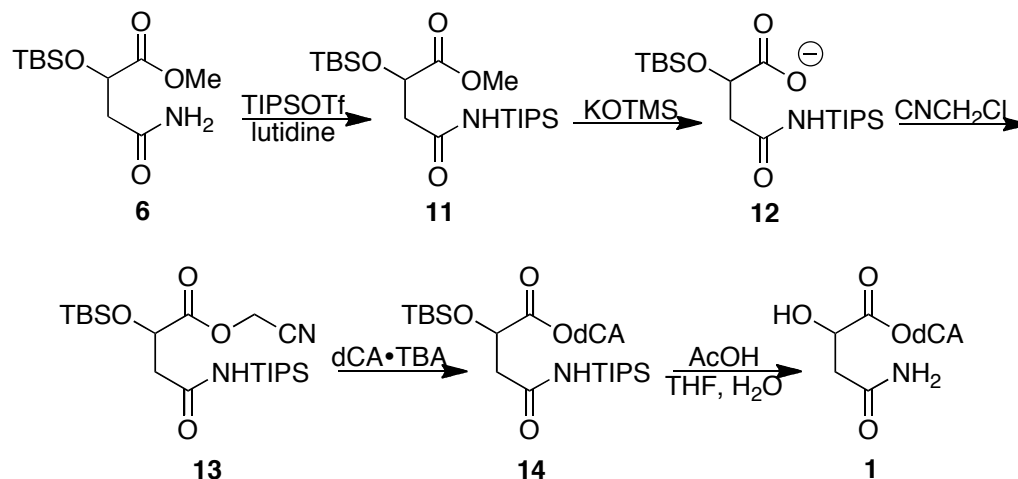
dCA).⁷ First, Nah-methyl ester **5** was made by Fischer esterification, followed by TBS protection of the α -hydroxy group. At this point, only a series of transesterifications and a deprotection were necessary to access **1**, but the first step—cleavage of the methyl ester—proved very difficult. Only succinimide **7** was isolated under a number of reaction conditions. Interestingly, when **7** was allowed to stand for several days in aqueous base, the desired free acid **9** could be isolated, along with isomer **8**. In this basic hydrolysis reaction, there are two imide carbonyls susceptible hydroxide attack; they are desymmetrized by the OTBS group, which should activate the closer carbonyl electronically but deactivate it sterically. The experiment suggests that the electronic effect dominates the steric effect in this case, as the desired α -silyloxy acid **9** is formed preferentially over the isomeric β -silyloxy acid **8** by a ratio of 5:1. Direct lyophilization of the crude reaction mixture gave the carboxylate salt **9**, which could be directly converted to the cyanomethyl ester **10** by direct addition of chloroacetonitrile. Unfortunately, **10** could not be coupled to dCA. After several hours of reaction, no dCA ester could be identified by HPLC or TLC, and all cyanomethyl ester **10** had cyclized to **7**.

Table 3.1. Protecting group screen for the amide in asparagine. Protecting groups were screened on the basis of: (a) ease of synthesis; (b) ease of removal; (c) survival of potassium trimethylsilyloate treatment; and (d) survival of dCA coupling conditions.

Protecting group	PPh ₂	P(O)Ph ₂	Trityl	TBS	TBDPS	TIPS
ON	X	X	YES	YES	YES	YES
OFF	-	-	X	YES	YES	YES
KOTMS	-	-	-	X	X	YES
dCA Coupling	-	-	-	-	-	YES

The substrate needed to be modified to prevent imide formation. Two distinct strategies were envisioned: the amide could be tethered to make the ester physically inaccessible; or the nucleophilicity of the amide could be reduced through the addition of steric bulk. We chose the latter strategy, reasoning that this solution might be more broadly applicable to other asparagine derivatives. Nearly a dozen protecting groups were screened for this role (Table 3.1). The TIPS group showed the most promise in this screen. Incorporating this protecting group into the synthesis, primary amide **6** was

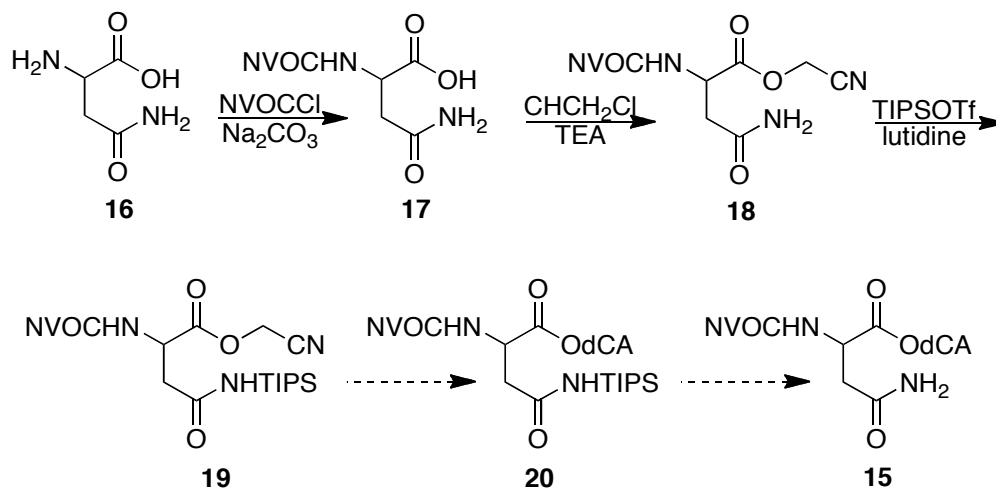
Scheme 3.3. Nah-dCA synthesis, route #3.



treated with TIPS triflate and base to give **11** (Scheme 3.3). Deprotection of this ester was accomplished with KOTMS in ether to give the salt **12**, which was immediately suspended in chloroacetonitrile to give the cyanomethyl ester **13**. To our relief, this compound successfully coupled to dCA, albeit in very low yields. This dCA ester was then successfully deprotected in a 1 : 1 : 3 mixture of water : THF : acetic acid to give Nah-dCA **1**.

The synthesis of Asn-dCA **15** required more than a simple extension of the Nah-dCA synthesis (Scheme 3.4). Given that literature precedent suggested that a cyanomethyl ester should be stable enough to survive all the steps of the Nah-dCA synthesis, we hoped to bypass the need for a methyl ester.⁸ Beginning with asparagine, treatment with nitroveratryl chloroformate in aqueous sodium carbonate yielded NVOC-Asn **17**. This compound was converted directly to cyanomethyl ester **18** by treatment with chloroacetonitrile and slow titration with triethylamine. Primary amide **18** could then be protected with TIPS triflate to give the coupling precursor **19**. Unfortunately, all that could be isolated from the dCA coupling reaction was succinimide and silylated

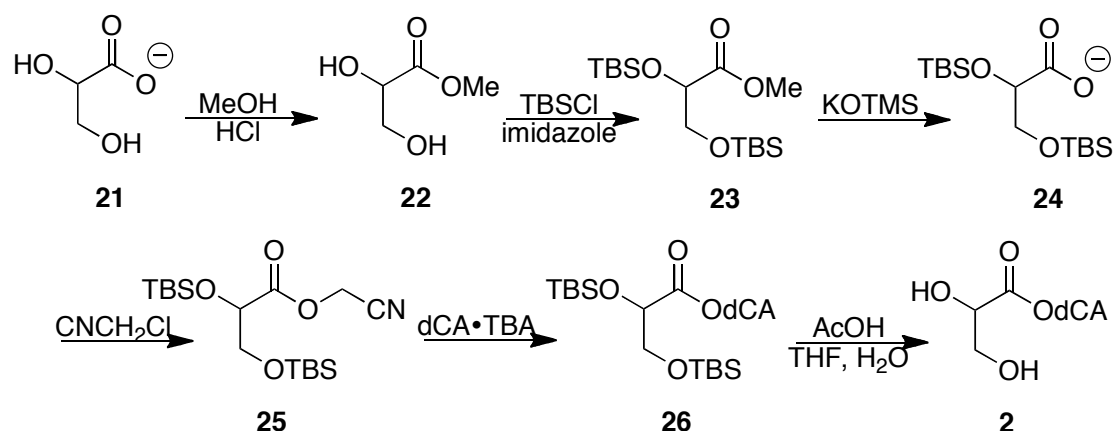
Scheme 3.4. Asn-dCA synthesis (failed).



dCA. These results suggest that the α -silyloxy cyanomethyl ester is more reactive than the α -N-carbamoyl cyanomethyl ester towards the dCA nucleophile. Clear precedent to support or challenge this observation is lacking: the Hammett parameters of methoxy and acetamido are roughly the same, but methoxy and acetamido are imperfect models for the electronics of OTBS and NHNVOC, respectively, and the Hammett parameters do not account for steric effects.⁹ Neither dCA-coupling reaction is homogeneous, so there may be solubility effects as well.

The synthesis of Sah-dCA (**2**) proceeded more smoothly (Scheme 3.5). Similar to the cyanomethyl esters of Nah and Aah, the cyanomethyl ester of Sah could not be separated from dCA by HPLC. It was therefore necessary to protect at least one of the hydroxyl groups. Starting with the calcium salt of glycerate (**21**), Fischer esterification yielded methyl ester **22**. TBS protection of both hydroxyl groups to give **23** was followed by KOTMS deprotection of the methyl ester to give carboxylate salt **24**. Addition of chloroacetonitrile to the salt yielded coupling precursor **25**. The coupling reaction of **25** and dCA proceeded smoothly to give protected product **26**. Deprotection in 1 : 1 : 3 of

Scheme 3.5. Sah-dCA synthesis.



water : THF : acetic acid yielded Sah-dCA **2**.

These syntheses demonstrate a strategy that may be more broadly applicable in the syntheses of other amino acid-dCA and α -hydroxy acid-dCA esters. Specifically, the one-pot conversion of methyl esters to cyanomethyl esters using the KOTMS-chloroacetonitrile sequence is demonstrated here for the first time. Often in other syntheses, there is a need to protect the ester with a group that is stable to acid and mild base. This method allows easy conversion of a methyl ester—which has those properties—to a cyanomethyl ester, which is the precursor activated ester needed for the dCA coupling/transesterification reaction.

Chemistry—General

All reactions were performed under argon using solvents that were dried and purified according to the method of Grubbs.¹⁰ All flasks and vials were oven dried at 122 °C and cooled in a desiccator box containing anhydrous calcium sulfate. Commercial reagents were purified according to the methods compiled by Armengo and Perrin.¹¹ Reactions were monitored by thin-layer chromatography on Merck Siligel 60-F₂₅₄. Compounds were visualized with UV lamp (254 nm) and stained with ceric ammonium molybdate solution. Column chromatography was carried out in accordance with the methods of Still¹² using EMD-Merck silica gel 60, 230-400 mesh ASTM. For dCA-coupling reactions, the reaction progress is monitored by analytical HPLC, and the reaction is ultimately quenched with a threefold (volume) excess of 1:1 acetonitrile: 10 mM aq. AcOH, which is then directly loaded onto the preparative HPLC. The standard HPLC method runs a gradient of 95:5 to 0:100 of 25 mM ammonium acetate, pH = 4.5: acetonitrile over a run time of 15 minutes. The product fraction(s) are then lyophilized to dryness. ¹H and ¹³C NMR spectra were acquired on a Varian Mercury 300 MHz spectrometer. High-resolution mass spectrometry was performed on a JEOL JMS-600H HRMS using an Electrospray Ion Source. Copies of NMR spectra of the synthesized compounds can be found in the supporting information section of our submission of this work to the *Journal of Biological Chemistry*.¹

Chemistry—Synthesis

Glycerate methyl ester (22). Glycerate, calcium salt dihydrate (286 mg, 2.0 mmol) was measured into a 100 mL round-bottomed flask. Methanol (40 mL) and toluene (10 mL) were then added, followed by HCl (1 mL, 12 N, 12 mmol). The mixture was stirred under reflux for 6 h, at which point the solvent was removed *in vacuo* to give 464 mg of a crude residue that was moved directly forward into the next step.

2,3-di-*tert*-butyldimethylsilylglycerate methyl ester (23). Glycerate methyl ester (464 mg crude residue, above) was dissolved in DMF (6 mL) in a 2 dram vial. TBSCl (906 mg, 6 mmol) and imidazole (544 mg, 8 mmol) were then added, and the reaction was stirred at room temperature for 12 h, at which point the reaction was concentrated *in vacuo* to ca. 1 mL, and dichloromethane (10 mL) was added. The precipitate was removed by filtration, and the filtrate was reduced *in vacuo* and purified by flash chromatography on silica (5% EtOAc in hexanes) to yield 421 mg (60% over 2 steps) 2,3-di-*tert*-butyldimethylsilylglycerate methyl ester. ^1H NMR (300 MHz, CDCl_3) δ 4.27 (dd, 1H, $J = 5.2, 6.2$ Hz), 3.80 (dd, 1H, $J_{\text{AB}} = 9.9$ Hz, $J_{\text{AX}} = 5.2$ Hz), 3.73 (dd, 1H, $J_{\text{AB}} = 9.9$ Hz, $J_{\text{AX}} = 6.6$ Hz), 3.70 (s, 3H), 0.88 (s, 9H), 0.85 (s, 9H), 0.07 (s, 3H), 0.05 (s, 3H), 0.03 (s, 3H), 0.02 (s, 3H). ^{13}C NMR (75 MHz, CDCl_3) δ 172.71, 74.21, 66.16, 51.99, 26.04, 25.94, 18.57, 18.52, -4.86, -4.87, -5.16, -5.25. LRMS (ES^+) calculated for $[\text{C}_{16}\text{H}_{36}\text{NaO}_4\text{Si}_2]$ ($[\text{M}+\text{Na}]^+$) 371.2, found 371.1.

2,3-di-*tert*-butyldimethylsilylglycerate cyanomethyl ester (25). 2,3-di-*tert*-butyldimethylsilylglycerate methyl ester (100 mg, 0.29 mmol) was measured into a 2 dram vial. Diethyl ether (3 mL) was added to dissolve the starting material, followed by potassium trimethylsilyloate (40.7 mg, 0.29 mmol). After 18 h, the potassium salt was isolated by filtration, washed with 2 x 1 mL ether, and dried *in vacuo*. The solid was then resuspended in chloroacetonitrile (3 mL) by sonication, and allowed to stir at room temperature for 6 hours. The reaction was then filtered through a plug of silica to yield the pure product as a colorless liquid: 66.7 mg (62% over 2 steps) 2,3-di-*tert*-butyldimethylsilylglycerate cyanomethyl ester. ¹H NMR (300 MHz, CDCl₃) δ 4.75 (s, 2H), 4.35 (t, 1H, *J* = 5.4 Hz), 3.81 (d, 2H, *J* = 5.4 Hz), 0.90 (s, 9H), 0.87 (s, 9H), 0.10 (s, 3H), 0.08 (s, 3H), 0.06 (s, 3H), 0.05 (s, 3H). ¹³C NMR (75 MHz, CDCl₃) δ 170.82, 114.24, 73.78, 65.92, 48.62, 26.01, 25.87, 18.48, -4.86, -4.90, -5.21, -5.24. HRMS (FAB⁺) calculated for [C₁₇H₃₆NO₄Si₂] ([M+H]⁺) 374.2183, found 374.2181.

2,3-di-*tert*-butyldimethylsilylglycerate dCA ester (26). 2,3-di-*tert*-butyldimethylsilylglycerate cyanomethyl ester (8.9 mg, 24 μmol) and dCA*2.4 TBA (8.2 mg, 6.5 μmol) were measured into a 1 dram vial. DMF (0.8 mL) was added, and the reaction was allowed to stir at room temperature for 24 h, at which point the reaction was quenched and purified by HPLC to yield 0.74 μmol (11%) 2,3-di-*tert*-butyldimethylsilylglycerate dCA ester. LRMS (ESI) calculated for [C₃₄H₅₇N₈O₁₆P₂Si₂] ([M-H]⁻) 951.3, found 951.4.

α -Hydroxy serine-dCA (2). 2,3-di-*tert*-butyldimethylsilylglycerate dCA ester (0.73 μ mol) in a 15 mL falcon tube was dissolved in water (0.2 mL), THF (0.2 mL) and AcOH (0.6 mL) and shaken at 37 °C for 24 h, at which point the reaction was lyophilized to give 0.24 μ mol (34%) α -Hydroxy serine-dCA. LRMS (ESI⁻) calculated for [C₂₂H₂₉N₈O₁₆P₂]⁻ ([M-H]⁻) 723.1, found 723.4.

4-amido-2-hydroxybutyrate methyl ester (5). 4-amido-2-hydroxybutyric acid (133 mg, 1.0 mmol)¹³ was measured into a 50 mL round-bottomed flask. Methanol (20 mL) and toluene (4 mL) were added, followed by HCl (0.5 mL, 12 N). The solution was refluxed for 3 h, at which point the solvent was removed *in vacuo*. The residue was resuspended in acetone (5 mL) and filtered to remove the solids. The filtrate was reduced *in vacuo* to give a crude yield of 145 mg. This residue was purified by flash chromatography on silica (50% acetone in dichloromethane) to yield 57.2 mg (39%) of the desired product as a white crystalline solid (note: the product was very difficult to elute off the silica). ¹H NMR (300 MHz, acetone-d₆) δ 7.05 (bs, 1H), 6.56 (bs, 1H), 4.73 (bs, 1H), 4.49 (m, 1H), 3.68 (s, 3H), 2.54-2.69 (m, 2H). ¹³C NMR (75 MHz, acetone-d₆) δ 174.02, 172.52, 68.00, 51.56, 39.58.

4-amido-2-*tert*-butyldimethylsiloxybutyrate methyl ester (6). 4-amido-2-hydroxybutyrate methyl ester (54 mg, 0.37 mmol) was measured into a 1 dram vial. DMF (350 μ L) was added to dissolve the starting material, followed by TBSCl (76 mg, 0.50 mmol) and imidazole (56 mg, 0.82 mmol). The solution was stirred at room temperature for 1 h, at which point dichloromethane (3.5 mL) was added. After 5

minutes stirring, a white precipitate fell out and was removed by filtration through a silica plug. The filtrate was reduced *in vacuo* and purified by flash chromatography on silica (7% acetone in dichloromethane) to yield 87.3 mg (91%) 4-amido-2-*tert*-butyldimethylsiloxybutyrate methyl ester. ^1H NMR (300 MHz, acetone- d_6) δ 6.33 (bs, 1H), 6.16 (bs, 1H), 4.57 (m, 1H), 3.67 (s, 3H), 2.51-2.66 (m, 2H), 0.84 (s, 9H), 0.06 (s, 3H), 0.03 (s, 3H). ^{13}C NMR (75 MHz, acetone- d_6) δ 173.18, 172.44, 69.40, 52.39, 41.50, 25.81, 18.38, -4.89, -5.37. LRMS (ESI $^+$) calculated for $[\text{C}_{11}\text{H}_{24}\text{NO}_4\text{Si}]^+$ ($[\text{M}+\text{H}]^+$) 262.1, found 261.9.

4-amido-2-*tert*-butyldimethylsiloxybutyrate cyanomethyl ester 9 (and regioisomer 8). 4-amido-2-*tert*-butyldimethylsiloxybutyrate methyl ester (46 mg, 0.18 mmol) was measured into a 2 dram vial. Methanol (2 mL) was added, and the vial was cooled to 0 °C. Aqueous lithium hydroxide (0.89 mL, 0.2 N, 0.18 mmol) was added over a period of 1 h, and the solution was allowed to reach room temperature (note: at the end of the addition period, TLC indicated the cyclic imide as the dominant species in the reaction mixture). After 5 days stirring, the reaction mixture was flash-frozen and lyophilized to dryness. Chloroacetonitrile (2 mL) and DMF (2 mL) were then poured over the dry salt, which slowly dissolved under stirring and sonication. After 4 h stirring at room temperature, the solvent volume was concentrated to ca. 0.5 mL; dichloromethane (4 mL) was then added, and the solids were removed by filtration through a silica plug. The filtrate was then reduced *in vacuo* and purified by flash chromatography (20% acetone in dichloromethane) to yield 14.8 mg (30%) 4-amido-2-*tert*-butyldimethylsiloxybutyrate

cyanomethyl ester and 3.5 mg (7%) of the regioisomer 4-amido-3-*tert*-butyldimethylsiloxybutyrate cyanomethyl ester.

4-(N-triisopropylsilyl)-amido-2-*tert*-butyldimethylsiloxybutyrate methyl ester (11).

4-amido-2-*tert*-butyldimethylsiloxybutyrate methyl ester (522 mg, 2.0 mmol) was measured into a 25 mL round-bottomed flask. Dichloromethane (4 mL) was added, and the flask was cooled to -10 °C. 2,6-Lutidine (465 µL, 4.0 mmol) was added in one portion, followed by the dropwise addition of triisopropylsilyl triflate (645 µL, 2.4 mmol). After 1 h stirring at 0 °C, toluene (8 mL) was added, and the solids were removed by filtration. The filtrate was reduced *in vacuo* and purified by flash chromatography on silica (15% EtOAc in hexanes) to yield 733.9 mg (87.8%) 4-(N-triisopropylsilyl)-amido-2-*tert*-butyldimethylsiloxybutyrate methyl ester. ¹H NMR (300 MHz, CDCl₃) δ 5.67 (bs, 1H), 4.51-4.56 (m, 1H), 3.69 (s, 3H), 2.72 (d, 2H, *J* = 5.1 Hz), 1.17-1.31 (m, 3H), 1.02 (dd, 18H, *J* = 7.5, 2.4 Hz), 0.88 (s, 9H), 0.12 (s, 3H), 0.07 (s, 3H). ¹³C NMR (75 MHz, CDCl₃) δ 175.12, 172.97, 69.34, 52.35, 42.99, 25.83, 18.44, 18.38, 18.37, 11.54, -4.73, -5.43. LRMS (ESI⁺) calculated for [C₂₀H₄₄NO₄Si₂]⁺ ([M+H]⁺) 418.3, found 418.3.

4-(N-triisopropylsilyl)-amido-2-*tert*-butyldimethylsiloxybutyrate cyanomethyl ester (13).

Potassium trimethylsilenote (71 mg, 0.5 mmol) was measured into a 2 dram vial, and diethyl ether (2.5 mL) was added. A solution of 4-(N-triisopropylsilyl)-amido-2-*tert*-butyldimethylsiloxybutyrate methyl ester (209 mg, 0.5 mmol) in ether (2.5 mL) was then added dropwise to this stirred suspension at 0 °C. After 9 h the solvent was removed *in*

vacuo and DMF (2 mL) was added to dissolve the residue. Chloroacetonitrile (2 mL) was then added, and the vial was stirred at room temperature for 10 h; the solvent was then removed *in vacuo*, and the residue was purified by flash chromatography on silica (12% → 16% EtOAc in hexanes) to yield 74.2 mg (34%) 4-(N-triisopropylsilyl)-amido-2-*tert*-butyldimethylsiloxybutyrate cyanomethyl ester. ¹H NMR (300 MHz, CDCl₃) δ 5.29 (bs, 1H), 4.64-4.83 (m, 3H), 2.69-2.82 (m, 2H), 1.20-1.33 (m, 3H), 1.05 (d, 18H, *J* = 7.5 Hz), 0.90 (d, 9H, *J* = 1.5 Hz), 0.14 (d, 3H, *J* = 1.5 Hz), 0.10 (d, 3H, *J* = 1.5 Hz). ¹³C NMR (75 MHz, CDCl₃) δ 174.33, 171.29, 114.10, 69.03, 48.93, 42.94, 25.74, 18.33, 17.87, 11.45, -4.82, -5.36. HRMS (FAB⁺) calculated for [C₂₁H₄₃N₂O₄Si₂]⁺ ([M+H]⁺) 443.2761, found 443.2765.

4-(N-triisopropylsilyl)-amido-2-*tert*-butyldimethylsiloxybutyrate dCA ester (14). 4-(N-triisopropylsilyl)-amido-2-*tert*-butyldimethylsiloxybutyrate cyanomethyl (11 mg, 25 μmol) and dCA*2.4 TBA (6 mg, 4.8 μmol) were measured into a 1 dram vial. DMF (0.8 mL) was added, and the reaction was allowed to stir at room temperature for 6 h, at which point the reaction was quenched and purified by HPLC to yield 0.14 μmol (2.9%) 4-(N-triisopropylsilyl)-amido-2-*tert*-butyldimethylsiloxybutyrate dCA ester (a significant amount of free dCA was also present). LRMS (ESI⁻) calculated for [C₃₈H₆₄N₉O₁₆P₂Si₂]⁻ ([M-H]⁻) 1020.3, found 1020.5.

α-Hydroxy asparagine-dCA (1). 4-(N-triisopropylsilyl)-amido-2-*tert*-butyldimethylsiloxybutyrate dCA ester (0.14 μmol) in a 15 mL falcon tube was dissolved in water (0.3 mL), THF (0.3 mL), and AcOH (0.9 mL) and shaken at 37 °C for 42 h, at which point the

reaction was lyophilized to give 0.12 μmol (86%) α -Hydroxy asparagine-dCA. LRMS (ESI⁻) calculated for $[\text{C}_{23}\text{H}_{30}\text{N}_9\text{O}_{16}\text{P}_2]^-$ ($[\text{M}-\text{H}]^-$) 750.1, found 750.5.

4-(N-tert-butyl-diphenylsilyl)-amido-2-tert-butyl-dimethylsiloxybutyrate methyl ester.

4-amido-2-tert-butyl-dimethylsiloxybutyrate methyl ester (92.5 mg, 0.35 mmol) and dimethylaminopyridine (4 mg, 0.035 mmol) were measured into a 1 dram vial. Dichloromethane (0.7 mL) was added, followed by triethylamine (99 μL , 0.71 mmol). The vial was cooled to 0 °C and TBDPSCl (118 μL , 0.46 mmol) was added dropwise. After 7 h the solvent was removed *in vacuo*, and the residue was purified by flash chromatography on silica (12% \rightarrow 20% EtOAc in hexanes) to yield 125.3 mg (71%) 4-(N-tert-butyl-diphenylsilyl)-amido-2-tert-butyl-dimethylsiloxybutyrate methyl ester. ¹H NMR (300 MHz, CDCl₃) δ 7.63-7.70 (m, 4H), 7.34-7.42 (m, 6H), 6.32 (bs, 1H), 4.62 (m, 1H), 3.73 (s, 3H), 2.85 (m, 2H), 1.10 (s, 9H), 0.89 (s, 1H), 0.14 (s, 3H), 0.09 (s, 3H). ¹³C NMR (75 MHz, CDCl₃) δ 174.86, 173.06, 135.63, 135.57, 135.08, 132.82, 132.74, 129.89, 129.74, 127.96, 69.40, 52.47, 43.18, 27.85, 26.82, 25.88, 18.50, -4.67, -5.36. LRMS (ESI⁺) calculated for $[\text{C}_{27}\text{H}_{42}\text{NO}_4\text{Si}_2]^+$ ($[\text{M}+\text{H}]^+$) 500.3, found 500.4.

4-(N-tert-butyl-dimethylsilyl)-amido-2-tert-butyl-dimethylsiloxybutyrate methyl ester.

4-amido-2-tert-butyl-dimethylsiloxybutyrate methyl ester (45.6 mg, 0.18 mmol) and dimethylaminopyridine (2 mg, 0.018 mmol) were measured into a 2 dram vial. Dichloromethane (0.35 mL) and triethylamine (49 μL , 0.35 mmol) were added to dissolve the solids, and TBSCl (32 mg, 0.21 mmol) was then added. The reaction was stirred at room temperature for 90 minutes, then the solvent was removed *in vacuo*, and

the residue was purified by flash chromatography on silica (12% → 20% EtOAc in hexanes) to yield 43.3 mg (66%) 4-(N-*tert*-butyldimethylsilyl)-amido-2-*tert*-butyldimethylsilyloxybutyrate methyl ester. ¹H NMR (300 MHz, CDCl₃) δ 5.56 (bs, 1H), 4.54-4.60 (m, 1H), 3.70 (s, 3H), 2.57-2.74 (m, 2H), 0.89 (d, 18H), 0.20 (s, 3H), 0.18 (s, 3H), 0.11 (s, 3H), 0.08 (s, 3H). ¹³C NMR (75 MHz, CDCl₃) δ 175.22, 173.13, 69.54, 52.34, 43.58, 26.31, 25.86, 18.42, 17.30, -4.77, -4.88, -5.05, -5.36. LRMS (ESI⁺) calculated for [C₁₇H₃₈NO₄Si₂]⁺ ([M+H]⁺) 376.2, found 376.2.

4-amido-2-(*o*-nitroveratrylamino)-butyrate cyanomethyl ester (18). Compound **17** (103 mg, 0.28 mmol) was measured into a 2 dram vial. DMF (4 mL) was added, followed by chloroacetonitrile (1 mL) and TEA (60 μL, 0.43 mmol) was added in portions over 3 h at room temperature. The reaction was then poured over 0.5 N aq. HCl (75 mL) and extracted with 5 x 20 mL ethyl acetate. The organic extracts were concentrated *in vacuo* to ca. 5 mL, at which point the crystalline white product was isolated by filtration. Yield was 84 mg (74 %). HRMS (FAB⁺) calculated for [C₁₆H₁₉N₄O₉]⁺ ([M+H]⁺) 411.1152, found 411.1143.

4-(N-triisopropylsilyl)-amido-2-(*o*-nitroveratrylamino)-butyrate cyanomethyl ester (19). Compound **18** (20 mg, 0.05 mmol) was measured into a 2 dram vial and suspended in DCM (2 mL). Addition of TIPSOTf (18 μL, 0.07 mmol), followed by slow addition of lutidine (8 μL, 0.07 mmol), caused the starting material to dissolve within 30 min. The reaction mixture was then reduced *in vacuo* and purified by chromatography (silica, acetone) to give 18.9 mg (68 %) of a white crystalline solid. ¹H NMR (300 MHz,

acetone- d_6) δ 7.73 (s, 1H), 7.23 (s, 1H), 6.99 (d, 1H, $J = 8.7$ Hz), 6.39 (s, 1H), 5.40-5.56 (m, 2H), 4.98 (m, 2H), 4.66-4.76 (m, 1H), 3.98 (s, 3H), 3.95 (s, 3H), 2.89-3.11 (m, 2H), 1.22-1.37 (m, 3H), 1.07 (d, 18H). ^{13}C NMR (75 MHz, acetone- d_6) δ 176.33, 171.55, 156.54, 155.02, 149.27, 129.21, 115.79, 110.87, 109.01, 64.03, 56.83, 56.65, 51.81, 50.23, 39.36, 18.29, 12.31, -4.48. HRMS (FAB $^+$) calculated for $[\text{C}_{25}\text{H}_{39}\text{N}_4\text{O}_9\text{Si}]^+$ ($[\text{M}+\text{H}]^+$) 567.2486, found 567.2503.

References

¹ We have published portions of this work previously: An Intersubunit Hydrogen Bond in the Nicotinic Acetylcholine Receptor that Contributes to Channel Gating, K. R. Gleitsman, S. M. A. Kedrowski, H. A. Lester and D. A. Dougherty, *J. Biol. Chem.*, **2008**, *283*, 35638-35643.

² (a) Ellman, J., Mendel, D., Anthonycahill, S., Noren, C.J. and Schultz, P.G., Biosynthetic Method for Introducing Unnatural Amino-Acids Site-Specifically into Proteins, *Methods in Enzymology*, **1991**, *202*, 301-336. (b) In Vivo Incorporation of Unnatural Amino Acids into Ion Channels in a *Xenopus* Oocyte Expression System. M. W. Nowak, J. P. Gallivan, S. K. Silverman, C. G. Labarca, D. A. Dougherty, and H. A. Lester, in *Methods in Enzymology*, **1998**, *293*, *Ion Channels, Part B*, E. P. Conn, Ed., Academic Press: San Diego, pp. 504-529. (c) Nicotinic Receptor Binding Site Probed with Unnatural Amino-Acid Incorporation in Intact Cells. M. W. Nowak, P. C. Kearney, J. R. Sampson, M. E. Saks, C. G. Labarca, S. K. Silverman, W. Zhong, J. Thorson, J. N. Abelson, N. Davidson, P. G. Schultz, D. A. Dougherty, and H. A. Lester, *Science*, **1995**, *268*, 439-442.

³ (a) Chapman, E.; Thorson, J. S.; Schultz, P. G. *J. Am. Chem. Soc.* **1997**, *119*, 7151-7152. (b) Koh, J. T.; Cornish, V. W.; Schultz, P. G. *Biochemistry* **1997**, *36*, 11314-11322. (c) Wales, T. E.; Fitzgerald, M. C. *J. Am. Chem. Soc.* **2001**, *123*, 7709-7710.

⁴ See ref. 2a.

⁵ England, P.M., Lester, H.A. and Dougherty, D.A., Incorporation of esters into proteins: Improved synthesis of hydroxyacyl tRNAs, *Tetrahedron Letters*, **1999**, *40*, 6189-6192.

⁶ Deechongkit, S., You, S.L. and Kelly, J.W., Synthesis of all nineteen appropriately protected chiral alpha-hydroxy acid equivalents of the alpha-amino acids for Boc solidphase depsi-peptide synthesis, *Organic Letters*, **2004**, *6*, 497-500.

⁷ See ref. 5.

⁸ Rothman, D.M., Petersson, E.J., Vazquez, M.E., Brandt, G.S., Dougherty, D.A. and Imperiali, B., Caged phosphoproteins, *Journal of the American Chemical Society*, **2005**, *127*, 846-847.

⁹ An Examination of Structure-Reactivity Relationships. Ritchie, C. D.; Sager, W. F. *Prog. Phys. Org. Chem.* **1964**, *2*, 323.

¹⁰ Pangborn, A. B.; Giardello, M. A.; Grubbs, R. H.; Rosen, R. K.; Timmers, F. J. *Organometallics* **1996**, *15*, 1518-1520.

¹¹ Perrin, D. D.; Armarego, W. L. F. *Purification of Laboratory Chemicals*. 3rd Edition. Pergamon Press: Oxford, **1988**.

¹² Still, W. C.; Kahn, M.; Mitra, a. *Journal of Organic Chemistry* **1978**, *43*, 2923-2925.

¹³ See ref. 6.

Section 1: Chapter 4

Probing a Key Hydrogen Bond in the Nicotinic Acetylcholine Receptor through Mutant Cycle Analysis¹

Abstract: Though much is now known about the structure of the nicotinic acetylcholine receptor (nAChR) binding site, relatively little is understood about how the binding event is communicated to the channel gate, causing the pore to open. Here we use mutant cycle analysis with the novel unnatural residue α -hydroxyserine (Sah) to identify a key hydrogen bond near the binding site that is involved in the gating pathway. This hydrogen bond is between the backbone N-H of α S191 in loop C and the sidechain of γ D174/ δ D180—which had originally been identified as a key binding residue for cationic agonists.

The Cys-loop family of ligand-gated ion channels is involved in mediating fast synaptic transmission throughout the central and peripheral nervous systems.² These neuroreceptors are among the molecules of learning, memory, and sensory perception, and they are implicated in numerous neurological disorders, including Alzheimer's disease, Parkinson's disease, and schizophrenia. The muscle nicotinic acetylcholine receptor (nAChR) is arguably the best-studied member of the Cys-loop family. This heteropentameric receptor is composed of homologous, but functionally distinct, subunits arranged symmetrically around a central ion-conducting pore with the stoichiometry $\alpha_2\beta\gamma\delta$. The agonist binding sites are located at the interfaces between the $\alpha:\gamma$ and $\alpha:\delta$ subunits. The binding of two agonist molecules induces a conformational change that leads to the opening of the ion channel.

It is now widely appreciated that a tryptophan residue (α W149) plays a key role in neurotransmitter binding by forming a cation- π interaction with the quaternary ammonium group of acetylcholine,³ a result supported by structural data. However, many

other important residues in the immediate vicinity of the binding site have been identified. In a classic experiment on the *Torpedo* nAChR (a close homologue of the muscle subtype), Czajkowski and Karlin concluded that an aspartate (γ D174/ δ D180) from the complementary binding subunit could come within 9 Å of the agonist binding site.⁴ Mutation of this residue severely impacted receptor function, leading to a proposal that the negative charge of this aspartate interacted with the positive charge of the agonist.⁵ Subsequently, however, both the crystal structure of acetylcholine-binding protein (AChBP, a soluble protein homologous to the extracellular domain of the nAChR)⁶ and the 4 Å cryo-EM structure of *Torpedo* nAChR⁷ showed that this residue is positioned quite far from the agonist binding site (Figure 4.1). Single-channel studies suggest that this residue is primarily important for ligand-induced channel gating rather than agonist binding.⁸

γ D174/ δ D180 is part of loop F, the most remote of the six loops originally proposed by Changeux to contribute to the agonist binding site.⁹ In the carbamylcholine-bound AChBP structure,¹⁰ a different F loop anionic residue, γ E176/ δ E182 (AChBP E163), is positioned near loop C of the agonist binding site (Figure 4.1). Specifically,

γ E176/ δ E182 is within hydrogen bonding distance of the backbone N-H at α S191, which is located on the C loop between the aromatic binding box residue α Y190 and the vicinal

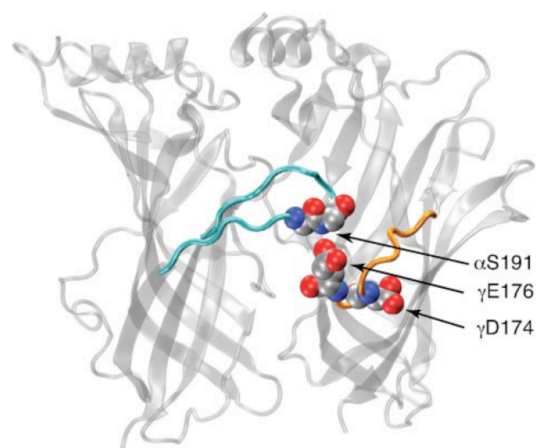


Figure 4.1. AChBP, carbamoylcholine-bound (1UV6). The C loop (cyan) and F loop (orange) are highlighted.

disulfide formed by α C192 and α C193. Loop F is generally disordered in the AChBP and nAChR structures, and hydrogen-deuterium exchange mass spectrometry on AChBP reveals that loop F and loop C are the most conformationally dynamic segments of the protein.¹¹ It is generally accepted that agonist binding draws loop C inward, capping the aromatic binding pocket.¹² In contrast, crystal structures of AChBP with antagonists bound reveal loop C pulled away from the agonist binding site. Distinctions between antagonist- and agonist-induced motions have also been observed in loop F.¹³ As such, many investigators favor a gating model involving a contraction of the agonist binding site around an agonist molecule that is largely mediated by movements in loops C and F, though little is known about the nature of the specific interactions involved in this systolic motion.

In the process of probing the backbone flexibility surrounding the nAChR binding box, we mutated α S191 to α -hydroxyserine (Sah). This produces an ester backbone linkage at this position, while preserving the side chain. Along with increasing backbone flexibility, this mutation removes the hydrogen bond-donating N-H group and replaces it

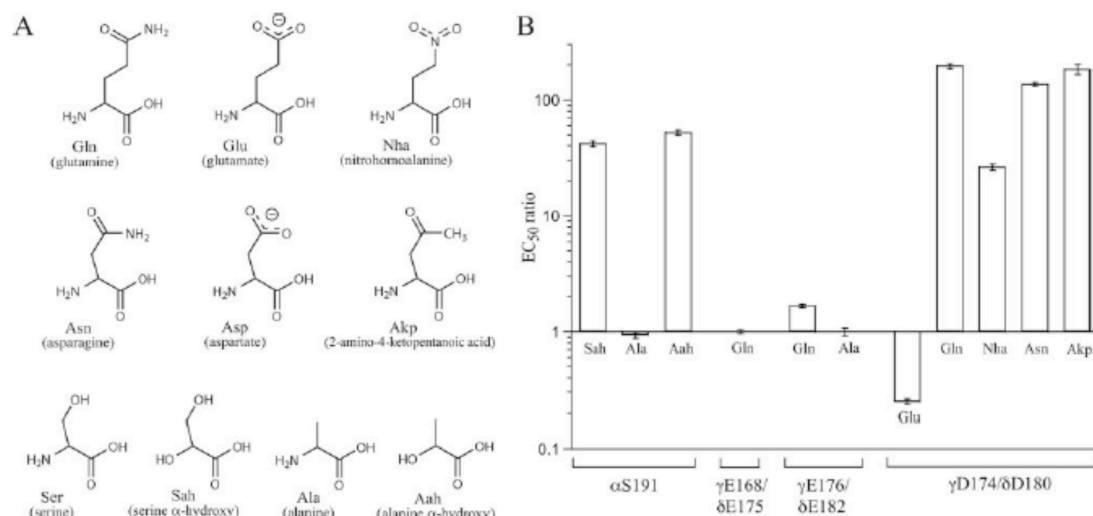


Figure 4.2. (a) Residues used in this study. (b) EC_{50} ratios (mutant/wild-type). For Gln and Nha, ratios were calculated relative to Glu rather than wild-type (Asp).

Table 4.1. Mutant EC₅₀ dataIn all cases, the β -subunit contains an L9'S mutation.

Mutant	EC ₅₀	Double mutant	EC ₅₀	$\Delta\Delta G$
	μM		μM	<i>kcal/mol</i>
$\alpha\beta\gamma\delta$	1.2 \pm 0.04			
$\alpha S191\beta\gamma\delta$ Sah	50 \pm 2.3			
$\alpha\beta\gamma E176A\delta E182A$	1.2 \pm 0.08	$\alpha S191Sah/\beta\gamma E176A/\delta E182A$	32 \pm 1.7	0.27 \pm 0.06
$\alpha\beta\gamma E176Q\delta E182Q$	2.0 \pm 0.10	$\alpha S191Sah/\beta\gamma E176Q/\delta E182Q$	51 \pm 2.4	0.29 \pm 0.03
$\alpha\beta\gamma E168Q\delta E175Q$	1.2 \pm 0.02	$\alpha S191Sah/\beta\gamma E168Q/\delta E175Q$	37 \pm 1.2	0.18 \pm 0.05
$\alpha\beta\gamma D174E\delta D180E$	0.3 \pm 0.01	$\alpha S191Sah/\beta\gamma D174E/\delta D180E$	15 \pm 0.90	0.12 \pm 0.05
$\alpha\beta\gamma D174Q\delta D180Q$	59 \pm 2.0	$\alpha S191Sah/\beta\gamma D174Q/\delta D180Q$	96 \pm 5.2	1.9 \pm 0.05
$\alpha\beta\gamma D174Nha\delta D180Nha$	7.9 \pm 0.40	$\alpha S191Sah/\beta\gamma D174Nha/\delta D180Nha$	31 \pm 1.9	1.4 \pm 0.05
$\alpha\beta\gamma D174N\delta D180N$	160 \pm 2.7	$\alpha S191Sah/\beta\gamma D174N\delta/D180N$	190 \pm 12	2.1 \pm 0.05
$\alpha\beta\gamma D174Akp\delta D180Akp$	220 \pm 19	$\alpha S191Sah/\beta\gamma D174Akp\delta/D180Akp$	190 \pm 12	2.3 \pm 0.15
$\alpha S191\beta\gamma\delta$ Ala	1.1 \pm 0.06	$\alpha S191Ala/\beta\gamma D174N\delta/D180N$	230 \pm 8.0	0.25 \pm 0.04
$\alpha S191\beta\gamma\delta$ Aah	63 \pm 2.4	$\alpha S191Aah/\beta\gamma D174N\delta/D180N$	130 \pm 7.6	2.5 \pm 0.04

with a non-hydrogen bond-donating O (Figure 4.2). We have performed similar backbone mutations at several positions in the nAChR, and typically the consequences are not dramatic.¹⁴ However, at $\alpha S191$, this subtle mutation leads to a 40-fold increase in EC₅₀ (Table 4.1). We also made alanine and α -hydroxyalanine (Aah) mutations at this site. The side chain mutation alone had minimal impact on receptor function, producing no shift in EC₅₀. However, receptor function of the $\alpha S191Aah$ mutant was dramatically impaired relative to $\alpha S191Ala$, confirming that the backbone—and not the side chain—at $\alpha S191$ is important for receptor function. We also made an analogous $\alpha Asn94Nah$ mutation at a site that is similarly adjacent to the binding box, and the EC₅₀ shift from wild type was minor.

To evaluate the potential hydrogen bond from $\alpha S191$ to $\gamma E176/\delta E182$, we made several mutations at this glutamate. Surprisingly, all mutations have minimal impact, suggesting no critical role for this residue. Another nearby loop F glutamate residue, $\gamma E169/\delta E175$, was also evaluated. Again, no significant impact was seen.

In sharp contrast, even the subtlest mutations at $\gamma D174/\delta D180$ produce large effects upon receptor function, a result that others have also seen.¹⁵ We first studied asparagine, glutamate, and glutamine mutations at this site. The $\gamma D174E/\delta D180E$ mutant

exhibits a modest ~threefold decrease in EC_{50} . However, the γ D174N/ δ D180N and γ D174Q/ δ D180Q mutants produce substantial (> 100-fold) changes to the EC_{50} .

Fundamentally, the results of these conventional mutations strongly implicate the side chain of γ D174/ δ D180 in an electrostatic interaction, such as an ion pair or hydrogen bond. However, changing the side chain functionality from a carboxylate to an amide not only neutralizes the charge on the side chain, it also desymmetrizes it and introduces a potential hydrogen bond donor. To better understand the role of γ D174/ δ D180, we incorporated two unnatural amino acids.

Nitrohomoalanine (Nha) is an analogue of glutamate that contains a nitro (NO_2) group, which is isosteric and isoelectronic to a carboxylate, but it has no charge and is a much weaker hydrogen bond acceptor (Figure 4.2a).¹⁶ Incorporation of Nha at γ D174/ δ D180 yields a slightly less dramatic effect than the γ D174N/ δ D180N and γ D174Q/ δ D180Q mutants, producing a 24-fold shift in EC_{50} relative to γ D174E/ δ D180E. Thus, charge neutralization at this site significantly affects receptor function but cannot fully account for the EC_{50} shift seen in the γ D174N/ δ D180N and γ D174Q/ δ D180Q mutants.

The second unnatural amino acid analogue incorporated at γ D174/ δ D180 was 2-amino-4-ketopentanoic acid (Akp). Akp is isoelectronic to Asp, but possesses a methyl ketone functionality in place of the carboxylate. As such, Akp is a desymmetrized analogue of Asp—similar to Asn—but it has different electrostatic properties (less polar, weaker hydrogen bond acceptor, and cannot donate a hydrogen bond). When Akp is incorporated at γ D174/ δ D180, its effect upon receptor function is roughly as deleterious as the Asn mutation. Mutations at individual binding sites ($\alpha_2\beta\gamma$ D174N δ and

$\alpha_2\beta\gamma\delta$ D180N) showed substantial (~50-fold) and approximately equivalent increases in whole cell EC_{50} .

Mutant cycle analyses were performed between several of the side chain mutations at γ D174/ δ D180 and the α S191Sah mutation (Figure 4.3). Briefly, mutant cycle analysis is used to determine the pairwise interaction energy between two residues in a protein using the equation given in

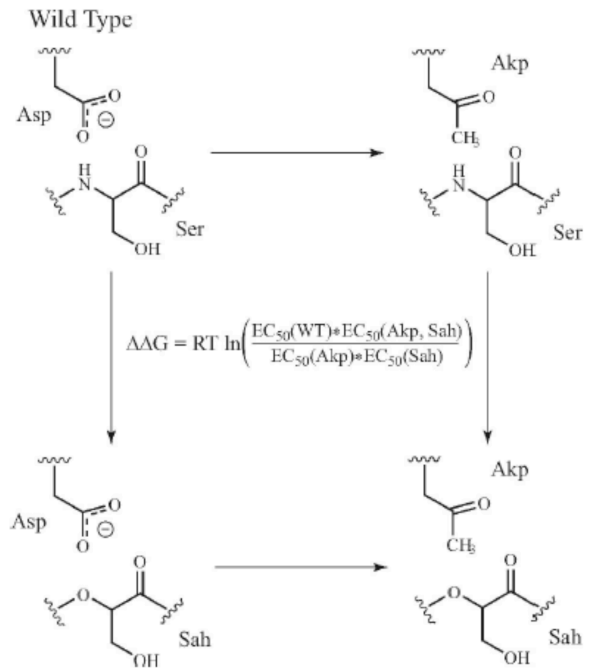


Figure 4.3. Mutant cycle analysis for α Ser191Sah and γ Asp174Akp/ δ Asp180Akp.

Figure 4.3. If the two residues do not interact, the change in free energy for the simultaneous mutation of both residues should simply be the sum of the free energy of each of the individual mutations. However, for residues that interact, the change in free energy for the double mutation will be non-additive. EC_{50} -based mutant cycle analysis

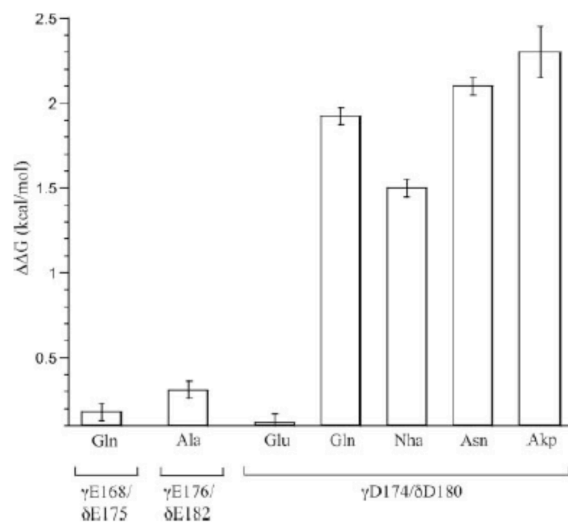


Figure 4.4. Mutant cycle coupling energies.

has been used to investigate interactions in Cys-loop receptors by other researchers.¹⁷

Lengthening the side chain (γ D174E/ δ D180E) has no impact on the interaction between these two residues ($\Delta\Delta G = 0.12$ kcal/mol; Figure 4.4). In contrast, mutant cycle analysis between

γ D174N/ δ D180N and α S191Sah indicates a large energetic coupling ($\Delta\Delta G = 2.1$ kcal/mol). A smaller but still quite significant effect is seen for the mutant cycle analysis between γ D174Nha/ δ D180Nha and α S191Sah ($\Delta\Delta G = 1.4$ kcal/mol). Mutant cycle analyses of γ D174N/ δ D180N with α S191A and α S191Aah further support the conclusion that the interaction between these residues involves the backbone of α S191 and not the side chain (α S191Ala: $\Delta\Delta G = 0.25$; α S191Aah: $\Delta\Delta G = 2.3$ kcal/mol). Comparable mutant cycle analyses of the two glutamates of loop F, γ E176/ δ E182 and γ E169/ δ E175, with α S191Sah showed no significant coupling.

The AChBP crystal structures transformed the study of nAChRs by providing high-resolution structural data about the ligand binding domain of these proteins. In addition to refining our existing structural knowledge of the receptor—obtained from decades of careful biochemical research—it served as a valuable starting point for new structure-function studies on the receptor. However, AChBP is not a ligand-gated ion channel and, in fact, shares less than 25% homology with its nearest Cys-loop relative, the $\alpha 7$ nAChR. As such, some fundamental structural differences presumably exist between AChBP and actual Cys-loop receptors, particularly pertaining to residues involved in mediating communication between the binding site and the ion channel pore.

Arguably the biggest discrepancy between the AChBP structures and prior biochemical studies of the nAChR concerns the loop F residue γ D174/ δ D180. A remarkable cross-linking study in the *Torpedo* nAChR indicated that this residue can come within 9 Å of the vicinal disulfide on the C loop, located at the heart of the agonist binding site.¹⁸ Yet, in AChBP the residue that aligns with γ D174/ δ D180 is not at all near

the agonist binding site. In addition, the cryo-EM structure of the *Torpedo* nAChR, which is believed to be in the desensitized or closed state, places this residue tucked deeply inside a β -sheet-lined hydrophobic pocket, over 15 Å from loop C.

While γ D174/ δ D180 is remote to the agonist binding site in AChBP, another loop F anionic residue, γ E176/ δ E182, appears to make a hydrogen bond to a backbone N-H that is integral to the aromatic box of the agonist binding site when the agonist carbamylcholine is bound. Using nonsense suppression methodology, we have been able to specifically remove the backbone N-H in question by replacing α S191 with its α -hydroxy analogue. Consistent with the AChBP images, this subtle structural change has a large effect on receptor function, suggesting that a hydrogen bond to this moiety is important. However, consistent with prior mutational analyses, we find that γ E176/ δ E182 does not play a large role in receptor function. This suggests that AChBP provides only an imperfect model of the muscle nAChR in this region. Given that the sequence alignment in this region shows a number of insertions in nAChR relative to AChBP—combined with the fact that the F loop is believed to be involved in gating the nAChR (AChBP does not gate)—it is not surprising that AChBP would be an unreliable model here.

Our results indicate that the hydrogen-bonding partner for the backbone N-H of α S191 in the nAChR is instead the side chain of γ D174/ δ D180. Based on the available structural and functional data, we suggest that this hydrogen bond exists in the open state only. As others have seen, a number of mutations of this side chain profoundly affect receptor function. Here we employ several relatively subtle mutations. The fact that substantial functional consequences are seen suggests a precise structural role for this

side chain in at least one state crucial for activating the channel. Furthermore, all mutations at γ D174/ δ D180 that significantly impact function also show strong coupling to the α S191Sah backbone mutation via mutant cycle analysis. The nature of the coupling is expected from the hydrogen bonding model: mutation at either site has a strong effect; however, once the α S191Sah mutation is introduced—removing any possible hydrogen bonding interaction—mutations at γ D174/ δ D180 have a *much* smaller impact. Interestingly, no specific role for the side chain of α S191 is found, as the α S191A mutant gives essentially wild-type behavior.¹⁹ However, when the alanine side chain is combined with the α -hydroxy backbone mutation, the same coupling to γ D174/ δ D180 is observed.

We propose that the movement of loop F of the complementary subunit from a position remote to the agonist binding site to one of close proximity to loop C of the principal subunit is a key early structural change associated with nAChR gating. Driving this structural reorganization is the formation of a hydrogen bond between the side chain of γ D174/ δ D180 and the backbone N-H of α S191. In the closed state of the wild-type receptor, α S191 and the C loop project out into solution, away from the bulk of the receptor, while γ D174/ δ D180 of the F loop projects deep within a hydrophobic cavity. Though the energetic desolvation penalty of burying a charged residue within a hydrophobic cavity is significant,²⁰ it alone is apparently not sufficient to overcome other structural elements that bias this conformation of the F loop. However, agonist binding induces a centripetal movement of the C loop, bringing the backbone N-H of α S191 in closer proximity to the F loop. This structural change makes possible a hydrogen bond between γ D174/ δ D180 and the C loop backbone. We hypothesize that the formation of

this hydrogen bond, along with the energetic solvation benefit of moving γ D174/ δ D180 into an aqueous environment, provides sufficient driving force to move γ D174/ δ D180 out of its pocket, inducing a movement of the F loop toward the C loop.²¹ This structural rearrangement of loop F contributes to the gating pathway. Using rate-equilibrium free energy relationships, Auerbach and coworkers have also concluded that γ D174/ δ D180 moves early in the gating process.²²

Our results provide an explanation for the cross-linking studies of Czajkowski and Karlin,²³ and they are not in conflict with available structural information. Though the cryo-EM images of the *Torpedo* receptor show greater than 20 Å separation between α S191 and γ D174/ δ D180 in the closed state, the distance of less than 9 Å that is suggested by the crosslinking studies is still plausible, provided that the residues are free to move closer. A comparison of AChBP structures with and without agonist bound likewise shows that motions of loops C and F are the dominant structural rearrangements that occur when agonist binds. The fact that the hydrogen bond acceptor in loop F differs between AChBP and nAChR is not surprising, given that loop F is strongly implicated in nAChR gating and AChBP did not evolve to have a gating function.

This model is also consistent with the γ 174/ δ 180 mutants described here. Lengthening the sidechain of this key F loop residue (γ D174E/ δ D180E) effects a modest improvement in receptor function, either because the longer sidechain can more easily reach its α S191 hydrogen bonding partner, or because it fits more poorly in the hydrophobic pocket, destabilizing the closed state. Any mutation that eliminates side chain charge has a significant impact on function, which is expected, given that these mutant side chains are poorer hydrogen bond acceptors and that they experience a much

lower energetic solvation benefit upon moving from the hydrophobic pocket into an aqueous environment.

In conclusion, mutant cycle analysis involving a novel backbone mutant has identified an important interaction between an F loop residue that has long been thought to contribute to receptor function and the peptide backbone of loop C. The hydrogen bond between the side chain of γ D174/ δ D180 and the backbone of α S191 likely forms upon agonist binding and is part of the agonist-induced conformational changes that lead to channel opening. Along with contributing new insights into the gating pathway of the nAChR, our results reconcile a long-standing discrepancy between early biochemical studies of the receptor and structural models from the AChBP systems.

Biology—Mutagenesis

Conventional mutagenesis and unnatural mutagenesis, with the site of interest mutated to either an amber stop codon or a four-base frameshift codon (at α S191), were achieved by a standard Stratagene QuikChange protocol. Sequencing through both strands confirmed the presence of the desired mutation. Mouse muscle embryonic nAChR in the pAMV vector was used. All the mutations were made in the presence of a background transmembrane mutation (β L9'S) that lowers whole-cell EC_{50} .²⁴ In addition, the α -subunits contain an HA epitope in the M3-M4 cytoplasmic loop for Western blot studies. Control experiments show that this epitope does not detectably alter EC_{50} . mRNA was prepared by *in vitro* runoff transcription using the Ambion (Austin, TX) T7 mMessage mMachine kit. For conventional mutants, a total of 2.0-4.0 ng of mRNA was injected in a ratio of 2:1:1:1 of α : β : γ : δ . For suppression with unnatural amino and hydroxy acids, a total of 4.0 ng of mRNA was injected in an α : β : γ : δ subunit ratio of 10:1:1:1. Typically, 25 ng of tRNA was injected per oocyte along with mRNA in a ratio of 1:1 with a total volume of 50 nL/cell. As a negative control for suppression, truncated 74-nucleotide tRNA or truncated tRNA ligated to dCA was co-injected with mRNA in the same manner as fully charged tRNA. Data from experiments where currents from these negative controls were greater than 10% of the experimental were excluded. Frameshift suppression at α S191 was used for simultaneous incorporation of two unnatural residues.²⁵

Biology—Electrophysiology

The function of mutant receptors was evaluated using two-electrode voltage clamp. Stage V-VI oocytes of *Xenopus laevis* were employed. Oocyte recordings were made 12-48 h postinjection in two-electrode voltage clamp mode using the OpusXpress 6000A instrument (Axon Instruments, Union City, CA). Oocytes were superfused with a Ca²⁺-free ND96 solution at flow rates of 1 mL/min before application, 4 mL/min during drug application, and 3 mL/min during wash. Holding potential was -60 mV. Data were sampled at 125 Hz and filtered at 50 Hz. Drug applications were 15 s in duration. Acetylcholine chloride was purchased from Sigma/Aldrich/RBI. Solutions ranging from 0.01 mM to 5000 mM were prepared in Ca²⁺-free ND96 from a 1 M stock solution. Dose-response data were obtained for a minimum of 8 concentrations of agonists and for a minimum of five cells. Dose-response relations were fitted to the Hill equation to determine EC₅₀ and Hill coefficient values. The dose-response relations of individual oocytes were examined and used to determine outliers. The reported EC₅₀ values are from the curve fit of the averaged data.

References:

-
- ¹ We have published this work previously: An Intersubunit Hydrogen Bond in the Nicotinic Acetylcholine Receptor that Contributes to Channel Gating, K. R. Gleitsman, S. M. A. Kedrowski, H. A. Lester and D. A. Dougherty, *J. Biol. Chem*, **2008**, 283, 35638-35643.
- ² (a) Corringer, P. J., Le Novere, N., and Changeux, J. P. *Annu Rev Pharmacol Toxicol* **2000**, 40, 431-458. (b) Grutter, T., and Changeux, J. P. *Trends Biochem Sci*, **2001**, 26, 459-463. (c) Karlin, A. *Nat Rev Neurosci* **2002**, 3, 102-114.
- ³ Zhong, W., Gallivan, J. P., Zhang, Y., Li, L., Lester, H. A., and Dougherty, D. A. *Proc Natl Acad Sci U S A*, **1998**, 95, 12088-12093.
- ⁴ Czajkowski, C., and Karlin, A. *J Biol Chem*, **1991**, 266, 22603-22612.
- ⁵ (a) Czajkowski, C., and Karlin, A. *J Biol Chem*, **1995**, 270, 3160-3164. (b) Czajkowski, C., Kaufmann, C., and Karlin, A. *PNAS*, **1993**, 90, 6285-6289.
- ⁶ Brejc, K., van Dijk, W. J., Klaassen, R. V., Schuurmans, M., van Der Oost, J., Smit, A. B., and Sixma, T. K. *Nature*, **2001**, 411, 269-276.
- ⁷ (a) Miyazawa, A., Fujiyoshi, Y., Stowell, M., and Unwin, N. *J Mol Biol*, **1999**, 288, 765-786. (b) Unwin, N. *Journal of Molecular Biology*, **2005**, 346, 967-989.
- ⁸ (a) Akk, G., Zhou, M., and Auerbach, A. *Biophys J*, **1999**, 76, 207-218. (b) Sine, S. M., Shen, X. M., Wang, H. L., Ohno, K., Lee, W. Y., Tsujino, A., Brengmann, J., Bren, N., Vajsar, J., and Engel, A. G. *J Gen Physiol*, **2002**, 120, 483-496.
- ⁹ Corringer, P. J., Le Novere, N., and Changeux, J. P. *Annu Rev Pharmacol Toxicol*, **2000**, 40, 431-458.
- ¹⁰ Sixma, T. K., and Smit, A. B. *Annu Rev Biophys Biomol Struct*, **2003**, 32, 311-334.
- ¹¹ Shi, J., Koeppe, J. R., Komives, E. A., and Taylor, P. *J Biol Chem*, **2006**, 281, 12170-12177.
- ¹² Hansen, S. B., Sulzenbacher, G., Huxford, T., Marchot, P., Taylor, P., and Bourne, Y. *EMBO J*, **2005**, 24, 3635-3646.
- ¹³ Hibbs, R. E., Radic, Z., Taylor, P., and Johnson, D. A. *J Biol Chem*, **2006**, 281, 39708-39718.
- ¹⁴ England, P. M., Zhang, Y., Dougherty, D. A., and Lester, H. A. *Cell*, **1999**, 96, 89-98.

¹⁵ (a) Martin, M., Czajkowski, C., and Karlin, A. *J Biol Chem*, **1996**, 271, 13497-13503.

(b) Martin, M. D., and Karlin, A. *Biochemistry*, **1997**, 36, 10742-10750.

¹⁶ Although nitroalanine, the analogue of aspartate, would be ideal, it is not chemically compatible with the nonsense suppression methodology. Given that the mutation γ D174E/ δ D180E produces a very modest EC₅₀ shift and that γ D174N/ δ D180N and γ D174Q/ δ D180Q show similar effects on receptor function, the comparison of Nha to Glu can be considered meaningful.

¹⁷ (a) Kash, T. L., Jenkins, A., Kelley, J. C., Trudell, J. R., and Harrison, N. L. *Nature*, **2003**, 421, 272-275. (b) Price, K. L., Millen, K. S., and Lummis, S. C. *J Biol Chem*, **2007**, 282, 25623-25630. (c) Venkatachalan, S. P., and Czajkowski, C. *Proc Natl Acad Sci U S A*, **2008**.

¹⁸ Czajkowski, C., and Karlin, A. *J Biol Chem*, **1991**, 266, 22603-22612.

¹⁹ In AChBP structures, the α S191 side chain also makes hydrogen bonds to γ E176/ δ E182.

²⁰ Based on the hydrophobicity constant, π , the expected desolvation penalty for an aspartic acid residue would be on the order of \sim 1 kcal/mol (Eisenberg&McLachlan *Nature* **1986**, 319 (16), 199-203).

²¹ The possibility of a salt bridge forming here can be eliminated, given that there are no basic residues in the C loop or in its vicinity.

²² Grosman, C., Zhou, M., and Auerbach, A. *Nature*, **2000**, 403, 773-776.

²³ Czajkowski, C., and Karlin, A. *J Biol Chem*, **1991**, 266, 22603-22612.

²⁴ (a) Filatov, G. N., and White, M. M. *Mol Pharmacol*, **1995**, 48, 379-384. (b) Labarca, C., Nowak, M. W., Zhang, H., Tang, L., Deshpande, P., and Lester, H. A. *Nature*, **1995**, 376, 514-516.

²⁵ Rodriguez, E. A., Lester, H. A., and Dougherty, D. A. *Proc Natl Acad Sci U S A*, **2006**, 103, 8650-8655.

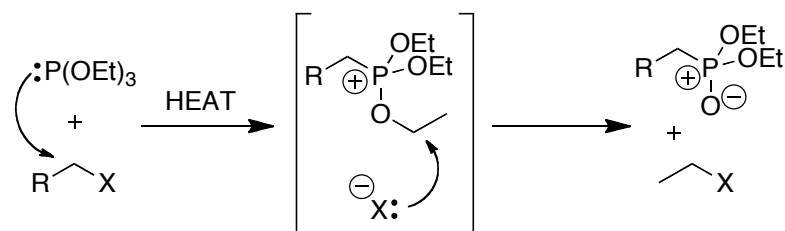
Section 2: Chapter 5

The Room Temperature Wolff-Kishner-Type Reductive Deoxygenation of Acyl Phosphonates: A One-Pot Transformation of Carboxylic Acids into Alkyl Phosphonates¹

Abstract: *The reductive deoxygenation of acyl phosphonates using a Wolff-Kishner-like sequence is described. This transformation allows direct access to alkyl phosphonates from acyl phosphonates at room temperature. The method can be combined with acyl phosphonate synthesis into a one-pot, four-step procedure for the conversion of carboxylic acids into alkyl phosphonates.*

Phosphonates are a key functional group in both organic synthesis and biological chemistry.² In synthesis, they are a direct precursor of olefins through the Horner-Wadsworth-Emmons reaction.³ In biological chemistry, their unique structure and charge distribution give them an important role in pharmaceuticals⁴ and phosphoester mimicry.⁵ Phosphonates have traditionally been accessed through the Arbuzov reaction:^{6,7} a double S_N2 process between an alkyl halide and a trialkylphosphite (Scheme 5.1), and this remains the most commonly employed route today. Notable exceptions include aryl/vinyl phosphonates,⁸ whose corresponding halides cannot readily participate in S_N2 reactions, and α-hydroxy/α-amino

phosphonates,⁹ whose corresponding halides are unstable.

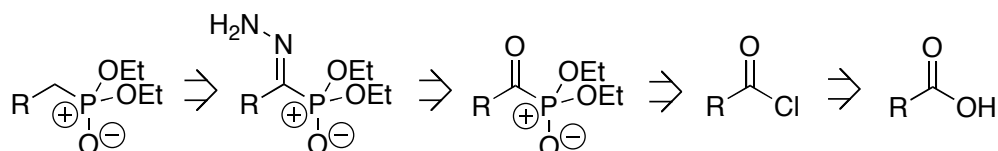


Despite its prevalence, the Arbuzov reaction has two key drawbacks. First, the elevated temperatures typically required limit the scope of substrates suitable for the reaction. Second, the reaction generates one equivalent of alkyl halide, which can react

with the phosphite under the reaction conditions to reduce yield and reaction efficiency. A modification using dialkylphosphite salts instead of trialkylphosphites eliminates the problem of new alkyl halide generation, but the yields are typically poorer, and this strategy is much less used.¹⁰ A number of other strategies for alkyl phosphonate synthesis have been developed,^{11,12} most notably the transition metal-mediated hydrophosphonylation of olefins with cyclic five-membered hydrogen phosphonates.¹³ Yet even this reaction is limited by the phosphite component scope and prolonged heating. Here we present a room-temperature alternative to the Arbuzov reaction that allows for the synthesis of phosphonates from carboxylic acids.

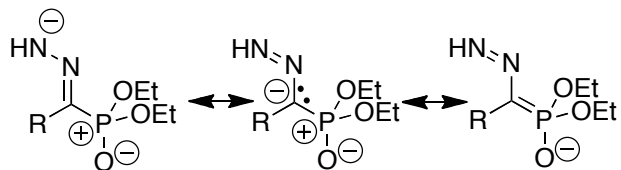
We began with the observation that the Arbuzov reaction of acyl halides is strikingly mild in comparison to the alkyl variant, often going to completion in several minutes at room temperature.¹⁴ Second, we noted that these acyl phosphonates can form isolable hydrazones,¹⁵ in contrast to most other carboxylic acid derivatives. This led us to consider the possibility that such acyl phosphonates could be deoxygenated through a Wolff-Kishner-type reduction to give alkyl phosphonates. Such a reaction would allow alkyl phosphonates to be readily accessed from carboxylic acid precursors (Scheme 5.2). At first glance such a proposal may seem unattractive, given that Wolff-Kishner conditions are quite harsh (the frequently-used Huang-Minlon modification calls for ethylene glycol and potassium hydroxide at 200 °C).^{16,17} However, we reasoned that the electron-withdrawing phosphonate group could stabilize the carbanionic character of the

Scheme 5.2. Retrosynthesis of phosphonates from carboxylic acids



presumed key intermediate (Scheme 5.3). The related transition state stabilization would allow this reaction variant to be much milder.

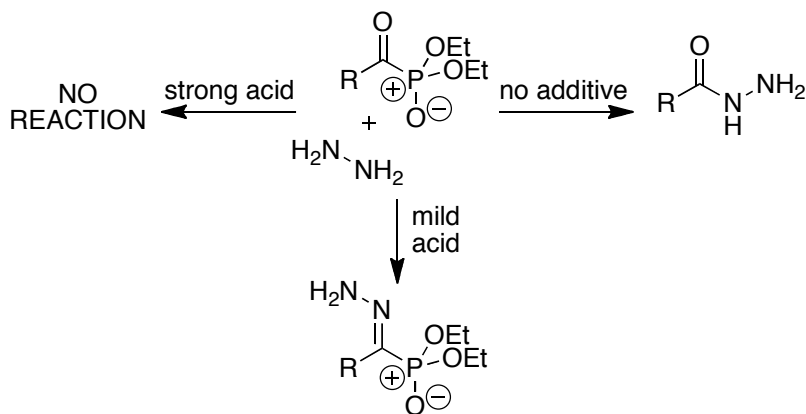
Scheme 5.3. Electron-withdrawing phosphonate stabilizes the key intermediate



To test this proposal, we synthesized the hydrazone of diethyl propionylphosphonate. Guided by several reports of low temperature (≤ 100 °C) Wolff-Kishner reductions,¹⁸ we slowly added the hydrazone to a rapidly stirring mixture of ten equivalents potassium *tert*-butoxide in dimethyl sulfoxide at room temperature. Pleasingly, a trace amount of diethyl propylphosphonate could be detected in the crude reaction mixture by ³¹P NMR. After exploring a variety of reaction conditions with the screening robot in the Caltech Center for Catalysis and Chemical Synthesis, we found that good ($\geq 70\%$) yields of diethyl propylphosphonate could be obtained at room temperature using potassium *tert*-butoxide in a 50% *v/v* tetrahydrofuran:*tert*-butanol solvent mixture.

We then turned our attention toward the hydrazone-formation step, seeking conditions that would allow the crude hydrazone to be used directly in the base-promoted

Scheme 5.4. Hydrazone formation is pH-dependent.



reduction step. Using propionyl phosphonate as the model substrate, we found that moderately acidic conditions worked best: strongly acidic

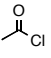
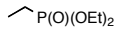
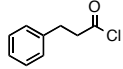
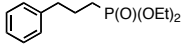
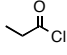
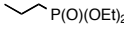
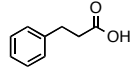
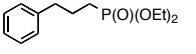
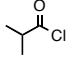
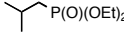
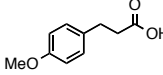
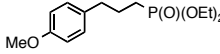
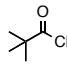
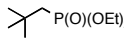
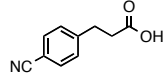
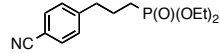
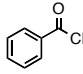
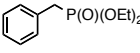
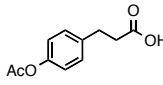
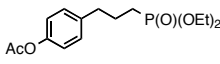
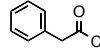
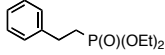
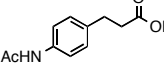
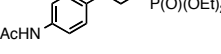
conditions led to no reaction, while pH-neutral and basic conditions led to decomposition of the starting material into propionyl hydrazide and diethylphosphite (Scheme 5.4). These observations are consistent with the trends observed in the formation of Schiff bases and related structures,¹⁹ except—in this case—higher pHs lead to decomposition rather than merely slower rates. The observed decomposition products are consistent with elimination of the phosphite from the presumed tetrahedral intermediate, indicating that the elimination of phosphite is favored under basic or neutral conditions, while the elimination of water is favored under acidic conditions.

We next sought to combine the hydrazone-formation and reduction steps. Since hydrazone formation is a reversible process, we anticipated that the direct addition of base to the water-containing hydrazone-formation reaction would lead to the same decomposition products observed previously (dialkylphosphite and propionyl hydrazide). This prediction was confirmed in practice under a variety of conditions. Similarly, when one equivalent of water was added to the reduction reaction of the purified hydrazone, the yield was dramatically reduced. Therefore, water must be removed from the hydrazone-forming reaction prior to its treatment with base. Adding desiccants to the reaction mixture (e.g., MgSO_4 , molecular sieves, etc.) gave low and inconsistent yields of the propyl phosphonate, even when the desiccant was filtered off prior to base addition. Evaporation of the liquid reactions under hi-vacuum failed to remove all the water, and the resultant oils gave poor yields of phosphonate when the reduction conditions were applied. However, when benzene was used as solvent in combination with a solid acid additive such as benzoic acid, the reaction mixture could be flash-frozen and placed under hi-vacuum to effectively remove all water, leaving behind a powdery solid matrix

of hydrazone and benzoic acid. Applying the reduction conditions to the residual lyophilized powder gave the phosphonate in consistently satisfactory yields.

Having arrived at a two-step, one-pot deoxygenation of propionyl phosphonate, we set out to explore the substrate scope of this transformation, only to realize that the starting acyl phosphonates could be purified only by distillation (in our hands, these compounds would not crystallize as solids, and they decomposed during chromatography). Fortunately, the “acyl-Arbuzov” reaction is quite clean, and the crude product can be used directly after the *in vacuo* removal of the volatile chloroethane, eliminating any possible side reactions involving this byproduct. This led us to a one-pot, three-step (or four-step, in cases where the acid chloride is formed *in situ*) sequence for the direct conversion of acid chlorides/carboxylic acids to diethyl phosphonates. The optimized sequence is as follows. First, the acid is treated with oxalyl chloride and catalytic dimethylformamide in dichloromethane. After removal of solvent and excess reagent *in vacuo*, the acid chloride is redissolved in dichloromethane and treated with one equivalent of triethylphosphite at 0 °C. Solvent and byproduct are again removed *in vacuo*; then, benzene and two molar equivalents benzoic acid are added to the residue. Dropwise addition of a slight molar excess of commercially available 1.0 M hydrazine in THF solution yields the hydrazone in several minutes. This solution is then lyophilized to give a finely dispersed solid mixture of benzoic acid and the hydrazone. The solid is then dissolved in 50% *v/v* tetrahydrofuran:*tert*-butanol and treated with three equivalents of 0.6 M potassium *tert*-butoxide in 50% *v/v* tetrahydrofuran:*tert*-butanol at room temperature. Solid potassium benzoate immediately precipitates, and typical reactions turn yellow in color; gas evolution can be observed immediately. The reaction is then

Table 5.1. Acyl Arbuzov-reductive deoxygenation reactions

				$\text{R}-\overset{\text{O}}{\parallel}{\text{C}}-\text{Cl}/\text{OH} \xrightarrow[\text{4) 3.0 equiv KOtBu}]{\begin{array}{l} \text{1) 1.2 equiv (COCl)}_2^{\text{a}} \\ \text{2) 1.0 equiv P(OEt)}_2 \\ \text{3) 1.05 equiv N}_2\text{H}_4, \text{ 2.0 equiv BzOH} \end{array}} \text{R}-\text{P(O)(OEt)}_2$			
entry	substrate	product	yield (%) ^b	entry	substrate	product	yield (%) ^b
1			58 (83)	7			74 (90)
2			74 (90)	8			69 (91)
3a 3b ^c			35 (70) 45 (77)	9			65 (90)
4			< 5	10			58 (87)
5a 5b ^d			21 (59) 30 (67)	11			< 5
6			65 (87)	12			< 5

(a) oxalyl chloride used where necessary; (b) number in parentheses represents per-step yield; (c) four equiv benzoic acid used in hydrazone formation; (d) two equiv o-bromobenzoic acid used.

quenched with water, washed with saturated sodium bicarbonate, and purified by flash column chromatography to yield the pure phosphonate.

This reaction works well for simple carboxylic acids, yielding $\geq 58\%$ for the sequence, corresponding to nearly 90% per step (Table 5.1). However, yields fall significantly for alpha-branched substrates (entries 3-5). NMR analysis of the reaction of isobutyryl chloride indicated that the acyl phosphonate is formed in high yield, but much of it decomposed to diethylphosphite and isobutyryl hydrazide during the hydrazone formation step. These are the same side products that we observed when trying to form the hydrazone of propionyl phosphonate under basic conditions (Scheme 5.4). Given that alpha branching leads to a more sterically crowded tetrahedral intermediate, we postulate that this steric crowding increases the effective nucleofugality of the bulky phosphite substituent relative to water. Having previously established that acid biases the

tetrahedral intermediate towards the elimination of water over phosphite, we performed the same reaction using slightly more acidic conditions. Consistent with our hypotheses, this adjustment led to a small improvement in yield but a much slower reaction (entry 3b). Benzoyl chloride also gave poor yields (entry 5). Alpha branching may contribute to the low yield, but there are likely some electronic factors also in play, as benzoyl phosphonate is much less reactive than other acyl phosphonates under the hydrazone-forming reaction conditions (reaction times are 100-1000-fold longer).

Functional groups such as ethers (entry 9) and nitriles (entry 10) are well tolerated by the reaction, while amides (entry 11) and esters (entry 12) give poor yields, presumably due to the reaction of the carboxyl group with the hydrazine. While there are thus some limitations to the scope of this reaction sequence, it compares favorably to the conventional Arbuzov reaction in many cases.

In conclusion, we have developed a one-pot protocol for the Wolff-Kishner type reductive deoxygenation of acyl phosphonates. We have further adapted this reaction to develop a one-pot sequence for the synthesis of alkyl phosphonates from carboxylic acids. We anticipate that this new reaction will offer a low-temperature alternative to the Arbuzov reaction for the synthesis of this important class of compounds.

Chemistry—General

All reactions were performed under argon using solvents that were dried and purified according to the method of Grubbs.²⁰ All flasks and vials were oven dried at 122 °C and cooled in a desiccator box containing anhydrous calcium sulfate. But for the exceptions listed here, commercial reagents were purified according to the methods compiled by Armengo and Perrin.²¹ Potassium *t*-butoxide, anhydrous *t*-butanol, and 1.0 M hydrazine in THF solution were used as purchased from Aldrich without further purification and stored under argon. Hydrocinnamic acids that could not be purchased were synthesized from the corresponding benzaldehyde according to a literature procedure.²² Reactions were monitored by thin-layer chromatography on Merck Siligel 60-F₂₅₄. Compounds were visualized with a UV lamp (254 nm) and stained with potassium permanganate solution. Column chromatography was carried out in accordance with the methods of Still²³ using EMD-Merck silica gel 60, 230-400 mesh ASTM. ¹H, ³¹P, and ¹³C NMR spectra were acquired on a Varian Mercury 300 MHz spectrometer. High-resolution mass spectrometry was performed on a JEOL JMS-600H HRMS using an Electrospray Ion Source. NMR spectra for the compounds synthesized here can be found in the supporting information of the original publication.¹

Chemistry—Synthesis

Diethyl ethylphosphonate (Table 5.1, entry 1). Acetyl chloride (72 μL , 1 mmol) was added to dichloromethane (8 mL) in a 25 mL round-bottomed flask and cooled on an icebath. Triethylphosphite (171 μL , 1 mmol) was then added dropwise to this chilled solution under stirring, then the reaction was allowed to come to room temperature. After two hours stirring, the reaction was reduced *in vacuo*, and benzoic acid (245 mg, 2 mmol) was added directly to the residue, followed by benzene (10 mL). The mixture was stirred to dissolve completely, then hydrazine solution (1.05 mL, 1.0 M in THF, 1.05 mmol) was added dropwise under rapid stirring. After 90 minutes, the reaction was flash-frozen and lyophilized. After lyophilization, 1:1 v/v tetrahydrofuran:*tert*-butanol (10 mL) was added to the flask and stirred to dissolve the solid. Potassium *tert*-butoxide solution (5 mL, 0.6 M in 1:1 v/v tetrahydrofuran:*tert*-butanol, 3 mmol) was then added to the stirring solution in one portion. After 6 h room temperature stirring, the reaction was diluted with ethyl acetate (50 mL), quenched with 1 N HCl (20 mL), washed with saturated sodium bicarbonate (2 x 15 mL), then with brine (15 mL), dried on sodium sulfate, reduced *in vacuo*, then purified by flash chromatography on silica (15% acetone in dichloromethane) to give the desired product as a colorless liquid; 97.0 mg (58.4%). ^1H NMR (300 MHz, CDCl_3) δ 3.98-4.12 (m, 4H), 1.62-1.68, (dq, 2H, $J = 18.2, 7.8$ Hz), 1.28 (t, 3H, $J = 7.1$ Hz), 1.11 (dt, 6H, $J = 20.0, 7.8$ Hz); ^{13}C NMR (75 MHz, CDCl_3) δ 61.4, 61.3, 19.7, 17.8, 16.4, 16.5, 6.5, 6.4; ^{31}P NMR (121 MHz, CDCl_3) δ 33.6; HRMS (FAB $^+$) calculated for $[\text{C}_6\text{H}_{16}\text{O}_3\text{P}]$ ($[\text{M}+\text{H}]^+$) 167.0837, found 167.0836.²⁴

Diethyl propylphosphonate. (Table 5.1, entry 2). Propionyl chloride (87 μL , 1 mmol) was added to dichloromethane (8 mL) in a 25 mL round-bottomed flask and cooled on an icebath. Triethylphosphite (171 μL , 1 mmol) was then added dropwise to this chilled solution under stirring, then the reaction was allowed to come to room temperature. After one hour stirring, the reaction was reduced *in vacuo*, and benzoic acid (245 mg, 2 mmol) was added directly to the residue, followed by benzene (10 mL). The mixture was stirred to dissolve completely, then hydrazine solution (1.05 mL, 1.0 M in THF, 1.05 mmol) was added dropwise under rapid stirring. After 60 minutes, the reaction was flash-frozen and lyophilized. After lyophilization, 1:1 v/v tetrahydrofuran:*tert*-butanol (10 mL) was added to the flask and stirred to dissolve the solid. Potassium *tert*-butoxide solution (5 mL, 0.6 M in 1:1 v/v tetrahydrofuran:*tert*-butanol, 3 mmol) was then added to the stirring solution in one portion. After 6 h room temperature stirring, the reaction was diluted with ethyl acetate (50 mL), quenched with 1 N HCl (20 mL), washed with saturated sodium bicarbonate (2 x 15 mL), then with brine (15 mL), dried on sodium sulfate, reduced *in vacuo*, then purified by flash chromatography on silica (10% acetone in dichloromethane) to give the desired product as a colorless liquid; 133.8 mg (74.3 %). ^1H NMR (300 MHz, CDCl_3) δ 3.93-4.11 (m, 4H), 1.48-1.70, (m, 4H), 1.25 (t, 6H, $J = 7.1$ Hz), 0.92-0.97 (m, 3H); ^{13}C NMR (75 MHz, CDCl_3) δ 61.3, 61.2, 28.6, 26.7, 16.4, 16.3, 16.1, 16.0, 15.3, 15.1; ^{31}P NMR (121 MHz, CDCl_3) δ 32.2; HRMS (FAB $^+$) calculated for $[\text{C}_7\text{H}_{18}\text{O}_3\text{P}]$ ($[\text{M}+\text{H}]^+$) 181.0994, found 181.1003.²⁵

Diethyl *sec*-butylphosphonate. (Table 5.1, entry 3b). 2-Methylpropionyl chloride (106 mg, 1 mmol) was added to dichloromethane (8 mL) in a 25 mL round-bottomed flask and

cooled on an icebath. Triethylphosphite (171 μL , 1 mmol) was then added dropwise to this chilled solution under stirring, then the reaction was allowed to come to room temperature. After one hour stirring, the reaction was reduced *in vacuo*, and benzoic acid (500 mg, 4 mmol) was added directly to the residue, followed by benzene (10 mL). The mixture was stirred to dissolve completely, then hydrazine solution (1.05 mL, 1.0 M in THF, 1.05 mmol) was added dropwise under rapid stirring. After 60 minutes, the reaction was flash-frozen and lyophilized. After lyophilization, 1:1 v/v tetrahydrofuran:*tert*-butanol (7 mL) was added to the flask and stirred to dissolve the solid. Potassium *tert*-butoxide solution (8 mL, 0.6 M in 1:1 v/v tetrahydrofuran:*tert*-butanol, 5 mmol) was then added to the stirring solution in one portion. After 12 h room temperature stirring, the reaction was diluted with ethyl acetate (50 mL), quenched with 1 N HCl (20 mL), washed with saturated sodium bicarbonate (2 x 15 mL), then with brine (15 mL), dried on sodium sulfate, reduced *in vacuo*, then purified by flash chromatography on silica (12% acetone in dichloromethane) to give the desired product as a colorless liquid; 88.5 mg (45.6 %). ^1H NMR (300 MHz, CDCl_3) δ 3.96-4.14 (m, 4H), 1.95-2.12 (m, 1H), 1.63 (dd, 2H, $J = 18.2, 6.8$ Hz), 1.28 (t, 6H, $J = 7.1$ Hz), 1.01 (dd, 6H $J = 6.7, 1.0$ Hz); ^{13}C NMR (75 MHz, CDCl_3) δ 61.2, 61.1, 35.4, 33.6, 24.1, 24.0, 23.7, 23.7, 16.5, 16.4; ^{31}P NMR (121 MHz, CDCl_3) δ 31.6; HRMS (FAB $^+$) calculated for $[\text{C}_8\text{H}_{20}\text{O}_3\text{P}]$ ($[\text{M}+\text{H}]^+$) 195.1150, found 195.1173.²⁶

Diethyl benzylphosphonate. (Table 5.1, entry 5b). Benzoyl chloride (117 μL , 1 mmol) was added to dichloromethane (8 mL) in a 25 mL round-bottomed flask and cooled on an icebath. Triethylphosphite (171 μL , 1 mmol) was then added dropwise to this chilled

solution under stirring, then the reaction was allowed to come to room temperature. After one hour stirring, the reaction was reduced *in vacuo*, and *ortho*-bromobenzoic acid (400 mg, 2 mmol) was added directly to the residue, followed by benzene (10 mL). The mixture was stirred, then hydrazine solution (1.05 mL, 1.0 M in THF, 1.05 mmol) was added dropwise under rapid stirring. After 6 hours, the reaction was flash-frozen and lyophilized. After lyophilization, 1:1 v/v tetrahydrofuran:*tert*-butanol (10 mL) was added to the flask and stirred to dissolve the solid. Potassium *tert*-butoxide solution (5 mL, 0.6 M in 1:1 v/v tetrahydrofuran:*tert*-butanol, 3 mmol) was then added to the stirring solution in one portion. After 4 h room temperature stirring, the reaction was diluted with ethyl acetate (50 mL), quenched with 1 N HCl (20 mL), washed with saturated sodium bicarbonate (2 x 15 mL), then with brine (15 mL), dried on sodium sulfate, reduced *in vacuo*, then purified by flash chromatography on silica (15% acetone in dichloromethane) to give the desired product as a colorless liquid; 68.6 mg (30.1 %). ¹H NMR (300 MHz, CDCl₃) δ 7.23-7.31 (m, 5H), 3.95-4.06 (m, 4H), 3.15 (d, 2H, *J* = 21.6 Hz), 1.24 (t, 6H, *J* = 7.1 Hz); ¹³C NMR (75 MHz, CDCl₃) δ 131.6, 131.6, 129.8, 129.7, 128.5, 128.5, 126.9, 126.8, 62.1, 62.1, 34.3, 33.2, 16.4, 16.3; ³¹P NMR (121 MHz, CDCl₃) δ 26.4; HRMS (FAB⁺) calculated for [C₁₁H₁₈O₃P] ([M+H]⁺) 229.0994, found 229.1005.²⁷

Diethyl 2-phenylethylphosphonate. (Table 5.1, entry 6). Phenylacetyl chloride (154 mg, 1 mmol) was added to dichloromethane (8 mL) in a 25 mL round-bottomed flask and cooled on an icebath. Triethylphosphite (171 μL, 1 mmol) was then added dropwise to this chilled solution under stirring, then the reaction was allowed to come to room temperature. After two hours stirring, the reaction was reduced *in vacuo*, and benzoic

acid (245 mg, 2 mmol) was added directly to the residue, followed by benzene (10 mL). The mixture was stirred to dissolve completely, then hydrazine solution (1.05 mL, 1.0 M in THF, 1.05 mmol) was added dropwise under rapid stirring. After 60 minutes, the reaction was flash-frozen and lyophilized. After lyophilization, 1:1 v/v tetrahydrofuran:*tert*-butanol (10 mL) was added to the flask and stirred to dissolve the solid. Potassium *tert*-butoxide solution (5 mL, 0.6 M in 1:1 v/v tetrahydrofuran:*tert*-butanol, 3 mmol) was then added to the stirring solution in one portion. After 6 h room temperature stirring, the reaction was diluted with ethyl acetate (50 mL), quenched with 1 N HCl (20 mL), washed with saturated sodium bicarbonate (2 x 15 mL), then with brine (15 mL), dried on sodium sulfate, reduced *in vacuo*, then purified by flash chromatography on silica (15% acetone in dichloromethane) to give the desired product as a yellow liquid; 158.1 mg (65.3 %). ¹H NMR (300 MHz, CDCl₃) δ 7.16-7.30 (m, 5H), 4.03-4.13 (m, 4H), 2.85-2.94 (m, 2H), 1.98-2.10 (m, 2H), 1.30 (t, 6H *J* = 7.0 Hz); ¹³C NMR (75 MHz, CDCl₃) δ 141.1, 140.8, 128.5, 128.0, 126.3, 61.6, 61.5, 28.6, 28.5, 28.5, 26.6, 16.5, 16.4; ³¹P NMR (121 MHz, CDCl₃) δ 30.8; HRMS (FAB⁺) calculated for [C₁₂H₂₀O₃P] ([M+H]⁺) 243.1150, found 243.1158.²⁷

Diethyl 3-phenylpropyl-1-phosphonate. (Table 5.1, entry 7). 3-Phenylpropionyl chloride (149 μL, 1 mmol) was added to dichloromethane (8 mL) in a 25 mL round-bottomed flask and cooled on an icebath. Triethylphosphite (171 μL, 1 mmol) was then added dropwise to this chilled solution under stirring, then the reaction was allowed to come to room temperature. After two hours stirring, the reaction was reduced *in vacuo*, and benzoic acid (245 mg, 2 mmol) was added directly to the residue, followed by

benzene (10 mL). The mixture was stirred to dissolve completely, then hydrazine solution (1.05 mL, 1.0 M in THF, 1.05 mmol) was added dropwise under rapid stirring. After 90 minutes, the reaction was flash-frozen and lyophilized. After lyophilization, 1:1 v/v tetrahydrofuran:*tert*-butanol (10 mL) was added to the flask and stirred to dissolve the solid. Potassium *tert*-butoxide solution (5 mL, 0.6 M in 1:1 v/v tetrahydrofuran:*tert*-butanol, 3 mmol) was then added to the stirring solution in one portion. After 6 h room temperature stirring, the reaction was diluted with ethyl acetate (50 mL), quenched with 1 N HCl (20 mL), washed with saturated sodium bicarbonate (2 x 15 mL), then with brine (15 mL), dried on sodium sulfate, reduced *in vacuo*, then purified by flash chromatography on silica (100% ethyl acetate) to give the desired product as a faintly yellow liquid; 189.0 mg (73.8 %). ¹H NMR (300 MHz, CDCl₃) δ 7.12-7.28 (m, 5H), 3.95-4.12 (m, 4H), 2.64-2.69 (t, 2H, *J* = 7.4 Hz), 1.84-1.97 (m, 2H), 1.64-1.75 (m, 2H), 1.27 (t, 6H *J* = 7.1 Hz); ¹³C NMR (75 MHz, CDCl₃) δ 141.0, 141.0, 128.4, 128.3, 126.0, 61.4, 61.3, 36.5, 36.3, 26.0, 24.2, 24.1, 24.1, 16.5, 16.4; ³¹P NMR (121 MHz, CDCl₃) δ 32.0; HRMS (FAB⁺) calculated for [C₁₃H₂₂O₃P] ([M+H]⁺) 257.1307, found 257.1302.²⁷

Diethyl 3-phenylpropyl-1-phosphonate. (Table 5.1, entry 8). 3-Phenylpropionic acid (150 mg, 1 mmol) was dissolved in dichloromethane (10 mL) in a 25 mL round-bottomed flask and cooled on an icebath. Oxalyl chloride (100 μL, 1.2 mmol) was added in one portion under stirring, and the reaction was allowed to come to room temperature. After 12 hours the reaction was reduced *in vacuo*, then the residue was redissolved in dichloromethane (8 mL) and cooled on an icebath. Triethylphosphite (171 μL, 1 mmol) was then added dropwise to this chilled solution under stirring, then the reaction was

allowed to come to room temperature. After two hours stirring, the reaction was reduced *in vacuo*, and benzoic acid (245 mg, 2 mmol) was added directly to the residue, followed by benzene (10 mL). The mixture was stirred to dissolve completely, then hydrazine solution (1.05 mL, 1.0 M in THF, 1.05 mmol) was added dropwise under rapid stirring. After 90 minutes, the reaction was flash-frozen and lyophilized. After lyophilization, 1:1 v/v tetrahydrofuran:*tert*-butanol (10 mL) was added to the flask and stirred to dissolve the solid. Potassium *tert*-butoxide solution (5 mL, 0.6 M in 1:1 v/v tetrahydrofuran:*tert*-butanol, 3 mmol) was then added to the stirring solution in one portion. After 6 h room temperature stirring, the reaction was diluted with ethyl acetate (50 mL), quenched with 1 N HCl (20 mL), washed with saturated sodium bicarbonate (2 x 15 mL), then with brine (15 mL), dried on sodium sulfate, reduced *in vacuo*, then purified by flash chromatography on silica (100% ethyl acetate) to give the desired product as a faintly yellow liquid; 177.0 mg (69.1 %). ¹H NMR (300 MHz, CDCl₃) δ 7.15-7.30 (m, 5H), 3.97-4.15 (m, 4H), 2.66-2.71 (t, 2H, *J* = 7.4 Hz), 1.84-1.99 (m, 2H), 1.66-1.78 (m, 2H), 1.29 (t, 6H *J* = 7.1 Hz); ¹³C NMR (75 MHz, CDCl₃) δ 141.0, 141.0, 128.5, 128.4, 126.0, 61.4, 61.3, 36.5, 36.3, 26.0, 24.2, 24.1, 16.5, 16.4; ³¹P NMR (121 MHz, CDCl₃) δ 32.0; HRMS (FAB⁺) calculated for [C₁₃H₂₂O₃P] ([M+H]⁺) 257.1307, found 257.1302.

Diethyl 3-(4-methoxyphenyl)propyl-1-phosphonate. (Table 5.1, entry 9). 3-(4-methoxyphenyl) propionic acid (180 mg, 1 mmol) was dissolved in dichloromethane (10 mL) in a 25 mL round-bottomed flask and cooled on an icebath. Oxalyl chloride (100 μL, 1.2 mmol) was added in one portion under stirring, and the reaction was allowed to come to room temperature. After 12 hours the reaction was reduced *in vacuo*, then the residue

was redissolved in dichloromethane (8 mL) and cooled on an icebath. Triethylphosphite (171 μ L, 1 mmol) was then added dropwise to this chilled solution under stirring, then the reaction was allowed to come to room temperature. After two hours stirring, the reaction was reduced *in vacuo*, and benzoic acid (245 mg, 2 mmol) was added directly to the residue, followed by benzene (10 mL). The mixture was stirred to dissolve completely, then hydrazine solution (1.05 mL, 1.0 M in THF, 1.05 mmol) was added dropwise under rapid stirring. After 90 minutes, the reaction was flash-frozen and lyophilized. After lyophilization, 1:1 v/v tetrahydrofuran:*tert*-butanol (10 mL) was added to the flask and stirred to dissolve the solid. Potassium *tert*-butoxide solution (5 mL, 0.6 M in 1:1 v/v tetrahydrofuran:*tert*-butanol, 3 mmol) was then added to the stirring solution in one portion. After 6 h room temperature stirring, the reaction was diluted with ethyl acetate (50 mL), quenched with 1 N HCl (20 mL), washed with saturated sodium bicarbonate (2 x 15 mL), then with brine (15 mL), dried on sodium sulfate, reduced *in vacuo*, then purified by flash chromatography on silica (100% ethyl acetate) to give the desired product as a faintly yellow liquid; 187.4 mg (65.5 %). ^1H NMR (300 MHz, CDCl_3) δ 7.03-7.06 (m, 2H), 6.77-6.80 (m 2H), 3.94-4.12 (m, 4H), 3.74 (s, 3H), 2.60 (t, 2H, $J = 7.4$ Hz), 1.79-1.93 (m, 2H), 1.62-1.75 (m, 2H), 1.27 (t, 6H $J = 7.1$ Hz); ^{13}C NMR (75 MHz, CDCl_3) δ 157.9, 133.1, 133.0, 129.3, 113.8, 61.4, 61.3, 55.2, 35.6, 35.4, 25.9, 24.3, 24.3, 24.0, 16.5, 16.4; ^{31}P NMR (121 MHz, CDCl_3) δ 32.2; HRMS (FAB $^+$) calculated for $[\text{C}_{14}\text{H}_{23}\text{O}_4\text{P}]$ ($[\text{M}+\text{H}]^+$) 286.1334, found 286.1342.

Diethyl 3-(4-cyanophenyl)propyl-1-phosphonate. (Table 5.1, entry 10). 3-(4-cyanophenyl) propionic acid (175 mg, 1 mmol) was dissolved in dichloromethane (10

mL) in a 25 mL round-bottomed flask and cooled on an icebath. A drop of dimethylformamide was added. Oxalyl chloride (100 μ L, 1.2 mmol) was added in one portion under stirring, and the reaction was allowed to come to room temperature. After 12 hours the reaction was reduced *in vacuo*, then the residue was redissolved in dichloromethane (8 mL) and cooled on an icebath. Triethylphosphite (171 μ L, 1 mmol) was then added dropwise to this chilled solution under stirring, then the reaction was allowed to come to room temperature. After two hours stirring, the reaction was reduced *in vacuo*, and benzoic acid (245 mg, 2 mmol) was added directly to the residue, followed by benzene (10 mL). The mixture was stirred to dissolve completely, then hydrazine solution (1.05 mL, 1.0 M in THF, 1.05 mmol) was added dropwise under rapid stirring. After 90 minutes, the reaction was flash-frozen and lyophilized. After lyophilization, 1:1 v/v tetrahydrofuran:*tert*-butanol (10 mL) was added to the flask and stirred. Potassium *tert*-butoxide solution (5 mL, 0.6 M in 1:1 v/v tetrahydrofuran:*tert*-butanol, 3 mmol) was then added to the stirring mixture in one portion. After 6 h room temperature stirring, the reaction was diluted with ethyl acetate (50 mL), quenched with 1 N HCl (20 mL), washed with saturated sodium bicarbonate (2 x 15 mL), then with brine (15 mL), dried on sodium sulfate, reduced *in vacuo*, then purified by flash chromatography on silica (20% acetone in dichloromethane) to give the desired product as a colorless liquid; 163.5 mg (58.2 %). ^1H NMR (300 MHz, CDCl_3) δ 7.51-7.55 (m, 2H), 7.23-7.27 (m 2H), 3.96-4.13 (m, 4H), 2.73 (t, 2H, $J = 7.5$ Hz), 1.83-1.97 (m, 2H), 1.63-1.74 (m, 2H), 1.27 (t, 6H $J = 7.1$ Hz); ^{13}C NMR (75 MHz, CDCl_3) δ 146.7, 132.2, 129.3, 118.9, 110.0, 61.6, 61.5, 36.5, 36.3, 25.9, 24.0, 23.8, 23.7, 16.5, 16.4; ^{31}P NMR (121 MHz, CDCl_3) δ 31.3; HRMS (FAB $^+$) calculated for $[\text{C}_{14}\text{H}_{21}\text{O}_3\text{NP}]$ ($[\text{M}+\text{H}]^+$) 282.1259, found 282.1262.

References

- ¹ We have published this work previously: Room-Temperature Alternative to the Arbuzov Reaction: The Reductive Deoxygenation of Acyl Phosphonates. Kedrowski, S. M. A.; Dougherty, D. A. *Organic Letters*, **2010**, 12(18), 3990–3993
- ² (a) Engel, R.; Cohen, J. I. *Synthesis of carbon-phosphorus bonds*; 2nd ed.; CRC Press: Boca Raton, FL, **2004**. (b) Savignac, P.; Iorga, B. *Modern phosphonate chemistry*; CRC Press: Boca Raton, FL, **2003**.
- ³ (a) Boutagy, J.; Thomas, R. *Chem. Rev.* **1974**, 74, 87. (b) Horner, L.; Hoffmann, H.; Wippel, H. G. *Chem. Ber.-Recl.* **1958**, 91, 61. (c) Horner, L.; Hoffmann, H.; Wippel, H. G.; Klahre, G. *Chem. Ber.-Recl.* **1959**, 92, 2499. (d) Wadsworth, W.; Emmons, W. D. *J. Am. Chem. Soc.* **1961**, 83, 1733.
- ⁴ (a) De Clercq, E. *Nat. Rev. Drug Discov.* **2002**, 1, 13. (b) De Clercq, E.; Holy, A. *Nat. Rev. Drug Discov.* **2005**, 4, 928. (c) Metcalf, W. W.; van der Donk, W. A. *Ann. Rev. Biochem.* **2009**, 78, 65. (d) Okuhara, M.; Goto, T. *Drugs Exp. Clin. Res.* **1981**, 7, 559. (e) Okuhara, M.; Kuroda, Y.; Goto, T.; Okamoto, M.; Terano, H.; Kohsaka, M.; Aoki, H.; Imanaka, H. *J. Antibiot.* **1980**, 33, 13. (f) White, A. K.; Metcalf, W. W. *Ann. Rev. Microbiol.* **2007**, 61, 379.
- ⁵ (a) Brandt, G. S. Ph.D. Dissertation, California Institute of Technology, Pasadena, CA, **2003**. (b) Chen, L.; Wu, L.; Otaka, A.; Smyth, M. S.; Roller, P. P.; Burke, T. R.; Denhertog, J.; Zhang, Z. Y. *Biochem. Biophys. Res. Commun.* **1995**, 216, 976. (c) Engel, R. *Chem. Rev.* **1977**, 77, 349. (d) Nieschalk, J.; Ohagan, D. *J. Chem. Soc., Chem. Commun.* **1995**, 719. (e) Oleksyszyn, J.; Powers, J. C. *In Proteolytic Enzymes: Serine and Cysteine Peptidases*; Academic Press Inc: San Diego, **1994**; 244, 423. (f) Panigrahi, K.; Eggen, M.; Maeng, J. H.; Shen, Q. R.; Berkowitz, D. B. *Chem. Biol.* **2009**, 16, 928 (g) Petersson, E. J. Ph.D Dissertation, California Institute of Technology, Pasadena, CA, **2005**. (h) Rothman, D. M.; Petersson, E. J.; Vazquez, M. E.; Brandt, G. S.; Dougherty, D. A.; Imperiali, B. *J. Am Chem Soc.* **2005**, 127, 846. (i) Zheng, W. P.; Schwarzer, D.; LeBeau, A.; Weller, J. L.; Klein, D. C.; Cole, P. A. *J. Biol. Chem.* **2005**, 280, 10462. (j) Zheng, W. P.; Zhang, Z. S.; Ganguly, S.; Weller, J. L.; Klein, D. C.; Cole, P. A. *Nat. Struct. Biol.* **2003**, 10, 1054.

⁶ Also known as the Michaelis-Arbuzov reaction.

⁷ (a) Arbuzov, A. *J. Russ. Phys. Chem. Soc.* **1906**, 38. (b) Arbuzow, B. A. *Pure Appl. Chem.* **1964**, 9, 307. (c) Bhattacharya, A. K.; Thyagarajan, G. *Chem. Rev.* **1981**, 81, 415. (d) Michaelis, A., Kaehne, R. *Chem. Ber.* **1898**, 31, 1048.

⁸ Aryl/vinyl phosphonates can be readily prepared by a variety of transition metal-mediated coupling reactions of the corresponding aryl/vinyl halides: (a) Gelman, D.; Jiang, L.; Buchwald, S. L. *Org. Lett.* **2003**, 13, 2315. (b) Hirao, T.; Masunaga, T.; Yamada, N.; Ohshiro, Y.; Agawa, T. *Bull. Chem. Soc. Jpn.* **1982**, 55, 909. (c) Kohler, M. C.; Sokol, J. G.; Stockland, R. A. *Tetrahedron Lett.* **2009**, 50, 457. (d) Schwan, A. L. *Chem. Soc. Rev.* **2004**, 33, 218. (e) Tavs, P. *Chem. Ber.-Recl.* **1970**, 103, 2428.

⁹ α -hydroxy/ α -amino phosphonates are typically prepared from dialkyl phosphites and the corresponding carbonyl/imine: (a) Gazizov, T. K.; Pyndyk, A. M.; Sudarev, Y. I.; Podobedov, V. B.; Kovalenko, V. I.; Pudovik, A. N. *B. Acad. Sci. USSR Ch.* **1978**, 27, 2319. (b) Pudovik, A. N.; Konovalova, I. V. *Synthesis-Stuttgart* **1979**, 81.

¹⁰ Michaelis, A.; Becker, T. H. *Chem. Ber.* **1897**, 30, 1003. See also ref. 1a, p. 7.

¹¹ (a) Chatterjee, A. K.; Choi, T.-L.; Grubbs, R. H. *Synlett* **2001**, 1034. (b) Inokawa, S.; Nakatsukasa, Y.; Horisaki, M.; Yamashita, M.; Yoshida, H.; Ogata, T. *Synthesis-Stuttgart* **1977**, 179. (c) Lee, K.; Wiemer, D. F. *J. Org. Chem.* **1991**, 56, 5556. (d) Maloney, K. M.; Chung, J. Y. L. *J. Org. Chem.* **2009**, 74, 7574. (e) Milburn, R. R.; McRae, K.; Chan, J.; Tedrow, J.; Larsen, R.; Faul, M. *Tetrahedron Lett.* **2009**, 50, 870. (f) Oshikawa, T.; Yamashita, M. *Bull. Chem. Soc. Jpn.* **1990**, 63, 2728. (g) Renard, P.-Y.; Vayron, P.; Leclerc, E.; Valleix, A.; Mioskowski, C. *Angew. Chem., Int. Ed.* **2003**, 42, 2389. (h) Suzuki, K.; Hashimoto, T.; Maeta, H.; Matsumoto, T. *Synlett* **1992**, 125. (i) Zheng, S.; Barlow, S.; Parker, T. C.; Marder, S. R. *Tetrahedron Lett.* **2003**, 44, 7989.

¹² (a) Deprele, S.; Montchamp, J.-L. *J. Org. Chem.* **2001**, 66, 6745. (b) Ganapathy, S.; Sekhar, B. B. V. S.; Cairns, S. M.; Akutagawa, K.; Bentrude, W. G. *J. Am. Chem. Soc.* **1999**, 121, 2085. (c) Stiles, A. R.; Vaughan, W. E.; Rust, F. F. *J. Am. Chem. Soc.* **1958**, 80, 714. (d) Tayama, O.; Nakano, A.; Iwahama, T.; Sakaguchi, S.; Ishii, Y. *J. Org. Chem.* **2004**, 69, 5494.

-
- ¹³ (a) Bravo-Altamirano, K.; Montchamp, J.-L. *Tetrahedron Lett.* **2007**, *48*, 5755. (b) Coudray, L.; Montchamp, J.-L. *Eur. J. Org. Chem.* **2008**, 3601. (c) Han, L.-B.; Mirzaei, F.; Zhao, C.-Q.; Tanaka, M. *J. Am. Chem. Soc.* **2000**, *122*, 5407. (d) Reichwein, J. F.; Patel, M. C.; Pagenkopf, B. L. *Org. Lett.* **2001**, *3*, 4303. (e) Xu, Q.; Han, L.-B. *Org. Lett.* **2006**, *8*, 2099.
- ¹⁴ Berlin, K. D.; Taylor, H. A. *J. Am. Chem. Soc.* **1964**, *86*, 3862. See also ref. 5b.
- ¹⁵ (a) Ben Akacha, A.; Barkallah, S.; Baccar, B. *Phosphorus, Sulfur Silicon Relat. Elem.* **1992**, *69*, 163. (b) Yuan, C. Y.; Chen, S. J.; Xie, R. Y.; Feng, H. Z.; Maier, L. *Phosphorus, Sulfur Silicon Relat. Elem.* **1995**, *106*, 115.
- ¹⁶ (a) Kishner, N. *J. Russ. Chem. Soc.* **1911**, 43. (b) Wolff, L. *Liebigs Ann. Chem.* **1912**, *394*, 23. (c) Wolff, L. *Liebigs Ann. Chem.* **1912**, *394*, 86.
- ¹⁷ (a) Minlon, H. *J. Am. Chem. Soc.* **1946**, *68*, 2487. (b) Minlon, H. *J. Am. Chem. Soc.* **1949**, *71*, 3301.
- ¹⁸ (a) Cram, D. J.; Sahyun, M. R. V.; Knox, G. R. *J. Am. Chem. Soc.* **1962**, *84*, 1734. (b) Furrow, M. E.; Myers, A. G. *J. Am. Chem. Soc.* **2004**, *126*, 5436. (c) Grundon, M. F.; Henbest, H. B.; Scott, M. D. *J. Chem. Soc.* **1963**, 1855.
- ¹⁹ (a) Anderson, B. M.; Jencks, W. P. *J. Am. Chem. Soc.* **1960**, *82*, 1773. (b) Cordes, E. H.; Jencks, W. P. *J. Am. Chem. Soc.* **1962**, *84*, 832. (c) Jencks, W. P. *J. Am. Chem. Soc.* **1959**, *81*, 475.
- ²⁰ Pangborn, A. B.; Giardello, M. A.; Grubbs, R. H.; Rosen, R. K.; Timmers, F. J. *Organometallics* **1996**, *15*, 1518-1520.
- ²¹ Armarego, W. L. F.; Perrin, D. D. *Purification of Laboratory Chemicals*, 3rd ed., **1988**, Pergamon Press
- ²² Compain, P.; Gore, J.; Vatele, J.-M. *Synthetic Communications* **1995**, *25(19)*, 3075
- ²³ Still, W. C.; Kahn, M.; Mitra, A. *Journal of Organic Chemistry* **1978**, *43(14)*, 2923
- ²⁴ Wnuk, S. F.; Bergolla, L. A.; Garcia, P. I. *Journal of Organic Chemistry* **2002**, *67*, 3065
- ²⁵ Characterization data matched those of a sample of the compound purchased from Aldrich
- ²⁶ Patois, C.; *Bulletin de la Societe Chimique de France* **1993**, *VI30(5)*, 630

²⁷ Takahashi, H.; Inagaki, S.; Yoshii, N.; Gao, F.; Nishihara, Y.; Takagi, K. *Journal of Organic Chemistry* **2009**, *74*, 2794

Section 2: Chapter 6

The Reductive Coupling of Aldehydes/Ketones with Dialkyl Phosphites: A Mild and Orthogonal Alternative to the Arbuzov Reaction

Abstract: A new method for the synthesis of phosphonates through the reductive coupling of aldehydes/ketones and dialkyl phosphites is described. The reaction proceeds through a mesitylenesulfonyl hydrazone intermediate and shows broad substrate scope and functional group tolerance. The method tolerates azides and benzyl halides, making it complementary to the Arbuzov reaction. The new method does not work for aliphatic aldehydes, but progress towards modifying the methodology to work for these substrates is presented.

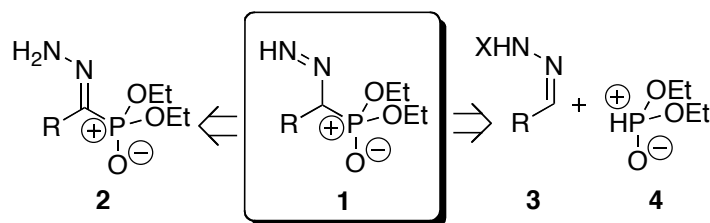
Chapter 5 presented a novel method for the conversion of carboxylic acids to phosphonates in a single pot, first by generating the acyl phosphonate through an Arbuzov-type mechanism, then by deoxygenating that intermediate using a Wolff-Kishner-type mechanism.¹ This route is mechanistically novel, but the use of strong acids and bases limits the functional group compatibility of the method, and the multiple rounds of reagent addition and solvent exchange diminish its attractiveness from a practical perspective. For these reasons it falls short of our goal of a methodology for phosphonate formation that is milder than and orthogonal to the conventional Arbuzov reaction.²

The acyl phosphonate deoxygenation method is presumed to proceed through diazene intermediate **1**, which rapidly decomposes into nitrogen gas and the desired product (Scheme 6.1). In the deoxygenation method, this intermediate is formed by the terminal deprotonation of hydrazone **2**; we rationalized that this intermediate may also be accessible through the nucleophilic addition of a dialkyl phosphite **4** into tosylhydrazone

3. If so, then a method could be envisioned in which aldehydes or ketones could be directly converted into phosphonates via combination with tosylhydrazide and a dialkyl phosphite.

The literature contains strong precedent for such a reductive coupling strategy. The Myers lab has developed a multistep strategy using a silyl-

Scheme 6.1. The key diazene **1** that presumably leads to product phosphonate could arise in multiple ways.



protected tosylhydrazone intermediate for the reductive coupling of aldehydes and organolithium compounds.³ Organic cyanides⁴ and tert-butyl ethers⁵ can also be accessed in a single operational step using this strategy. Bertz and Dabbaugh demonstrated the application of this strategy using phosphine oxides in a two-step process.⁶ Inokawa, et al. reported the route envisioned here: the reductive coupling of ketones with dialkylphosphites to give phosphonates using tosylhydrazone (Scheme 6.2).⁷ However, Inokawa's reported methodology suffers several key drawbacks. First, it uses three steps, requiring the isolation and purification of the hydrazone intermediate **3** and the hydrazone-phosphite tetrahedral adduct **5**. Second, the overall sequence takes at least a week. Third, the authors only present five substrates, and none contain any functionality other than the ketone that is undergoing reaction.

Scheme 6.2. Phosphonates from ketones according to the method of Inokawa.

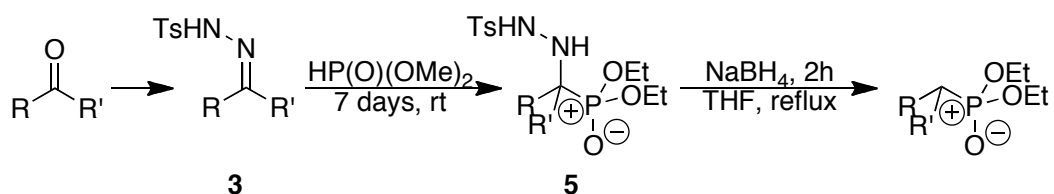
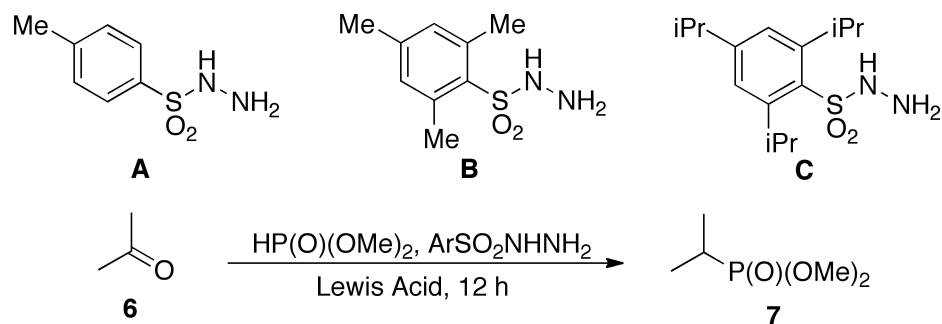


Table 6.1. Method development.

Lewis Acid	Hydrazide	Solvent	Temp.	Yield (GC %)
None	0.5 eq. A	MeCN	85 °C	< 5
10% $\text{BF}_3 \cdot \text{Et}_2\text{O}$	0.5 eq. A	MeCN	85 °C	10
10% Sc(OTf)_3	0.5 eq. A	MeCN	85 °C	49
10% Sc(OTf)_3	0.5 eq. B	MeCN	85 °C	66
10% Sc(OTf)_3	0.5 eq. C	MeCN	60 °C	54
10% Sc(OTf)_3	0.5 eq. B	MeCN	60 °C	66
2% Sc(OTf)_3	0.5 eq. B	MeCN	60 °C	65
2% Sc(OTf)_3	0.5 eq. B	Toluene	60 °C	> 95
2% Sc(OTf)_3	1.0 eq. B	Toluene	60 °C	> 95

Using acetone as a model substrate, we set out to develop a single-step protocol. Heating acetone, tosylhydrazide, and dimethylphosphite in a sealed vial at 85 °C for 12 hours in acetonitrile resulted in only trace product **7** (Table 6.1). Since addition of the phosphite into the hydrazone was the slowest step in the Inokawa protocol, we reasoned that the addition of a Lewis acid might accelerate this step by coordinating to the hydrazone and activating the electrophilic carbon toward attack from the phosphite. Upon screening, many Lewis acids offered improvement, but the best three were the trivalent trifluoromethanesulfonate salts of yttrium, scandium, and indium. These Lewis acids are

regarded as amongst the most azaphilic, lending support to the hypothesis that they function by coordinating to the hydrazone **3** to promote addition of the phosphite to form the tetrahedral adduct **5**.⁸

Other sulfonyl hydrazides were also screened. Mesitylenesulfonyl hydrazide consistently gave the best results of the commercially available sulfonyl hydrazides. The literature suggests that the bulkier mesitylene sulfinate is more reactive than the toluene sulfinate in the decomposition of the corresponding hydrazides and hydrazones.⁹ The bulkier 2,4,6-triisopropylbenzenesulfonyl hydrazide is known to be even more reactive in this regard, but its poor solubility under the reaction conditions may have led to the poorer results observed when it was screened. *o*-Nitrobenzenesulfonyl hydrazide led to much poorer results despite the reactivity trend; perhaps direct decomposition of this hydrazide under the reaction conditions becomes an issue.

Solvent, temperature, concentration, and stoichiometry were also screened. Noncoordinating solvents such as chloroform and toluene were shown to perform better than polar, coordinating solvents such as acetonitrile, dimethylsulfoxide, and tetrahydrofuran, perhaps because these solvents coordinate and sequester the Lewis acid catalyst. 60 °C was typically sufficient for the reactions to run to completion in 48 hours or less, while direct decomposition of the hydrazide became an issue at higher temperatures. For acetone and other ketone substrates, 1-2 mol% Lewis acid was typically sufficient, while benzaldehyde substrates benefitted from higher catalyst loadings: 10 mol% was typically sufficient. Pleasingly, superstoichiometric amounts of hydrazide relative to the aldehyde/ketone substrate provided little benefit to the yield, giving no need to add extra hydrazide, which could react with other functional groups in

Table 6.2. Reaction scope.

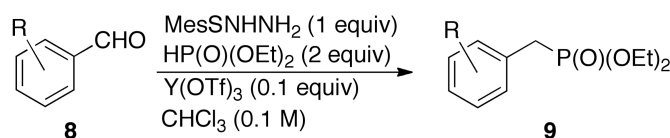
entry	substrate	product	yield (%)
1	 8a	 9a	89
2	 8b	 9b	60
3	 8c	 9c	59
4	 8d	 9d	71
5	 8e	 9e	66
6	 8f	 9f	60

a more complicated substrate. In contrast, optimized conditions require a one-equivalent excess of dialkyl phosphite, which fortunately (with respect to side reactions) is a much weaker nucleophile than mesitylenesulfonyl hydrazide. The excess phosphite—while often difficult to chromatographically separate from the product phosphonate—can be easily removed under high vacuum (in the case of dimethyl or diethyl phosphite). If the product phosphonate is also volatile, the phosphite can be selectively oxidized in the presence of the product phosphonate by treatment of the crude reaction product with

iodine in a water-methanol mixture at room temperature. The resulting phosphate diester monoanion can then be easily removed by extraction or chromatography. These optimized conditions yielded the desired phosphonate in yields > 95% by GC for the acetone test substrate.

In exploring the substrate scope, the reaction conditions proved to be tolerant of a wide range of functional groups (Table 6.2). Ethers (entry 1), amides, esters, cyanides, nitro compounds, benzyl chlorides (entry 4), benzyl bromides (entry 6), and azides (entries 2 & 3) all worked. In the case of benzaldehyde substrates, electron-rich substrates generally reacted faster and gave better yields than electron-poor substrates, but yields in excess of 50% could still be obtained for these substrates. The fact that nitro groups, azides, and benzyl halides are untouched by these reaction conditions is particularly exciting, because phosphonates containing these functional groups are not accessible through the Arbuzov reaction, illustrating the orthogonality of this new process (nitro compounds are reduced by trialkyl phosphites at high temperatures, though Arbuzov reactions can usually be run at a time/temperature where this is only a minor side-reaction).^{10,11}

Anilines and pyridines, which are incompatible with Arbuzov conditions due to their nucleophilic nitrogen, give poor yields under these conditions also (Table 6.3). When reactions using 4-dimethylaminobenzaldehyde and 4-formylpyridine were monitored by NMR, it was noted that the majority of the mass balance of the aldehyde substrate existed as the aldehyde, even after several hours of reaction. In contrast, only hydrazone was visible by ¹H NMR for other aldehyde substrates, even when the spectrum was taken just minutes after combining the reactants. To explore this further, one

Table 6.3. Additive screen for base-containing substrates

SUBSTRATE	YIELD (NMR)	TEMP	TIME	ADDITIVE I	ADDITIVE II
3,4-dimethoxy-	88%	60 °C	24 h		
4-dimethylamino-	0%	60 °C	24 h		
4-pyridinyl-	0%	60 °C	24 h		
3-pyridinyl-	0%	60 °C	24 h		
3,4-dimethoxy-	1%	80 °C	18 h	1 eq. pyridine	
3,4-dimethoxy-	63%	80 °C	18 h	1 eq. pyridine	1 eq. PTSA H2O
4-pyridinyl-	0%	80 °C	18 h	1 eq. PTSA H2O	
3,4-dimethoxy-	2%	80 °C	18 h	1 eq. pyridine	silica
3,4-dimethoxy-	1%	80 °C	18 h	1 eq. pyridine	MgSO4
3,4-dimethoxy-	23%	80 °C	18 h	1 eq. pyridine	TBSCl
3,4-dimethoxy-	1%	80 °C	18 h	1 eq. pyridine	mol. Sieves

equivalent of pyridine was added to the reaction of 3,4-dimethoxybenzaldehyde (**8a**). Extremely poor yields were obtained, and ¹H NMR showed a lot of unreacted aldehyde. Repeating the experiment with one equivalent of pyridine and one equivalent of *p*-toluenesulfonic acid led to nearly complete formation of the hydrazone in the first ten minutes of the reaction and a partial recovery of final phosphonate yield. These results suggest that the poor reactivity of the aniline- and pyridine-containing substrates arises from their basicity. In altering the protonation states of the species involved in hydrazone formation, base shifts the equilibrium toward the aldehyde and hydrazide, resulting in a much smaller pool of hydrazone to react productively.¹² If this is the case, Le Chatlier's Principle suggests that active removal of water from the reaction should also help to drive the reaction forward. Several desiccant additives were screened in the reaction 3,4-

dimethoxybenzaldehyde (**8a**) in the presence of one equivalent of pyridine, but they were all substantially less effective than one equivalent of strong acid.

Unfortunately, when 3-formylpyridine and 4-formylpyridine were subjected to the reaction conditions along with one equivalent of *p*-toluenesulfonic acid, very poor yields were obtained, perhaps because the resulting pyridinium substrate is so electron-poor. Further studies on these substrates were not performed due to time constraints, but these results suggest it might be possible to obtain good yields for substrates containing a pyridyl moiety, provided that an acid additive is used and that the reactive carbonyl is not adjacent to the ring.

Another substrate that gives low yields in this reaction is 4-methoxybenzaldehyde, which decomposes with the loss of methanol (methanol observed by ¹H NMR). This is strange, given that 3-methoxybenzaldehyde and 3,4-dimethoxybenzaldehyde both give good yields with no sign of methanol formation. Control reactions show that both hydrazide and phosphite are necessary for this decomposition. The mechanism of this decomposition is unclear, but the satisfactory reaction yields with 4-fluorobenzaldehyde (Table 6.2, entry 5) suggest that an S_NAr pathway is not at work.

For a number of substrates, the phosphonate yields seemed to plateau after 24-48 hours, even though some hydrazone remained (as judged by TLC). To explore this observation, the reaction of 4-bromomethylbenzaldehyde (**8f**) was monitored by ¹H and ³¹P NMR (Figure 6.1). Since hydrazone formation is very rapid and quantitative (within NMR detection limits), hydrazone was considered to be the starting material. Indeed, the rate of disappearance of hydrazone slowed late in the reaction, even more than would be

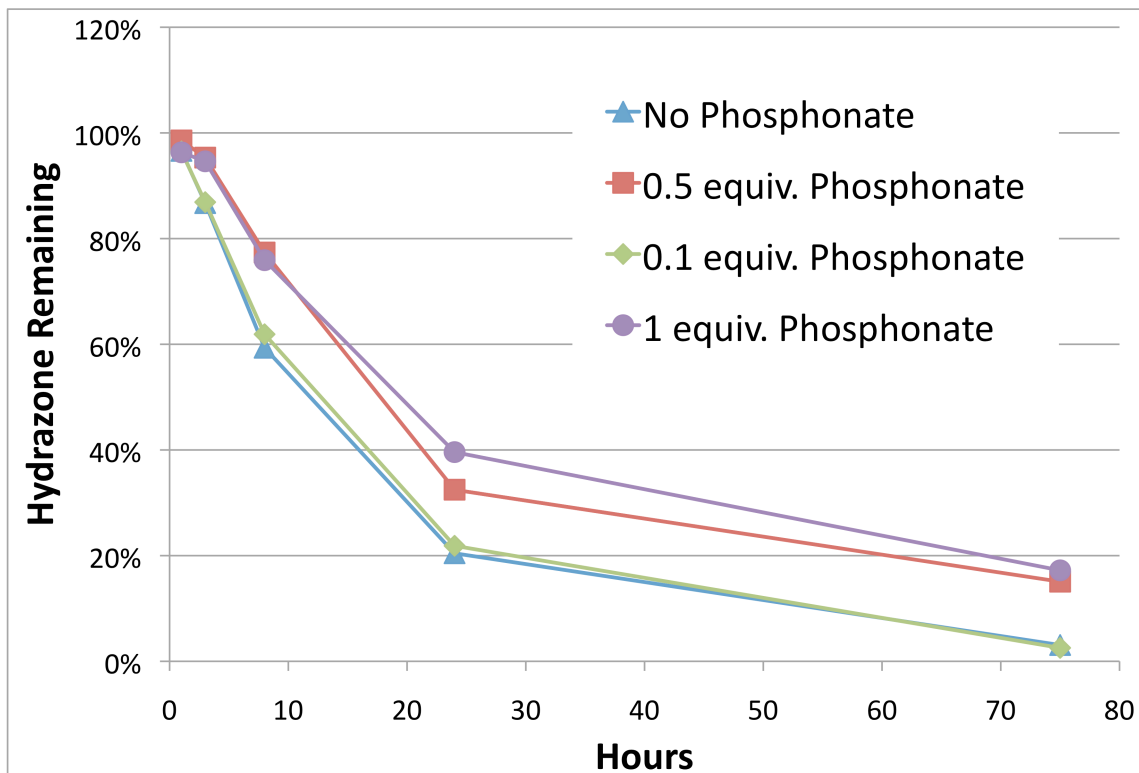


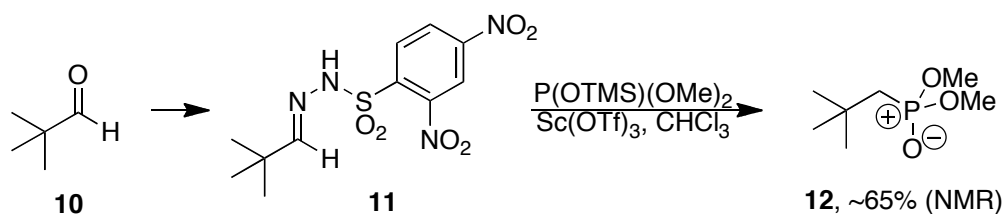
Figure 6.1. Effect of pre-added phosphonate on the rate of hydrazone consumption.

expected by first-order behavior. This remained the case even if extra phosphite was added after 12 hours. Since product inhibition can cause such a phenomenon, the experiment was repeated with varying proportions of phosphonate pre-added to the reaction. The reaction rate decreased as a function of pre-added phosphonate. These experiments were repeated using 3,4-methoxybenzaldehyde (**8a**) as substrate, and the results were similar, as the reaction had run to completion within eight hours under the standard conditions, but only two-thirds of the hydrazone had been consumed in that period of time when one equivalent of phosphonate had been pre-added. The reason for this product inhibition is unclear, but sequestration of the Lewis acid catalyst by the phosphonate product is one possible explanation.

Only poor phosphonate yields could be obtained for aliphatic aldehydes using the standard conditions, and most hydrazones did not crystallize readily. Pivaldehyde (**10**) was chosen as a model substrate to focus on because: the hydrazones could be crystallized; the NMR spectra have less splitting and are easier to interpret; and the sterically bulky neopentyl phosphonate **12** is difficult to access by the conventional Arbuzov reaction. Starting from pre-formed pivaldehyde tosylhydrazone, the tetrahedral adduct with dimethyl phosphite could be formed in several days at room temperature in benzene, but the reaction was significantly slower in other solvents. Heating the reaction actually led to lower conversion to the adduct, consistent with reports from Bertz and Dabbaugh claiming that heat drives the adduct-hydrazone equilibrium toward the hydrazone.¹³ Acid, base, and moderate heating were unable to convert it into the desired phosphonate product. Flash pyrolysis (250 °C) gave moderate yields of the phosphonate, but such conditions lacked the mildness and operational simplicity required for an attractive alternative to the Arbuzov reaction. (Unfortunately, this also made the GC useless as a tool for high-throughput screening of reaction conditions).

This reaction thus faced two problems: first, the adduct formation is too slow; second, adduct decomposition into the phosphonate is too slow. To address the first issue, dimethyl trimethylsilyl phosphite was tried as a more nucleophilic phosphite. Using this phosphite, adduct could be formed from the pivaldehyde tosylhydrazone within just

Scheme 6.3. Progress towards a method for synthesizing hindered phosphonates



several hours at room temperature. To address the second problem, it was reasoned that a hydrazide possessing a better arenesulfinate leaving group might be the answer. When pivaldehyde 2,4-dinitrobenzenesulfonylhydrazone (**11**) was combined with dimethyl trimethylsilyl phosphite in the presence of 10 mol% scandium triflate in chloroform, the desired dimethyl neopentyl phosphonate **12** formed in moderate yield in under a day at room temperature—an exciting result for such a sterically hindered substrate (Scheme 6.3). Unfortunately, this method could not be easily adapted to a single-step reaction starting from the aldehyde because the water generated in hydrazone formation readily decomposes the silyl phosphite. A quick screen of dessicant additives showed that a partial recovery of yields was possible, but a thorough examination of these conditions could not be done due to time constraints.

The first method described here works well for the direct conversion of ketones and with aromatic aldehydes into phosphonates. The methodology shows broad functional group tolerance and allows access to products that are inaccessible through the Arbuzov reaction. Significant progress towards adapting this method for aliphatic aldehydes was also achieved, and many avenues for exploration remain for developing such a method. For example, homogenous and heterogenous dessicants can be screened to remove water and enable the use of trimethylsilyl phosphites. Bulkier silyl phosphites (and other trisubstituted phosphites) can also be screened to see if they are less reactive toward water.

Chemistry—General

All reactions were performed under ambient air using untreated solvents unless otherwise noted. All flasks and vials were oven-dried at 122 °C and cooled in a desiccator box containing anhydrous calcium sulfate. Reagents were used as purchased without further purification. Phenylazide reactants were prepared by coupling the corresponding boronic acid with sodium azide.¹⁴ Reactions were monitored by thin-layer chromatography on Merck Siligel 60-F₂₅₄. Compounds were visualized with a UV lamp (254 nm) and stained with potassium permanganate solution. Column chromatography was carried out in accordance with the methods of Still¹⁵ using EMD-Merck silica gel 60, 230-400 mesh ASTM. ¹H, ³¹P, and ¹³C NMR spectra were acquired on a Varian Mercury 300 MHz spectrometer. High-resolution mass spectrometry was performed on a JEOL JMS-600H HRMS using an Electrospray Ion Source.

Chemistry—Synthesis

General Procedure, aldehyde-to-phosphonate reactions. Aldehyde (0.1 mmol), mesitylenesulfonyl hydrazide (21.4 mg, 0.1 mmol), and yttrium triflate (5.4 mg, 0.01 mmol) were measured into an oven-dried ½-dram vial with a disposable perylene stir-bar. Chloroform (1 mL) was added, and the vial was capped with a septum and stirred at room temperature for 10 minutes. Typically, the solids dissolved initially, but a small amount of precipitate appeared after several minutes. Diethyl phosphite (26 μ L, 0.2 mmol) was

then added, and the reaction was heated to 60 °C under stirring and monitored by TLC. Following the disappearance of the hydrazone (or if the rate of hydrazone disappearance has stalled), the reaction was filtered directly through a silica plug, eluting with 50% acetone in chloroform. This crude solution was then reduced *in vacuo* (often requiring 24 hours on the hi-vacuum pump to remove excess diethyl phosphite) and purified by flash chromatography on silica to give the desired product.

Diethyl 3,4-dimethoxybenzylphosphonate (9a). 8 hour reaction time. Chromatography using 15% acetone in dichloromethane; 25.5 mg (88.5%). ¹H NMR (300 MHz, CDCl₃) δ 6.78-6.86 (m, 3H), 3.9-4.1, (m, 4H), 3.87 (s, 3H), 3.85 (s, 3H), 3.08 (d, 2H, *J* = 21.2 Hz), 1.24 (t, 6H, *J* = 7.0 Hz); ¹³C NMR (126 MHz, CDCl₃) δ 148.82, 148.80, 148.00, 147.97, 123.88, 123.81, 121.93, 121.87, 112.91, 112.87, 111.19, 111.17, 62.09, 62.03, 55.85, 55.83, 33.75, 32.64, 16.44, 16.39; ³¹P NMR (121 MHz, CDCl₃) δ 26.70; HRMS (FAB⁺) calculated for [C₁₃H₂₂O₅P] ([M+H]⁺) 289.1205, found 289.1208.

Diethyl 4-azidobenzylphosphonate (9b). 36 hour reaction time. Chromatography using 10% acetone in dichloromethane; 16.1 mg (59.9%). ¹H NMR (300 MHz, CDCl₃) δ 7.29 (d, 2H, *J* = 8.5 Hz), 6.97 (d, 2H *J* = 7.8 Hz), 3.95-4.10 (m, 4H), 3.11 (d, 2H, *J* = 21.6 Hz) 1.24 (t, 6H, *J* = 7.0 Hz); ¹³C NMR (126 MHz, CDCl₃) δ 138.75, 131.12, 131.06, 128.38, 128.31, 119.15, 119.13, 62.18, 62.13, 33.71, 32.60, 16.41, 16.37; ³¹P NMR (121 MHz, CDCl₃) δ 25.95; HRMS (FAB⁺) calculated for [C₁₁H₁₇N₃O₃P] ([M+H]⁺) 270.1002, found 270.1009.

Diethyl 3-azidobenzylphosphonate (9c). 48 hour reaction time. Chromatography using 8% acetone in dichloromethane; 15.9 mg (59.1%). ^1H NMR (300 MHz, CDCl_3) δ 7.29 (t, 1H, $J = 7.7$ Hz), 7.08 (d, 1H $J = 7.6$ Hz), 6.89-6.98 (m, 2H), 3.97-4.09 (m, 4H), 3.12 (d, 2H, $J = 21.8$ Hz) 1.26 (t, 6H, $J = 7.0$ Hz); ^{13}C NMR (126 MHz, CDCl_3) δ 140.19, 133.76, 133.68, 129.85, 129.82, 126.41, 126.36, 120.30, 120.25, 117.60, 117.57, 62.24, 62.18, 34.19, 33.09, 16.41, 16.36; ^{31}P NMR (121 MHz, CDCl_3) δ 25.58; HRMS (FAB $^+$) calculated for $[\text{C}_{11}\text{H}_{17}\text{N}_3\text{O}_3\text{P}]$ ($[\text{M}+\text{H}]^+$) 270.1002, found 270.1014.

Diethyl 4-chloromethylbenzylphosphonate (9d). 24 hour reaction time. Chromatography using 10% acetone in dichloromethane; 19.6 mg (71.0%). ^1H NMR (300 MHz, CDCl_3) δ 7.25-7.35 (m, 4H), 4.56, (s, 2H), 3.95-4.10 (m, 4H), 3.16 (d, 2H, $J = 21.1$ Hz) 1.24 (t, 6H, $J = 7.0$ Hz); ^{13}C NMR (126 MHz, CDCl_3) δ 136.10, 131.97, 130.12, 130.08, 128.78, 62.21, 45.94, 34.27, 33.20, 16.40; ^{31}P NMR (121 MHz, CDCl_3) δ 25.97; HRMS (FAB $^+$) calculated for $[\text{C}_{12}\text{H}_{19}\text{ClO}_3\text{P}]$ ($[\text{M}+\text{H}]^+$) 277.0760, found 277.0769.

Diethyl 4-fluorobenzylphosphonate (9e). 48 hour reaction time. Chromatography using 7% acetone in dichloromethane; 16.2 mg (65.9%). ^1H NMR (300 MHz, CDCl_3) δ 7.22-7.30 (m, 2H), 6.99 (t, 2H $J = 8.6$ Hz), 3.94-4.08 (m, 4H), 3.11 (d, 2H, $J = 21.4$ Hz) 1.24 (t, 6H, $J = 7.0$ Hz); ^{13}C NMR (126 MHz, CDCl_3) δ 162.89, 162.86, 160.94, 160.91, 131.27, 131.22, 131.21, 131.16, 127.38, 127.35, 127.30, 127.28, 115.50, 115.48, 115.33, 115.31, 62.17, 62.12, 33.49, 32.38, 16.39, 16.35; ^{31}P NMR (121 MHz, CDCl_3) δ 26.09; ^{19}F NMR (282 MHz, CDCl_3) δ -116.02; HRMS (FAB $^+$) calculated for $[\text{C}_{11}\text{H}_{17}\text{FO}_3\text{P}]$ ($[\text{M}+\text{H}]^+$) 247.0894, found 287.0894.

Diethyl 4-bromomethylbenzylphosphonate (9f). 64 hour reaction time. Chromatography using 7% acetone in dichloromethane; 19.3 mg (60.1%). ^1H NMR (300 MHz, CDCl_3) δ 7.25-7.35 (m, 4H), 4.47, (s, 2H), 3.95-4.08 (m, 4H), 3.14 (d, 2H, $J = 21.7$ Hz) 1.24 (t, 6H, $J = 7.1$ Hz); ^{13}C NMR (126 MHz, CDCl_3) δ 136.41, 136.38, 132.08, 132.01, 130.19, 130.13, 129.25, 129.22, 62.19, 62.14, 34.11, 33.23, 33.03, 16.40, 16.35; ^{31}P NMR (121 MHz, CDCl_3) δ 25.93; HRMS (FAB $^+$) calculated for $[\text{C}_{12}\text{H}_{19}\text{BrO}_3\text{P}]$ ($[\text{M}+\text{H}]^+$) 321.0250, found 321.0241.

4-Chloromethylbenzaldehyde (8d). 4-Hydroxymethylbenzaldehyde¹⁶ (1.0 g, 7.3 mmol) was measured into a 25 mL round-bottomed flask with stirbar. Toluene (6 mL) and concentrated hydrochloric acid (6 mL) were added, and the mixture was rapidly stirred at reflux for 3 hours. The reaction was cooled and poured over ice (75 g) and extracted with ethyl acetate (3 x 25 mL). The organic layers were combined and washed with brine (20 mL), dried on magnesium sulfate, and reduced *in vacuo*. The residue was then purified by flash chromatography on silica (10% ethyl acetate in hexanes) to give a volatile white solid. 688 mg (61%). ^1H NMR (300 MHz, CDCl_3) δ 10.02 (s, 1H), 7.88 (d, 2H, $J = 8.3$ Hz), 7.57 (d, 2H, $J = 8.0$ Hz), 4.63 (s, 2H); ^{13}C NMR (126 MHz, CDCl_3) δ 191.56, 143.81, 136.18, 130.09, 129.09, 77.25, 77.00, 76.74, 45.23; HRMS (FAB $^+$) calculated for $[\text{C}_8\text{H}_7\text{OCl}]$ ($[\text{M}+\text{H}]^+$) 154.0185, found 154.0142.

4-Azidomethylbenzaldehyde. Sodium Azide (134 mg, 2.2 mmol) was measured into a 2 dram vial with stirbar. DMSO (5 mL) was added, and the mixture was allow to stir until

it dissolved (3 hours). 4-Chloromethylbenzaldehyde (309 mg, 2.0 mmol) was then added in one portion, and the reaction was allowed to stir at room temperature for 18 hours, at which point it was poured over ice-water (25 mL) and extracted with diethyl ether (4 x 20 mL). The organic layers were combined and washed with ice-water (3 x 10 mL), washed with brine (10 mL), dried on magnesium sulfate, and reduced *in vacuo* to give quantitative yield of a colorless oil. ^1H NMR (300 MHz, CDCl_3) δ 10.03 (s, 1H), 7.91 (d, 2H, $J = 8.2$ Hz), 7.50 (d, 2H, $J = 8.0$ Hz), 4.46 (s, 2H); ^{13}C NMR (126 MHz, CDCl_3) δ 191.65, 142.10, 136.15, 130.22, 128.48, 77.26, 77.01, 76.75, 54.27; HRMS (FAB $^+$) calculated for $[\text{C}_8\text{H}_7\text{N}_3\text{O}]$ ($[\text{M}+\text{H}]^+$) 161.0589, found 161.0593.

3-Chloromethylbenzaldehyde. Slightly impure 3-hydroxymethylbenzaldehyde¹⁷ (650 mg, ~4 mmol) was measured into a 25 mL round-bottomed flask with stirbar. Toluene (6 mL) and concentrated hydrochloric acid (6 mL) were added, and the mixture was rapidly stirred at reflux for 3 hours. The reaction was cooled and poured over ice (75 g) and extracted with ethyl acetate (3 x 25 mL). The organic layers were combined and washed with brine (20 mL), dried on magnesium sulfate, and reduced *in vacuo*. The residue was then purified by flash chromatography on silica (12% ethyl acetate in hexanes) to give a colorless liquid. 519.1 mg (~85%). ^1H NMR (300 MHz, CDCl_3) δ 10.03 (s, 1H), 7.91 (m, 1H), 7.85 (dm, 1H, $J = 7.6$ Hz), 7.67 (dm, 1H, $J = 7.6$ Hz), 7.55 (t, 1H, $J = 7.6$ Hz), 4.65 (s, 2H); HRMS (FAB $^+$) calculated for $[\text{C}_8\text{H}_7\text{OCl}]$ ($[\text{M}+\text{H}]^+$) 154.0185, found 154.0153.

4-Bromomethylbenzaldehyde (8f). 4-Hydroxymethylbenzaldehyde (680 mg, 5 mmol) was measured into a 25 mL round-bottomed flask with stirbar. Toluene (6 mL) and

concentrated hydrobromic acid (6 mL) were added, and the mixture was rapidly stirred at reflux for 3 hours. The reaction was cooled and poured over ice (75 g) and extracted with ethyl acetate (3 x 25 mL). The organic layers were combined and washed with brine (20 mL), dried on magnesium sulfate, and reduced *in vacuo* to give a white solid. 997 mg (quant.). ¹H NMR (300 MHz, CDCl₃) δ 10.02 (s, 1H), 7.87 (d, 2H, *J* = 8.3 Hz), 7.56 (d, 2H, *J* = 8.0 Hz), 4.52 (s, 2H); ¹³C NMR (126 MHz, CDCl₃) δ 191.50, 144.23, 136.11, 130.16, 129.67, 77.27, 77.02, 76.77, 31.98; HRMS (FAB⁺) calculated for [C₈H₇OBr] ([M+H]⁺) 197.9680, found 197.9632.

Dimethyl (2,2-dimethyl-1-(2-tosylhydrazinyl)propyl)phosphonate (pivaldehyde tosylhydrazone-dimethyl phosphite adduct). Pivaldehyde tosylhydrazone (25.4 mg, 0.1 mmol), scandium triflate (4.9 mg, 0.01 mmol), and methoxynaphthalene internal standard (2.8 mg, 0.02 mmol) were measured into an oven-dried ½ dram vial. Deuterated benzene (1 mL) was added, followed by dimethyl phosphite (18.3 μL, 0.2 mmol), and the mixture was shaken to dissolve and loaded into an NMR tube. ¹H and ³¹P NMR showed no adduct after 8 hours, but it was visible as a minor set of peaks (1:20 relative to the hydrazone) after 24 hours, and it was the dominant set of peaks (7:1 relative to the hydrazone) after 1 week. ¹H NMR (300 MHz, CDCl₃) δ 7.82 (d, 2H, *J* = 8.3 Hz), 7.32 (d, 2H, *J* = 8.3 Hz), 6.94 (m, 1H), 3.80 (d, 3H, *J* = 8.2 Hz), 3.76 (d, 3H, *J* = 8.1 Hz), 3.63 (t, 1H, *J* = 9.7 Hz), 2.86 (t, 1H, *J* = 10.5 Hz), 2.44 (s, 3H), 0.97 (s, 9H); ³¹P NMR (121 MHz, CDCl₃) δ 31.17.

Dimethyl (2,2-dimethyl-1-(2-tosylhydrazinyl)propyl)phosphonate (pivaldehyde tosylhydrazone-dimethyl phosphite adduct). Pivaldehyde tosylhydrazone (12.7 mg,

0.05 mmol) and scandium triflate (2.5 mg, 0.005 mmol) were measured into an oven-dried ½ dram vial. Deuterated chloroform (1 mL) was added, followed by dimethyl trimethylsilyl phosphite (19.1 μ L, 0.01 mmol), and the mixture was shaken to dissolve and loaded into an NMR tube. ^1H and ^{31}P NMR showed that conversion to the adduct was more than 50% complete after 2 hours, mostly complete after 6 hours, and it was complete in under 24 hours. In the absence of scandium triflate, no adduct formation whatsoever was visible by NMR in 24 hours.

Dimethyl neopentyl phosphonate (12). Pivaldehyde 2,4-dinitrobenzenesulfonyl hydrazide (16.5 mg, 0.05 mmol) and scandium triflate (2.5 mg, 0.005 mmol) were measured into a ½ dram vial with perylene stirbar. Chloroform was added, followed by dimethyl trimethylsilyl phosphite (19.1 μ L, 0.01 mmol). The reaction was allowed to stir at room temperature, and aliquots were removed periodically by syringe and examined by NMR. NMR after 24 hours showed ~65% yield, as determined by integration of the product methylene against all tert-butyl protons and all aromatic region protons. ^1H NMR (300 MHz, CDCl_3) δ 3.72 (d, 6H, J = 10.8 Hz), 1.75 (d, 2H, J = 18.7 Hz), 1.10 (d, 9H, J = 0.7 Hz); ^{31}P NMR (121 MHz, CDCl_3) δ 33.01.

Chemistry—Phosphite Oxidation Protocol

Dimethyl phosphite (2 drop, 0.1 mmol) was added to acetonitrile- d_3 (1.5 mL) and deuterated water (0.2 mL). Half of this solution was loaded into an NMR tube as a

control, while iodine (25 mg, 0.1 mmol) was added to the other half, and the mixture was sonicated to dissolve completely, then loaded into another NMR tube. After 10 minutes, a new set of methyl peaks were visible by ^1H NMR, and the conversion was complete within 1 hour. ^1H NMR (300 MHz, $\text{CD}_3\text{CN}/\text{D}_2\text{O}$) δ CONTROL: 6.61 (d, 1H, $J = 7044$ Hz), 3.73 (s, 1.3H), 3.63 (s, 3H), 3.59 (s, 3H); δ 1 HOUR: 4.71 (s, 2.3H), 3.55 (s, 3H), 3.51 (s, 3H); ^{31}P NMR (121 MHz, $\text{CD}_3\text{CN}/\text{D}_2\text{O}$) δ CONTROL: 11.10; δ 1 HOUR: 0.83. When dimethyl isopropyl phosphonate was subjected to the same conditions, no change was seen by NMR.

Chemistry—Kinetic Runs

4-Bromomethylbenzaldehyde (**8f**, 19.9 mg, 0.1 mmol), mesitylenesulfonyl hydrazide (21.4 mg, 0.1 mmol), yttrium triflate (5.4 mg, 0.01 mmol), and methoxynaphthalene internal standard (5.0 mg, 0.0316 mmol) were measured into an oven-dried $\frac{1}{2}$ dram vial with a disposable perylene stir-bar. CDCl_3 (1 mL) was added, and the vial was capped with a septum. In reactions where there was an additive, it was added at this time, and the reactions were stirred at room temperature for 15 minutes. Diethyl phosphite (26 μL , 0.2 mmol) was then added, and the reaction was heated to 60 $^\circ\text{C}$ under stirring. Periodic aliquots were taken in the following manner: the reactions were cooled, and 100 μL samples were taken, diluted with CDCl_3 (0.5 mL), and examined by ^1H and ^{31}P NMR. The reactions were immediately returned to the heat. The reactions shown are as follows:

- 1) no additive

- 3) 10 mol.% diethyl 4-methylbenzylphosphonate (2.4 μ L, 0.01 mmol)
- 4) 50 mol % diethyl 4-methylbenzylphosphonate (12.0 μ L, 0.05 mmol)
- 5) 100 mol % diethyl 4-methylbenzylphosphonate (24.0 μ L, 0.1 mmol).

Yields of hydrazone were calculated based on integration of the ^1H NMR peaks of its ortho-methyl groups (δ 2.72) relative to the methoxy group (δ 3.92) of the internal standard. Yields of phosphonate were calculated based on integration of the ^1H NMR peaks of its benzylic methylene (δ 3.20/3.13) relative to the methoxy group (δ 3.92) of the internal standard. Residual baseline was subtracted from each integration. Data in Table 6.S1. These results were qualitatively supported by the ^{31}P NMR spectra.

Table 6.S1. Reaction timecourse data (NMR) for Figure 6.1

	1 (standard conditions)			2 (20% Y)			3 (0.1 equiv. phosphonate)			4 (0.5 equiv. phosphonate)			5 (1.0 equiv. phosphonate)						
	0.316			0.316			0.316			0.316			0.316						
	IS		2.73	IS		2.73	IS		2.73	IS		2.73	IS		2.73				
	3.00	6.00		3.00	6.00		3.00	6.00		3.00	6.00		3.00	6.00					
1	0.88	5.38	1	0.92	6.03	1	0.93	5.68	1	0.92	5.74	1	0.83	5.06	1				
H-adj.	0.29	0.90	H-adj.	0.31	1.01	H-adj.	0.31	0.95	H-adj.	0.31	0.96	H-adj.	0.28	0.84	H-adj.				
pred.		5.57	pred.		5.82	pred.		5.89	pred.		5.82	pred.		5.25	pred.				
Yield	97%	0%	97%	Yield	104%	0%	104%	Yield	96%	96%	Yield	99%	99%	Yield	96%	96%			
	0.316		0.316			0.316			0.316			0.316			0.316				
	IS		2.73	IS		2.73	IS		2.73	IS		2.73	IS		2.73				
	3.00	2.00	6.00		3.00	2.00	6.00		3.00	2.00	6.00		3.00	2.00	6.00				
2	0.84	0.05	4.61	2	0.84	0.11	5.00	2	0.88	0.04	4.84	2	0.90	5.43	2	0.90	5.39		
H-adj.	0.28	0.03	0.77	H-adj.	0.28	0.06	0.83	H-adj.	0.29	0.02	0.81	H-adj.	0.30	0.00	0.91	H-adj.	0.30	0.00	0.90
pred.		1.77	5.32	pred.		1.77	5.32	pred.		1.86	5.57	pred.		1.90	5.70	pred.		1.90	5.70
Yield	90%	3%	87%	Yield	100%	6%	94%	Yield	89%	2%	87%	Yield	95%	0%	95%	Yield	95%	0%	95%
	0.316		0.316			0.316			0.316			0.316			0.316				
	IS		2.73	IS		2.73	IS		2.73	IS		2.73	IS		2.73				
	3.00	2.00	6.00		3.00	2.00	6.00		3.00	2.00	6.00		3.00	2.00	6.00				
3	0.90	0.49	3.38	3	0.89	0.89	2.97	3	0.85	0.53	3.33	3	0.87	0.29	4.26	3	0.82	0.32	3.94
H-adj.	0.30	0.25	0.56	H-adj.	0.30	0.45	0.50	H-adj.	0.28	0.27	0.56	H-adj.	0.29	0.14	0.71	H-adj.	0.27	0.16	0.66
pred.		1.90	5.70	pred.		1.88	5.63	pred.		1.79	5.38	pred.		1.84	5.51	pred.		1.73	5.19
Yield	85%	26%	59%	Yield	100%	47%	53%	Yield	91%	30%	62%	Yield	93%	16%	77%	Yield	94%	18%	76%
	0.316		0.316			0.316			0.316			0.316			0.316				
	IS		2.73	IS		2.73	IS		2.73	IS		2.73	IS		2.73				
	3.00	2.00	6.00		3.00	2.00	6.00		3.00	2.00	6.00		3.00	2.00	6.00				
4	0.85	1.41	1.10	4	0.87	1.69	0.19	4	0.86	1.31	1.19	4	0.90	1.20	1.85	4	0.85	1.05	2.13
H-adj.	0.28	0.71	0.18	H-adj.	0.29	0.85	0.03	H-adj.	0.29	0.66	0.20	H-adj.	0.30	0.60	0.31	H-adj.	0.28	0.53	0.36
pred.		1.79	5.38	pred.		1.84	5.51	pred.		1.81	5.44	pred.		1.90	5.70	pred.		1.79	5.38
Yield	99%	79%	20%	Yield	96%	92%	3%	Yield	94%	72%	22%	Yield	96%	63%	32%	Yield	98%	59%	40%
	0.316		0.316			0.316			0.316			0.316			0.316				
	IS		2.73	IS		2.73	IS		2.73	IS		2.73	IS		2.73				
	3.00	2.00	6.00		3.00	2.00	6.00		3.00	2.00	6.00		3.00	2.00	6.00				
5	0.82	1.73	0.16	5	0.76	1.80	0.16	5	0.87	1.59	0.14	5	0.65	1.32	0.62	5	0.67	1.32	0.73
H-adj.	0.27	0.87	0.03	H-adj.	0.25	0.90	0.03	H-adj.	0.29	0.80	0.02	H-adj.	0.22	0.66	0.10	H-adj.	0.22	0.66	0.12
pred.		1.73	5.19	pred.		1.60	4.81	pred.		1.84	5.51	pred.		1.37	4.11	pred.		1.41	4.24
Yield	103%	100%	3%	Yield	116%	112%	3%	Yield	89%	87%	3%	Yield	111%	96%	15%	Yield	111%	93%	17%
	0.00	-3.48			0.12	-3.40			-0.14	-3.67			-0.04	-1.89			-0.07	-1.76	

References

-
- ¹ Room-Temperature Alternative to the Arbuzov Reaction: The Reductive Deoxygenation of Acyl Phosphonates. Kedrowski, S. M. A.; Dougherty, D. A. *Organic Letters* **2010**, 12(18), 3990–3993.
- ² (a) Arbuzov, A. *J. Russ. Phys. Chem. Soc.* **1906**, 38. (b) Arbuzow, B. A. *Pure Appl. Chem.* **1964**, 9, 307. (c) Bhattacharya, A. K.; Thyagarajan, G. *Chem. Rev.* **1981**, 81, 415. (d) Michaelis, A.; Kaehne, R. *Chem. Ber.* **1898**, 31, 1048.
- ³ Highly Efficient Methodology for the Reductive Coupling of Aldehyde Tosylhydrazones with Alkylolithium Reagents. Myers, A. G.; Movassaghi, M. *J. Am. Chem. Soc.* **1998**, 120, 8891
- ⁴ Mesitylenesulfonylhydrazine and (1 α ,2 α ,6 β)-2,6-Dimethylcyclohexanecarbonitrile and (1 α ,2 β ,6 α)-2,6-Dimethylcyclohexanecarbonitrile as a Racemic Mixture. Reid, J. R.; Dufresne, R. F.; Chapman, J. *J. Organic Syntheses, Coll. Vol. 9*, **1998**, p.281; Vol. 74, **1997**, p.217.
- ⁵ Direct Conversion of Tosylhydrazones to tert-Butyl Ethers under Bamford-Stevens Reaction Conditions. Chandrasekhar, S.; Rajaiah, G.; Chandraiah, L.; Swamy, D. N. *Synlett.* **2001**, 11(26), 1779-1780.
- ⁶ (a) Addition of Diphenylphosphine Oxide to Arenesulfonylhydrazones: Novel Adducts from Tosylhydrazones and a New Synthesis of Alkyldiphenylphosphine Oxides from Trisylhydrazones. Bertz, S. H.; Dabbagh, G. *J. Am. Chem. Soc.* **1981**, 103(19), 5932-5934. (b) Improved Preparations of Some Arenesulfonylhydrazones. Bertz, S. H.; Dabbagh, G. *J. Org. Chem.* **1983**, 48, 116-119.
- ⁷ (a) A New Route to sec-Alkanephosphonates. Inokawa, S.; Nakatsukasa, Y.; Horisaki, M.; Yamashita, M.; Yoshida, H.; Ogata, T.; Inokawa, H. *Synthesis.* **1977**, 179-180. (b) Promotion of Dehydrazination by Nitrobenzenesulfonyl Group from Phosphorus-hydrazone Adducts. Yamashita, M.; Takeuchi, J.; Nakatani, K.; Oshikawa, T.; Inokawa, S. *Bull. Chem. Soc. Jpn.* **1985**, 58, 377-378.
- ⁸ (a) Orthogonal Lewis Acids: Catalyzed Ring Opening and Rearrangement of Acylaziridines. Ferraris, D.; Drury, W. J. III; Cox, C.; Lectka, T. *J. Org. Chem.* **1998**, 63, 4568-4569. (b) A Novel Classification of Lewis Acids on the Basis of Activity and

Selectivity. Kobayashi, S.; Busujima, T.; Nagayama, S. *Chem. Eur. J.* **2000**, 6(19), 3491-3494.

⁹ (a) Virgil, S., personal communication. (b) Mesitylenesulfonylhydrazide. Chamberlin, A. R.; Sheppeck, J. E. *e-EROS Encyclopedia of Reagents for Organic Synthesis*. **2001**. (c) p-Toluenesulfonylhydrazide. Chamberlin, A. R.; Sheppeck, J. E.; Goess, B.; Lee, C. *e-EROS Encyclopedia of Reagents for Organic Synthesis*. **2007**. (d) 2,4,6-Triisopropylbenzenesulfonylhydrazide. Chamberlin, A. R.; Sheppeck, J. E.; Somoza, A. *e-EROS Encyclopedia of Reagents for Organic Synthesis*. **2008**. (e) 2-Nitrobenzenesulfonylhydrazide. Myers, A. G.; Movassaghi, M. *e-EROS Encyclopedia of Reagents for Organic Synthesis*. **2003**. (f) 2,4-dinitrobenzenesulfonylhydrazide. Chamberlin, A. R.; Sheppeck, J. E. *e-EROS Encyclopedia of Reagents for Organic Synthesis*. **2001**. (g) references contained in b-f.

¹⁰ (a) New organic compounds of phosphorus. III. Phosphinemethylene derivatives and phosphinamines. Staudinger, H.; Meyer, J. *Helv. Chim. Acta.* **1919**, 2, 635-646. (b) Azides: their preparation and synthetic uses. Scriven, E. F. V.; Turnbull, K. *Chem. Rev.* **1988**, 88, 297-368.

¹¹ (a) The Reactivity of Organophosphorus Compounds. Part XIX. Reduction of Nitrocompounds by Triethyl Phosphite: a Convenient New Route to Carbazoles, Indoles, Indazoles, Triazoles, and Related Compounds. Cadogan, J. I. G.; Cameron-Wood, M.; MacKie, R. K.; Searle, R. J. G. *J. Chem. Soc.* **1965**, 4831-4837. (b) Direct Conversion of Benzylic and Allylic Alcohols to Phosphonates. Barney, R. J.; Richardson, R. M.; Wiemer, D. F. *J. Org. Chem.* **2011**, 76, 2875-2879. (c) The Michaelis-Arbuzov Rearrangement. Bhattacharya, A. K.; Thyagarajan, G. *Chem. Rev.* **1981**, 81, 415-430.

¹² (a) Anderson, B. M.; Jencks, W. P. *J. Am. Chem. Soc.* **1960**, 82, 1773. (b) Cordes, E. H.; Jencks, W. P. *J. Am. Chem. Soc.* **1962**, 84, 832. (c) Jencks, W. P. *J. Am. Chem. Soc.* **1959**, 81, 475.

¹³ (a) Addition of Diphenylphosphine Oxide to Arenesulfonylhydrazones: Novel Adducts from Tosylhydrazones and a New Synthesis of Alkyldiphenylphosphine Oxides from Trisylhydrazones. Bertz, S. H.; Dabbagh, G. *J. Am. Chem. Soc.* **1981**, 103(19), 5932-5934. (b) Improved Preparations of Some Arenesulfonylhydrazones. Bertz, S. H.;

Dabbagh, G. J. *Org. Chem.* **1983**, *48*, 116-119.

¹⁴ Copper(II)-Catalyzed Conversion of Aryl/Heteroaryl Boronic Acids, Boronates, and Trifluoroborates into the Corresponding Azides: Substrate Scope and Limitations. Grimes, K. D.; Gupte, A.; Aldrich, C. C. *Synthesis*, **2010**, *9*, 1441.

¹⁵ Still, W. C.; Kahn, M.; Mitra, A. *Journal of Organic Chemistry* **1978**, *43(14)*, 2923

¹⁶ Unsymmetrical, oxazolinyl-containing achiral and chiral NCN pincer ligand precursors and their complexes with palladium(II). Hao, X.-Q.; Wang, Y.-N.; Liu J.-R.; Wang, K.-L.; Gong, J.-F.; Song, M.-P. *J. Organometallic Chem.* **2010**, *695*, 82-89.

¹⁷ Unsymmetrical, oxazolinyl-containing achiral and chiral NCN pincer ligand precursors and their complexes with palladium(II). Hao, X.-Q.; Wang, Y.-N.; Liu J.-R.; Wang, K.-L.; Gong, J.-F.; Song, M.-P. *J. Organometallic Chem.* **2010**, *695*, 82-89.

Section 3: Chapter 7

Investigations into the Role of Nitrosylation of Cysteine Residues as a Posttranslational Protein Modification

Abstract: Cysteine nitrosylation as a posttranslational protein modification is considered. The site-specific incorporation of nitrosocysteine is not possible due to the fast rate of nitrosyl exchange between thiols. A system to quantify the energetics of the proposed nitrosothiol-aromatic interaction is outlined.

The 1998 Nobel Prize in Medicine was awarded to Ferid Murad, Robert Furchgott, and Louis Ignarro for “their discoveries concerning nitric oxide as a signaling molecule in the cardiovascular system”.¹ Specifically, they showed that nitric oxide is a naturally-produced hormone capable of traveling significant distances within the body and responsible for triggering dilation of the blood vessels through binding to the central heme in guanylyl cyclase.² Since their initial discoveries, a number of other physiological roles and mechanisms for nitric oxide have been reported.³ For example, nitric oxide has also been shown to bind to hemoglobin, enabling it to be carried longer distances in the bloodstream as part of a complex feedback mechanism for regulating oxygen delivery throughout the body.⁴ It has also been shown that nitric oxide can bind proteins at cysteine residues in addition to at iron.⁵

Outside of the circulatory system, nitric oxide has been shown to play a role in the central nervous system.⁶ The neuronal subtype of nitric oxide synthase is calcium activated,⁷ while the nitric oxide thus produced has been shown to down-modulate the N-methyl-D-aspartate (NMDA) receptor, thus providing a negative feedback for calcium influx.⁸

Because of its suspected role in memory formation, the NMDA receptor is of particular interest (Figure 7.1).⁹ As a ‘coincidence detector’, it requires glycine binding, glutamate binding, and membrane depolarization to activate. Furthermore, there are a number of sites for posttranslational modification that can influence current, activation, and/or interactions with other proteins. The lab

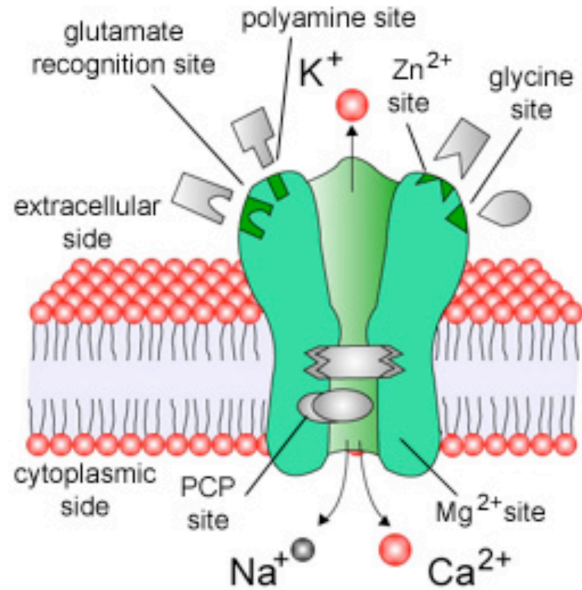


Figure 7.1. The NMDA receptor.

of Stuart Lipton demonstrated nitric oxide-induced down-modulation of the NMDA receptor that is reversible with dithiothreitol.¹⁰ They also performed an alanine scan of all the cysteine residues in the protein, showing that the NR2A C399A mutant is unresponsive to nitric oxide, suggesting that this is the key cysteine residue for nitrosylation. However, they lacked a method for selectively nitrosylating that residue in the wild-type receptor, which would provide stronger and more direct support of that hypothesis.

Given our lab’s expertise in the site-specific incorporation of unnatural amino acid residues,¹¹ we hoped that we might be able to site-specifically incorporate nitrosocysteine into the NMDA receptor to establish the key site of nitrosylation. This strategy could also be useful in studying other proteins that undergo cysteine nitrosylation. However, this first required some controls to explore the stability of the

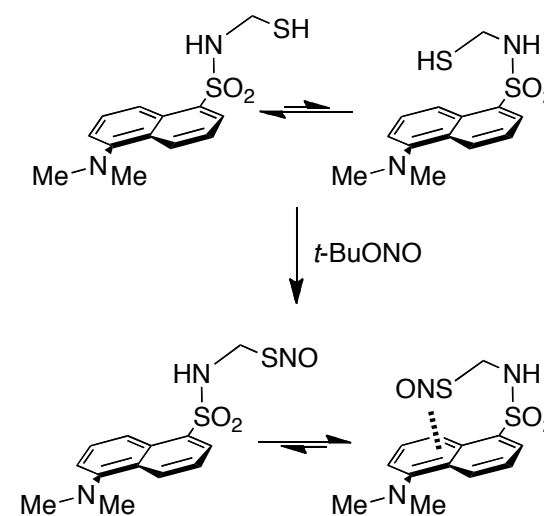
nitrosothiol group and whether it was sufficiently robust to survive our protocols for unnatural amino acid incorporation.

The literature reports that the energy barrier for uncatalyzed S-NO bond cleavage is too high (> 30 kcal/mol) to occur under physiological conditions.¹² However, there are other mechanisms by which a nitrosothiol might degrade.¹³

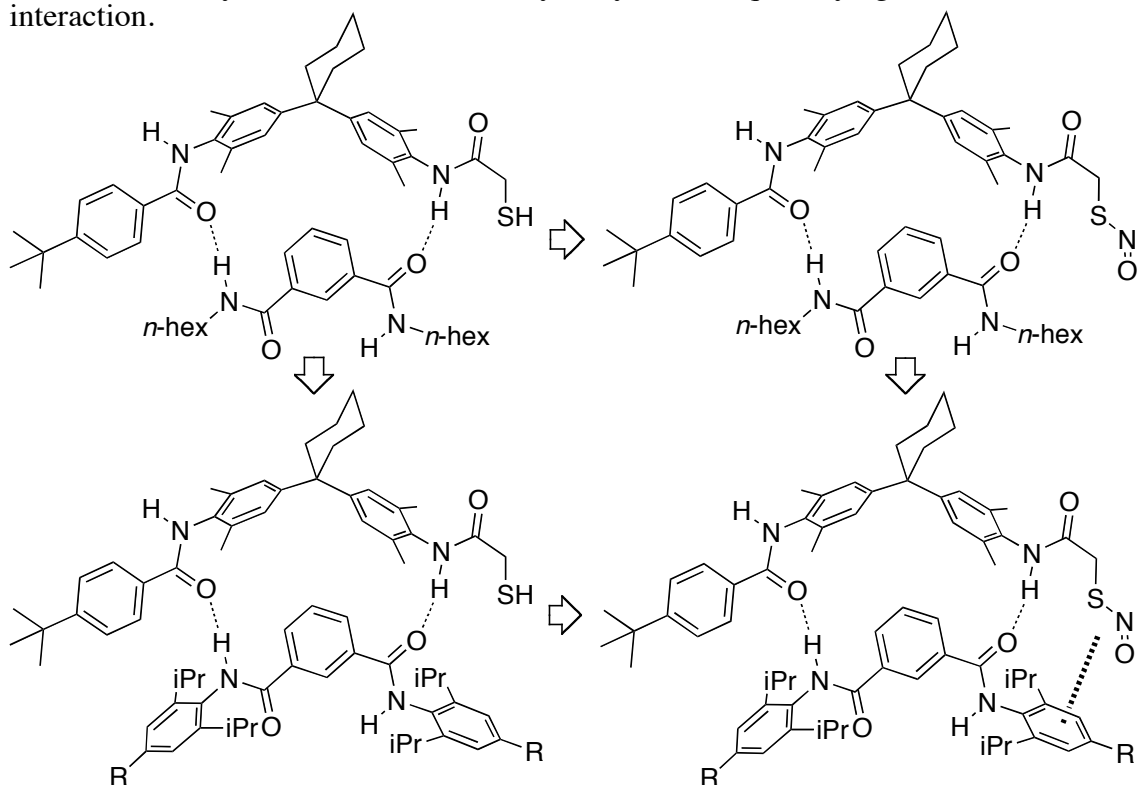
Specifically, nitrosyl transfer from one thiol to another is known to be a rather facile process.¹⁴ Sterically hindered thiols are known to react more slowly, but there are multiple literature reports of this happening on a timescale of minutes, consistent with our observations. Since our unnatural amino acid incorporation protocol requires in-cell incubation times of 1-2 days, site-specific incorporation of nitrosocysteine using this method is not feasible. Likewise, no feasible ‘caged’ nitrosocysteine residues could be envisioned,^{15,16} and more chemically stable structural analogs did not seem worth pursuing (e.g., the sulfur-to-carbon analog C-N=O would rapidly rearrange to the oxime and have radically different electronic properties).

For a posttranslational modification to alter protein function, the change must chemically alter its sterics and/or electronics sufficiently to induce a conformation change or change its binding affinity for other molecules. Glycosylation and ubiquitylation are

Scheme 7.1. It has been reported that fluorescence is reversibly quenched in these thiol-tethered dansyl derivatives (ref. 19).

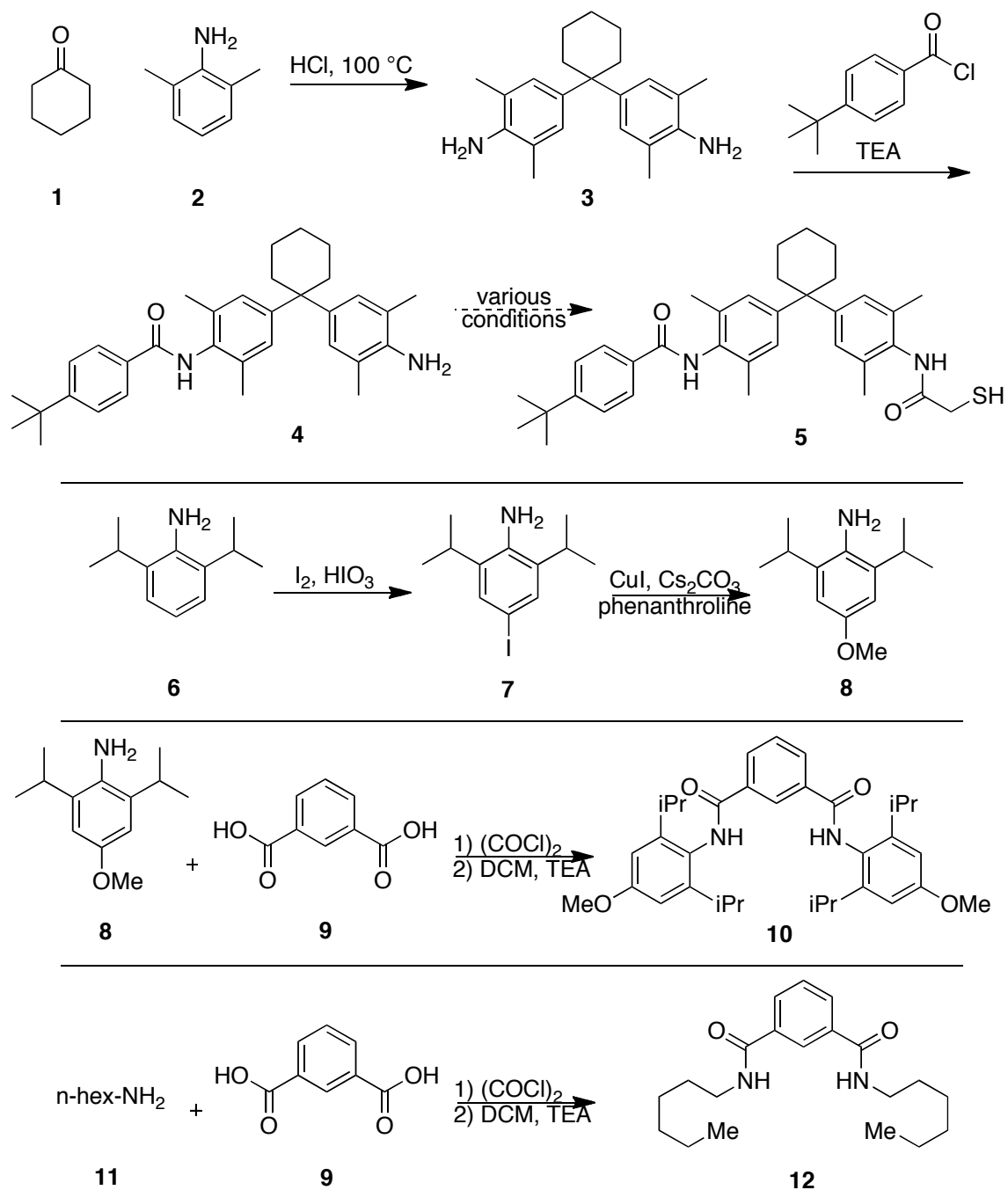


Scheme 7.2. A synthetic double mutant cycle system for quantifying the nitrosothiol- π interaction.



large enough to alter binding properties. Phosphorylation is a small change sterically, but it adds an ionic charge, which can produce a large effect. Nitric oxide binding at iron can displace other ligands or change the preferred coordination geometry of the metal. In contrast nitrosylation at sulfur is a more modest alteration. The nitrosyl group is so small that sterics are hardly altered, while the change from sulfhydryl involves no change in charge.

It has been proposed that cysteine nitrosylation meaningfully increases the residue's affinity for aromatic amino acids.¹⁷ This mechanism has been suggested to operate in the NMDA receptor, hemoglobin, and fibrinogen.¹⁸ However, there is scant evidence supporting how this could be possible on a chemical level. Specifically, there is one report in which a thiol tethered to a dansyl group exhibits some fluorescence

Scheme 7.3. Synthetic progress toward the double-mutant cycle system

quenching upon addition of a nitrosylating agent (Scheme 7.1).¹⁹ However, there is no rigorous quantification of this interaction, and the forces underlying it are unclear.

To answer these questions, we proposed a chemical double-mutant cycle experiment using a designed system modeled after those used by the lab of Chris Hunter

(Scheme 7.2).²⁰ This design should allow a value to be assigned to a nitrosothiol-aromatic interaction; if it is significant, computation could be done to further explore its basis. In the two contexts wherein interactions between specific nitrosothiols and specific aromatics have been reported, the aromatic residue was tyrosine. With a sample size of two, this could be pure coincidence, or it could suggest something unique about tyrosine (e.g., one could envision a hydrogen bond between the phenolic proton and the terminal oxygen of the nitrosothiol; Figure 7.2). For this reason, a phenol was chosen as the aromatic component of the mutant cycle studies.

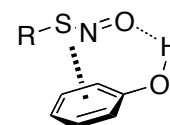


Figure 7.2. Phenol-nitrosothiol

Most reactions required to synthesize these molecules were well-precedented in the literature and proceeded without incident, but the last couple of steps gave some difficulty (Scheme 7.3). First, conditions that would cleanly deprotect the methyl ether of **10** without affecting the amide linkages could not be found. Second, the amide linkages in **5** proved difficult to forge. Given these challenges, along with our general skepticism towards the ‘nitrosothiol-aromatic interaction’, we chose to abandon this project after a predetermined time allotment had been exceeded.

Chemistry—General

All reactions were performed under argon using solvents that were dried and purified according to the method of Grubbs.²¹ All flasks and vials were oven dried at 122 °C and cooled in a desiccator box containing anhydrous calcium sulfate. Nitrosothiols were prepared using sodium nitrite according to literature procedure.²² The aryl iodide was synthesized according to the protocol of Ban.²³ Compounds whose syntheses are not presented here are known compounds prepared according to the methods of Hunter.²⁴ Reactions were monitored by thin-layer chromatography on Merck Siligel 60-F₂₅₄. Compounds were visualized with a UV lamp (254 nm) and stained with potassium permanganate solution. Column chromatography was carried out in accordance with the methods of Still²⁵ using EMD-Merck silica gel 60, 230-400 mesh ASTM. ¹H and ¹³C NMR spectra were acquired on a Varian Mercury 300 MHz spectrometer. High-resolution mass spectrometry was performed on a JEOL JMS-600H HRMS using an Electrospray Ion Source.

Chemistry—Synthesis

2,6-diisopropyl-4-methoxyaniline (8). 4-Iodo-2,6-Diisopropylaniline (3.03 g, 10 mmol), copper(I) iodide (190 mg, 1 mmol), phenanthroline (360 mg, 2 mmol), cesium carbonate (4.5 g, 14 mmol), and methanol (10 mL) were measured into a pressure tube with stirbar. The mixture was stirred on a oil bath at 110 °C for 20 h, then cooled, diluted with ethyl

acetate (50 mL), and filtered through a silica plug. The residue was then purified by flash chromatography on silica (10% ethyl acetate in hexanes) to give 1.39 g (67.1%).²⁶ ¹H NMR (300 MHz, CDCl₃) δ 6.67 (s, 2H), 3.80, (s, 3H), 3.48 (bs, 2H), 2.98 (septet, 2H, *J* = 6.9 Hz), 1.29 (d, 12H, *J* = 6.6 Hz); ¹³C NMR (126 MHz, CDCl₃) δ 152.98, 134.47, 134.04, 108.86, 55.78, 28.35, 22.66; LRMS (FAB⁺) calculated for [C₁₃H₂₂NO]⁺ ([M+H]⁺) 208.1696, found 208.1668.

bis[2,6-diisopropyl-4-methoxyaniline]-isophthaloyl diamide (10). 2,6-diisopropyl-4-methoxy aniline (1.48 g, 7.1 mmol) was added to 50 mL round-bottom flask with stirbar. Dichloromethane (10 mL) and triethylamine (1.04 mL, 7.5 mmol) were added by syringe, followed by the slow addition of isophthaloyl dichloride (3.4 mmol)²⁷ over 1 hour by syringe pump at room temperature. After 16 hours the reaction was diluted with dichloromethane (100 mL), washed with 1N aq. HCl (2 x 50 mL), washed with 2N aq. NaOH (1 x 50 mL), dried on sodium sulfate, and reduced *in vacuo*. The residue was then recrystallized from 40:60 dichloromethane:petroleum ether to give 1.17 g (63.2%). ¹³C NMR (126 MHz, CDCl₃) δ 166.53, 159.79, 148.11, 135.38, 130.46, 129.56, 126.26, 123.81, 109.28, 55.47, 29.34, 23.87.

References

¹ nobelprize.org

² (a) Nitric oxide activates guanylate cyclase and increases guanosine 3':5'-cyclic monophosphate levels in various tissue preparations. Arnold, W. P.; Mittal, C. K.; Katsuki, S.; Murad, F. *PNAS*, **1977**, 74(8), 3203-3207. (b) The obligatory role of endothelial cells in the relaxation of arterial smooth muscle by acetylcholine. Furchgott, R. F.; Zawadzki, J. V. *Nature* **1980**, 288, 373-377. (c) Activation of Soluble Guanylate Cyclase by NO-Hemoproteins Involves NO-Heme Exchange. Ignarro, L. J.; Adams, J. B.; Horwitz, P. M.; Wood, K. S. *J. Biol. Chem.*, **1986**, 261(11), 4997-5002. (d) Endothelium-derived relaxing factor produced and released from artery and vein is nitric oxide. Ignarro, L. J.; Buga, G. M.; Wood, K. S.; Byrns, R. E.; Chaudhuri, G. *PNAS*, **1987**, 84, 9265-9269.

³ (a) Protein S-nitrosylation: Purview and Parameters. Hess, D. T.; Matsumoto, A.; Kim, S.-O.; Marshall, H. E.; Stamler, J. S. *Nature Reviews*. **2005**, 6, 150-166. (b) Nitric Oxide Circulates in Mammalian Plasma Primarily as an S-Nitroso Adduct of Serum Albumin. Stamler, J. S.; Jaraki, O.; Osborne, J.; Simon, D. I.; Keaney, J.; Vita, J.; Singel, D.; Valeri, C. R.; Loscalzo, J. *PNAS*, **1992**, 89, 7674-7677. (c) Mechanism of p21Ras S-Nitrosylation and Kinetics of Nitric Oxide-Mediated Guanine Nucleotide Exchange. Heo, J.; Campbell, S. L. *Biochemistry*. **2004**, 43, 2314-2322. (d) The Skeletal Muscle Calcium Release Channel: Coupled O₂ Sensor and NO Signaling Functions. Eu, J. P.; Sun, J.; Xu, L.; Stamler, J. S.; Meissner, G. *Cell*. **2000**, 102, 499-509. (e) Nitric oxide activates TRP channels by cysteine S-nitrosylation. Yoshida, T.; Inoue, R.; Morii, T.; Takahashi, N.; Yamamoto, S.; Hara, Y.; Tominaga, M.; Shimizu, S.; Sato, Y.; Mori, Y. *Nature Chemical Biology*. **2006**, 2(11), 596-607.

⁴ (a) Chemical Physiology of Blood Flow Regulation by Red Blood Cells: The Role of Nitric Oxide and S-Nitrosohemoglobin. Singel, D. J.; Stamler, J. S. *Ann. Rev. Physiol.* **2005**, 67, 99-145. (b) S-nitrosohaemoglobin: a dynamic activity of blood involved in vascular control. Jia, L.; Bonaventura, C.; Bonaventura, J.; Stamler, J. S. *Nature*. **1996**, 380, 221-226. (c) Reactions between nitric oxide and haemoglobin under physiological conditions. Gow, A. J.; Stamler, J. S. *Nature*. **1998**, 391, 169-173. (d) Export by red

blood cells of nitric oxide bioactivity. Pawloski, J. R.; Hess, D. T.; Stamler, J. S. *Nature*. **2001**, *409*, 622-626. (e)

⁵ (a) Protein S-nitrosylation: Purview and Parameters. Hess, D. T.; Matsumoto, A.; Kim, S.-O.; Marshall, H. E.; Stamler, J. S. *Nature Reviews*. **2005**, *6*, 150-166. (b) Crystal Structure of the S-Nitroso Form of Liganded Human Hemoglobin. Chan, N.-L.; Rogers, P. H.; Arnone, A. *Biochemistry*. **1998**, *37*, 16459-16464.

⁶ (a) Nitric oxide as modulator of neuronal function. Prast, H.; Philippu, A. *Progress in Neurobiology*. **2001**, *64*, 51-68. (b) Nitric oxide, cell bioenergetics and neurodegeneration. Moncada, S.; Bolanos, J. P. J. *Neurochemistry*. **2006**, *97*, 1676-1689. (c) Protein S-nitrosylation: a physiological signal for neuronal nitric oxide. Jaffrey, S. R.; Erdjument-Bromage, H.; Ferris, C. D.; Tempst, P.; Snyder, S. H. *Nature Cell Biology*. **2001**, *3*, 193-197.

⁷ Intrinsic and Extrinsic Modulation of Nitric Oxide Synthase Activity. Roman, L. J.; Martasek, P.; Masters, B. S. S. *Chem. Rev.* **2002**, *102*, 1179-1189.

⁸ Cysteine regulation of protein function – as exemplified by NMDA-receptor modulation. Lipton, S. A.; Choi, Y.-B.; Takahashi, H.; Zhang, D.; Li, W.; Godzik, A.; Bankston, L. A. *TRENDS in Neurosciences*. **2002**, *25*(9), 474-480.

⁹ (a) The Glutamate Receptor Ion Channels. Dingledine, R.; Borges, K.; Bowie, D.; Traynelis, S. F. *Pharmacological Review*. **1999**, 7-61 and references therein. (b) The chemical biology of clinically tolerated NMDA receptor antagonists. Chen, H.-S. V.; Lipton, S. A. *J. Neurochemistry*. **2006**, *97*, 1611-1626.

¹⁰ Molecular basis of NMDA receptor-coupled ion channel modulation by S-nitrosylation. Choi, Y.-B.; Tanneti, L.; Le, D. A.; Ortiz, J.; Bai, G.; Chen, H.-S. V.; Lipton, S. A. *Nature Neuroscience*. **2000**, *3*(1), 15-21.

¹¹ (a) Nicotinic Receptor Binding Site Probed with Unnatural Amino-Acid Incorporation in Intact Cells. M. W. Nowak, P. C. Kearney, J. R. Sampson, M. E. Saks, C. G. Labarca, S. K. Silverman, W. Zhong, J. Thorson, J. N. Abelson, N. Davidson, P. G. Schultz, D. A. Dougherty, and H. A. Lester, *Science*, **1995**, *268*, 439-442. (b) Is the Brain Ready for Physical Organic Chemistry? D. A. Dougherty, *J. Phys. Org. Chem.*, **1998**, *11*, 334-340. (c) From Ab Initio Quantum Mechanics to Molecular Neurobiology: A Cation-pi Binding

Site in the Nicotinic Receptor. W. Zhong, J. P. Gallivan, Y. Zhang, L. Li, H. A. Lester, and D. A. Dougherty, *Proc. Natl. Acad. Sci. (USA)*, **1998**, *95*, 12088-12093. (d) A Cation- π Binding Interaction with a Tyrosine in the Binding Site of the GABAC Receptor. Sarah CR Lummis, Darren L Beene, Neil J. Harrison, Henry A. Lester, and Dennis A. Dougherty, *Chem. Biol.* **2005**, *12*, 993-997. (e) A Cation- π Interaction between Extracellular TEA and an Aromatic Residue in Potassium Channels, C. A. Ahern, A. L. Eastwood, H. A. Lester and D. A. Dougherty and Richard Horn, *J. Gen. Phys.* **2006**, *128*, 649-657. (f) Unnatural Amino Acid Mutagenesis of the GABA_A Receptor Binding Site Residues Reveals a Novel Cation- π Interaction Between GABA and b2 Tyr97. Padgett C.L., Hanek A.P., Lester H.A., Dougherty D.A. and Lummis S.C.R., *J. Neurosci.*, **2007**, *27*, 886-892. (g) A Cation- π Interaction in The Binding Site of The Glycine Receptor Mediated by a Phenylalanine Residue, S. A. Pless, K. S. Millen, A. P. Hanek, J. W. Lynch, H. A. Lester, S. C.R. Lummis, and D. A. Dougherty, *J. Neurosci.*, **2008**, *28*, 10937-10942. (h) Nicotine Binding to Brain Receptors Requires a Strong Cation- π Interaction X. Xiu*, N. L. Puskar*, J. A. P. Shanata, H. A. Lester, and D. A. Dougherty, *Nature*, **2009**, *458*, 534-537.

¹² (a) NO Affinities of S-Nitrosothiols: A Direct Experimental and Computational Investigation of RS-NO Bond Dissociation Energies. Lu, J.-M.; Wittborcht, J. M.; Wang, K.; Wen, Z.; Schlegel, H. B.; Wang, P. G.; Cheng, J.-P. *J. Am. Chem. Soc.* **2001**, *123*, 2903-2904. (b) Stamler, J. S.; Toone, E. J. *Curr. Opin. Chem. Biol.* **2002**, *6*, 779.; Bartberger, M. D.; Mannion, J. D.; Powell, S. C.; Stamler, J. S.; Houk, K. N.; Toone, E. *J. Am. Chem. Soc.* **2001**, *123*, 8868.

¹³ (a) Saville, B. *Analyst* **1958**, *83*, 670. (b) Mechanism of Nitric Oxide Release from S-Nitrosothiols. Singh, R. J.; Hogg, N.; Joseph, J.; Kalyanaraman, B. *J. Biol. Chem.* **1996**, *271(31)*, 18596-18603. (c) Ascorbic Acid and Reducing Agents Regulate the Fates and Functions of S-Nitrosothiols. Kashiba-Iwatsuki, M.; Kitoh, K.; Kasahara, E.; Yu, H.; Nisikawa, M.; Matsuo, M.; Inoue, M. *J. Biochem.* **1997**, *122*, 1208-1214.

¹⁴ (a) Kinetics and equilibria of S-nitrosothiol-thiol exchange between glutathione, cysteine, penicillamines and serum albumin. Meyer, D. J.; Kramer, H.; Ozer, N.; Coles, B.; Ketterer, B. *FEBS Letters*. **1994**, *345*, 177-180. (b) NO-Group transfer

(transnitrosation) between S-nitrosothiols and thiols. Part 2. Barnett, D. J.; Rios, A.; Williams, D. L. H. *J. Chem. Soc.—Perkins Trans.* **1995**, 1279-1282. (c) Scharfstein, J. S.; Keaney, J. F.; Slivka, A.; Welch, G. N.; Vita, J. A.; Stamler, J. S.; Loscalzo, J. *J. Clin. Invest.* **1994**, *94*, 1432. (d) Equilibrium and Kinetics Studies of Transnitrosation Between S-Nitrosothiols and Thiols. Wang, K.; Wen, Z.; Zhang, W.; Xian, M.; Cheng, J.-P.; Wang, P. G. *Bioorganic & Medicinal Chemistry Letters.* **2001**, *11*, 433-436.

¹⁵ (a) Incorporation of Caged Cysteine and Caged Tyrosine into a Transmembrane Segment of the Nicotinic Acetylcholine Receptor. K. D. Philipson, J. P. Gallivan, G. S. Brandt, D. A. Dougherty, and H. A. Lester. *Am. J. Physiol Cell Physiol*, **2001**, *281*, C195-C206. (b) Caged Phosphoproteins Deborah M. Rothman, E. James Petersson, M. Eugenio Vázquez, Gabriel S. Brandt, Dennis A. Dougherty*, Barbara Imperiali* *J. Am. Chem. Soc.*, **2005**, *127*, 846-847.

¹⁶ 4-Aryl-1,3,2-oxathiazolylium-5-olates as pH-Controlled NO-Donors: The Next Generation of S-Nitrosothiols. Lu, D.; Nadas, J.; Zhang, G.; Johnson, W.; Zweier, J. L.; Cardounel, A. J.; Villamena, F. A.; Wang, P. G. *J. Am. Chem. Soc.* **2007**, *129*, 5503-5514.

¹⁷ (a) Ramachandran, N.; Jacob, S.; Zielinski, B.; Curatola, G.; Mazzanti, L.; Mutus, B. *Biochim. Biophys. Acta.* **1999**, 1430, 149. (b) Cysteine regulation of protein function – as exemplified by NMDA-receptro modulation. Lipton, S. A.; Choi, Y.-B.; Takahashi, H.; Zhang, D.; Li, W.; Godzik, A.; Bankston, L. A. *TRENDS in Neurosciences.* **2002**, *25*(9), 474-480.

¹⁸ Evidence for S-nitrosothiol-dependent changes in fibrinogen that do not involve transnitrosation or thiolation. Akhter, S.; Vignini, A.; Wen, Z.; English, A.; Wang, P. G.; Mutus, B. *PNAS.* **2002**, *99*, 9172-9177.

¹⁹ Fluorophore-Labeled S-Nitrosothiols. Chen, X.; Wen, Z.; Xian, M.; Wang, K.; Ramachandran, N.; Tang, X.; Schlegel, H. B.; Mutus, B.; Wang, P. G. *J. Org. Chem.* **2001**, *66*, 6064-6073.

²⁰ (a) Chemical Double Mutant Cycles for the Measurement of Weak Intermolecular Interactions: Edge-to-Face Aromatic Interactions. H. Adams, F. J. Carver, C. A. Hunter, J. C. Morales and E. M. Seward *Angew. Chem. Int. Ed.* **1996**, *35*, 1542-1544. (b) A

Supramolecular System for Quantifying Aromatic Stacking Interactions. H. Adams, C. A. Hunter, K. R. Lawson, J. Perkins, S. E. Spey, C. J. Urch and J. M. Sanderson, *Chem. Eur. J.* **2001**, *7*, 4863-4877. (c) Substituent Effects on Cation- π Interactions: A Quantitative Study C. A. Hunter, C. M. R. Low, C. Rotger, J. G. Vinter and C. Zonta, *Proc. Natl. Acad. Sci. USA* **2002**, *99*, 4873-4876. (d) Substituent Effects on Edge-to-Face Aromatic Interactions. J. Carver, C. A. Hunter, D. J. Livingstone, J. F. McCabe and E. M. Seward, *Chem. Eur. J.* **2002**, *8*, 2848-2859.

²¹ Pangborn, A. B.; Giardello, M. A.; Grubbs, R. H.; Rosen, R. K.; Timmers, F. J. *Organometallics* **1996**, *15*, 1518-1520.

²² *Tetrahedron Letters* **1985**, 2013

²³ Synthesis and biological activity of novel 4-phenyl-1,8-naphthyridin-2(1H)-on-3-yl ureas: Potent acyl-CoA:cholesterol acyltransferase inhibitor with improved aqueous solubility. Ban, H.; Muraoka, M.; Ioriya, K.; Ohashi, N. *Bioorganic and Medicinal Chemistry Letters*. **2006**, *16*, 44-48.

²⁴ A Supramolecular System for Quantifying Aromatic Stacking Interactions. H. Adams, C. A. Hunter, K. R. Lawson, J. Perkins, S. E. Spey, C. J. Urch and J. M. Sanderson, *Chem. Eur. J.* **2001**, *7*, 4863-4877.

²⁵ Still, W. C.; Kahn, M.; Mitra, A. *Journal of Organic Chemistry* **1978**, *43(14)*, 2923

²⁶ Procedure adapted from: Copper-Catalyzed Coupling of Aryl Iodides with Aliphatic Alcohols. Wolter, M.; Nordmann, G.; Job, G. E.; Buchwald, S. L. *Organic Letters*. **2002**, *4(6)*, 973-976.

²⁷ as a 0.5M solution prepared from the diacid and oxalyl chloride

Section 3: Chapter 8

Synthetic Efforts Towards a Fluorinated Dopamine Analog

Abstract: *α,α -difluorodopamine was envisioned as a potential agonist for probing the binding site of the D2 dopamine receptor. Its synthesis was attempted, but it was ultimately shown that the molecule is highly unlikely to be stable enough for pharmacological testing.*

The dopamine D2 receptor is a G protein-coupled receptor that accepts dopamine (**1**) as its native ligand (Figure 8.1).¹ Studies in the Dougherty lab have implicated tryptophan

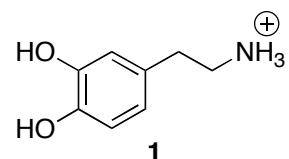


Figure 8.1. Dopamine

6.48 of the D2 receptor as involved in binding the ammonium moiety of dopamine.² This assignment was made through structure-function studies in which fluorinated tryptophan residues were incorporated at the 6.48 site. These experiments demonstrated that the receptor's sensitivity to dopamine is proportional to the cation-binding affinity of the π surface of the fluorinated tryptophan residue at position 6.48. This technique has been extensively demonstrated in various ligand-gated ion channels.³ However, Trp6.48 in the D2 receptor is peculiar in that the proportionality constant for this relationship is smaller than expected (in Coulombic terms) for a primary amine. Graphically speaking, the slope of the cation- π fluorination plot trendline is too shallow (Figure 8.2).

One possible explanation is that Trp6.48 is offset from the optimum binding geometry with the primary ammonium moiety of dopamine. In this case, the cation- π binding interaction could be better described as between Trp6.48 and the methylene adjacent to the ammonium moiety of dopamine (Figure 8.3).⁴ If that is true, increasing the

electrostatic potential of this methylene should increase the binding affinity of dopamine for the receptor, also causing a steeper slope in the fluorination plot of residue Trp6.48. We hypothesized this could be realized by synthesizing a dopamine analog that is fluorinated at the α -position, inductively increasing the electrostatic potential of the β -methylene (Scheme 8.1). Other molecules possessing this desired feature could be envisioned, but this molecule was the most attractive target because the steric deviation from dopamine is minimal, and it possesses no additional hydrogen bond donors or acceptors relative to dopamine. However, this molecule was unknown, and there was a possibility that the *p*-difluoromethylene phenol structure would be unstable, ejecting

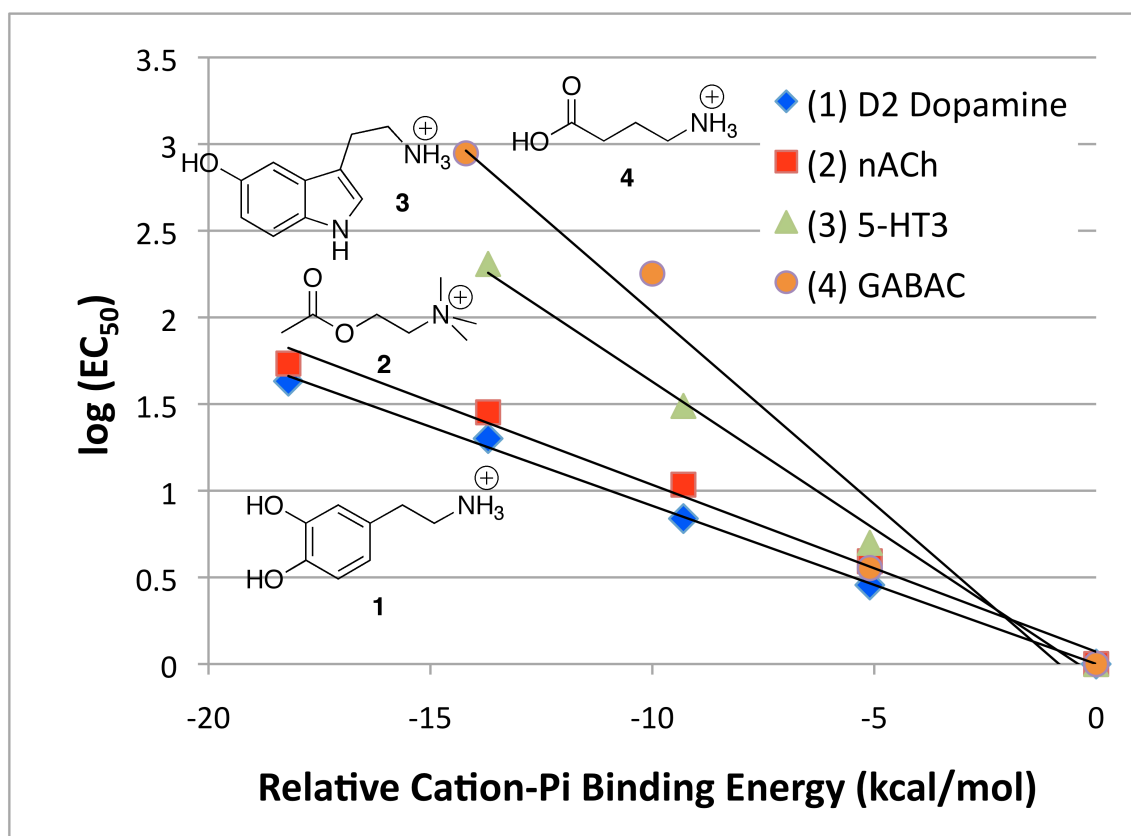


Figure 8.2. Cation- π fluorination plots for three ligand-gated ion channels and the D2 dopamine GPCR. Primary ammonium agonists are expected to give steeper fluorination slopes, yet the fluorination slope for dopamine in the D2 GPCR is shallow, similar to the slope for ACh in the nAChR.³ⁱ

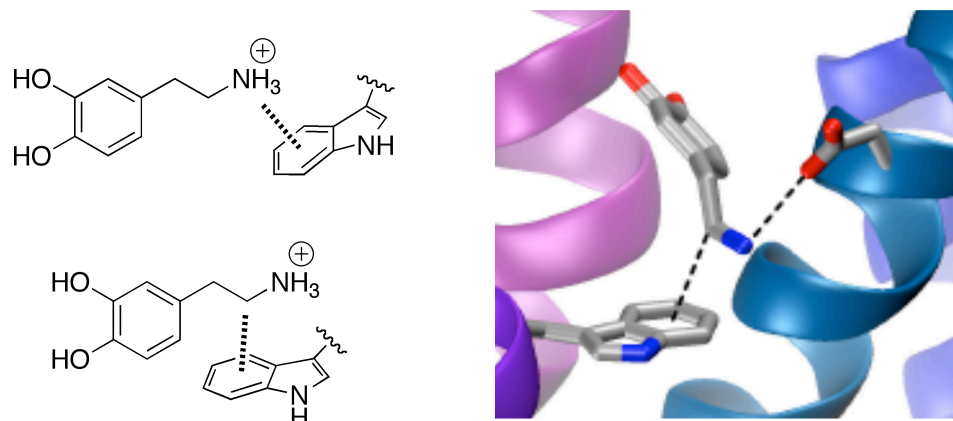


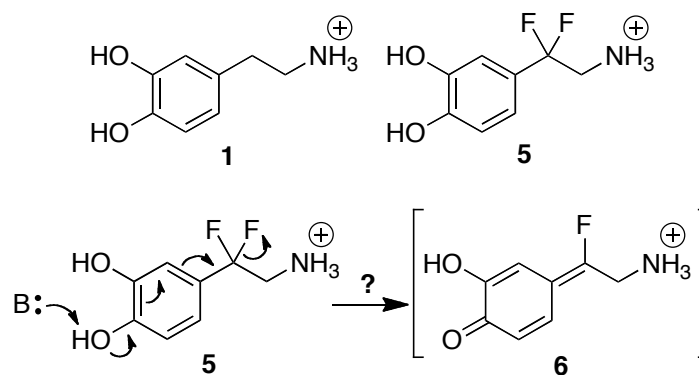
Figure 8.3. The shallow cation- π fluorination slope may arise from alignment of Trp residue with the methylene rather than the ammonium.

fluoride through a quinone methide-type intermediate.⁵ There is some literature precedent for this decomposition mode, but there is also some precedent suggesting the molecule would be stable—namely, the stability of aqueous *p*-trifluoromethylphenol.⁶

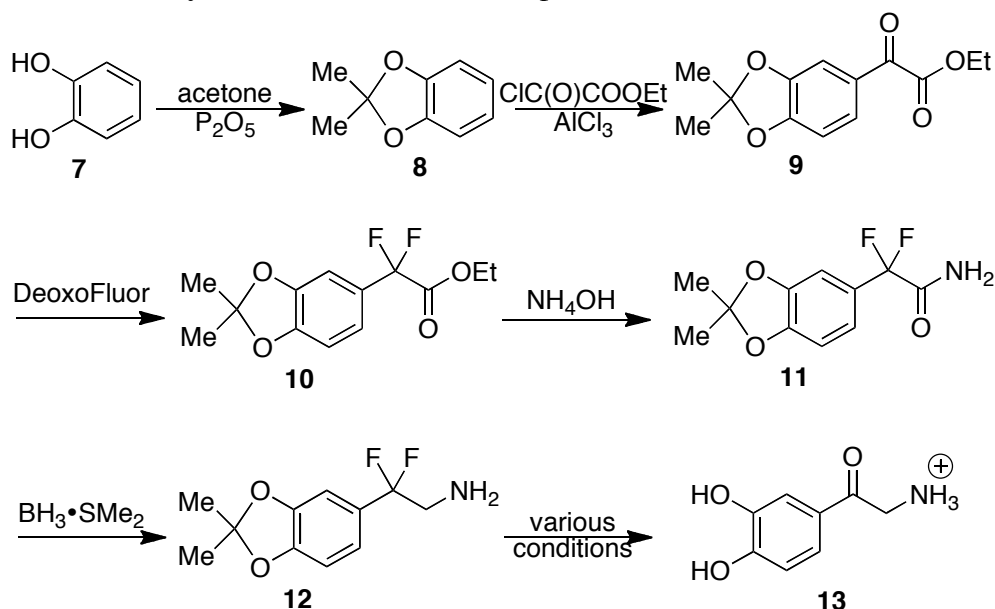
The target molecule was envisioned as rising from the acidic deprotection of catechol acetamide **12**, which itself could arise from the reduction from amide **11**, which is a known compound

(Scheme 8.2). In a forward sense, the protection of catechol with acetone was accomplished in hot toluene in the presence of phosphorus pentoxide. Submitting this

Scheme 8.1. Difluoride **5** may form a stronger cation- π than dopamine, but decomposition is a concern.



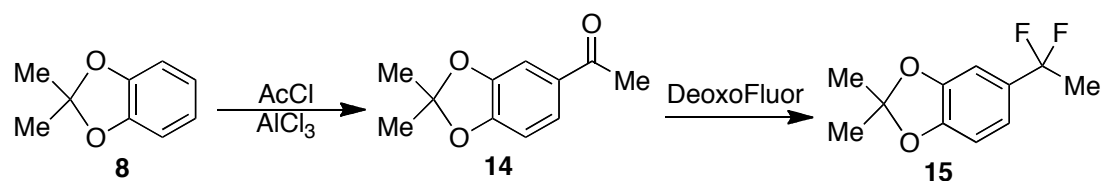
liquid to Friedel-Crafts conditions with ethyl chlorooxalate gave ketoacid **9** as a viscous orange liquid. Treatment of this compound with DeoxoFluor at room temperature over 3 days, followed by quench with aqueous ammonia yielded the difluorinated amide **11** as

Scheme 8.2. Synthesis of difluorinated dopamine **5** (failed).

fine, white, needle-like crystals. This solid was then reduced with borane-dimethylsulfide to give the primary amine **12** as a colorless liquid.

Methanolic HCl handily deprotected the acetonide, giving a white hydrochloride salt upon addition to diethyl ether. Unfortunately, NMR revealed that the geminal difluoride was no longer present and had instead hydrolyzed to a ketone (**13**). After screening a variety of conditions, it was discovered that low yields of the desired product could be isolated using chilled trifluoroacetic acid or boron trifluoride-etherate in dichloromethane. Interestingly, NMR of these deprotection mixtures showed that some amount of material was defluorinating prior to acetonide deprotection, which was surprising because a deprotonated phenolate intermediate was expected to be necessary to enable fluoride loss.

To explore this curiosity, a commercial sample of *p*-trifluoromethylphenol was exposed to a variety of the acidic deprotection conditions screened with acetonide **12**. Fluoride loss was not observed in any of these cases. When amide **11** was exposed to the

Scheme 8.3. Synthesis of difluoride **15**

acidic deprotection conditions, fluoride loss was observed. These results suggested that the β -nitrogen was necessary for the observed fluoride loss. To test this theory, difluoride **15** was synthesized (Scheme 8.3). When this compound was subjected to acidic acetonide deprotection conditions (TFA or *p*TSA in D₂O/CD₃OD, monitored by NMR), fluoride loss was still observed, but at a slower rate. This difference was not dramatic enough to invoke any major contribution from anchimeric assistance.

Even though small quantities of the desired compound could be synthesized, the stability tests showed that fluoride loss was enough of a concern that it would be uncertain whether a pure population of agonist is being observed in pharmacological tests. This project was therefore abandoned.

Chemistry—General

All reactions were performed under argon using solvents that were dried and purified according to the method of Grubbs.⁷ All flasks and vials were oven dried at 122 °C and cooled in a desiccator box containing anhydrous calcium sulfate. Commercial reagents were used as purchased. (3,4-(dimethylmethylene)dioxybenzene) difluoroacetamide **11** was prepared according to literature procedure.⁸ Reactions were monitored by thin-layer chromatography on Merck Siligel 60-F₂₅₄. Compounds were visualized with a UV lamp (254 nm) and stained with potassium permanganate solution. Column chromatography was carried out in accordance with the methods of Still⁹ using EMD-Merck silica gel 60, 230-400 mesh ASTM. ¹H, ³¹P, and ¹³C NMR spectra were acquired on a Varian Mercury 300 MHz spectrometer. High-resolution mass spectrometry was performed on a JEOL JMS-600H HRMS using an Electrospray Ion Source.

Chemistry—Synthesis

2-(3,4-(dimethylmethylene)dioxybenzene)-2,2-difluoro ethylamine (12). Amide **11** (1.94 g, 8 mmol) was measured into a 50 mL oven-dried round-bottomed flask with stirbar and condenser and purged 3x with argon. THF (20 mL) was added to dissolve the solid, and the clear, colorless solution was cooled on an icebath. Borane-dimethylsulfide (1.75 mL, 18.4 mmol)¹⁰ was then added to the stirring solution by syringe, and the reaction was allowed to reach room temperature under stirring. Some slight bubbling was

observed, and the reaction was monitored by TLC (2:1 hexanes:ethyl acetate; stain with ninhydrin). After 20 hours, the reaction was again cooled on an icebath, and 6N HCl (5 mL) was added dropwise with furious bubbling. This was allowed to stir a further 6 hours, then the reaction was basified and extracted with 3 x 20 mL ethyl acetate. The combined organic layers were washed with 1N NaOH (20 mL), brine (20 mL), dried on MgSO₄, and reduced *in vacuo* to give a yellow liquid. This residue was purified by chromatography on silica (40% ethyl acetate in hexanes) to give **12** as a colorless liquid (673 mg, 36.7%). ¹H NMR (300 MHz, CDCl₃) δ 6.88-6.93 (m, 1H), 6.82, (d, 1H, *J* = 1.5 Hz), 6.73 (d, 1H, *J* = 8.1 Hz), 3.12 (t, 2H, *J* = 14.4 Hz), 1.67 (s, 6H), 1.38 (bs, 2H); ¹³C NMR (126 MHz, CDCl₃) δ 148.99, 148.96, 147.87, 129.20, 128.84, 128.49, 125.11, 121.90, 119.04, 118.99, 118.90, 118.81, 108.20, 106.00, 105.92, 105.83, 50.09, 49.68, 49.26, 26.09; ¹⁹F NMR (282 MHz, CDCl₃) δ -104.0; HRMS (FAB⁺) calculated for [C₁₁H₁₄NO₂F₂] ([M+H]⁺) 230.0993, found 230.0990.

4-acetocatechol acetone (14). Aluminum chloride (2.0 g, 15 mmol) was measured into an oven-dried 25 mL round-bottomed flask with stirbar and purged 3x with argon. Dichloromethane (2 mL) was added, and the mixture was cooled on an icebath. Acetyl chloride (0.7 mL, 10 mmol) was then added dropwise over 30 minutes, followed by the dropwise addition of catechol acetone **8** (1.5 g, 10 mmol). The reaction was then allowed to warm to room temperature and stirred for 1 hour, then poured over 50 grams of ice. The mixture was extracted with dichloromethane, washed with saturated aqueous NaHCO₃, dried on MgSO₄, and reduced *in vacuo*. The residue was then purified by flash chromatography on silica (10% ethyl acetate in hexanes) to give **14** as a yellow oil (323

mg). ^1H NMR (300 MHz, CDCl_3) δ 7.51 (dd, 1H, $J = 1.8, 8.1$ Hz), 7.34, (d, 1H, $J = 1.8$ Hz), 6.75 (d, 1H, $J = 8.1$ Hz), 2.52 (s, 3H), 1.69 (s, 6H); ^{13}C NMR (126 MHz, CDCl_3) δ 196.58, 151.89, 148.15, 131.81, 124.53, 119.54, 108.06, 107.86, 26.64, 26.13; HRMS (FAB $^+$) calculated for $[\text{C}_{11}\text{H}_{12}\text{O}_3]$ ($[\text{M}+\text{H}]^+$) 192.0786, found 192.0788.

3,4-(dimethylmethylene)dioxybenzene-1,1-difluoroethane (15). Ketone **14** (295 mg, 1.5 mmol) was measured into an oven-dried 2 dram vial with stirbar and purged 3x with argon. DeoxoFluor (400 μL , 2.1 mmol) was added, and the mixture was stirred at room temperature for 40 hours. The reaction was then heated to 75 $^\circ\text{C}$ for 24 hours. The reaction was then cooled and quenched with ice and extracted with chloroform. The organic layer was dried on MgSO_4 and reduced *in vacuo*. The crude product was then filtered through a silica plug using 20% ethyl acetate in hexanes. The filtrate was then purified by flash chromatography on silica (5% ethyl acetate in hexanes) to give **15** (31.5 mg, 9.8%). ^1H NMR (300 MHz, CDCl_3) δ 6.94 (d, 1H, $J = 7.8$ Hz), 6.87, (d, 1H, $J = 1.8$ Hz), 6.72 (d, 1H, $J = 7.8$ Hz), 1.88 (t, 3H, $J = 17.7$ Hz), 1.68 (s, 6H); ^{13}C NMR (126 MHz, CDCl_3) δ 148.67, 147.75, 132.02, 131.66, 131.31, 125.16, 121.99, 118.88, 118.83, 118.26, 118.17, 118.09, 108.00, 105.60, 105.52, 105.44, 29.93, 26.53, 26.13, 26.08, 25.72; ^{19}F NMR (282 MHz, CDCl_3) δ -85.59 (q, $J = 18.0$ Hz).

References

- ¹ (a) The Dopamine Receptors. Neve, K. A. Humana Press: 2010, New York. (b) Molecular Biology of Dopamine Receptors. Sibley, D. R.; Monsma, F. J. *Trends in Pharmacological Sciences*, **1992**, 13(2), 61.
- ² Probing the Role of the Cation- π Interaction in the Binding Sites of GPCRs Using Unnatural Amino Acids, M. M. Torrice, K. S. Bower, H. A. Lester, D. A. Dougherty, *Proc. Natl. Acad. Sci.*, **2009**, 106, 11919-11924.
- ³ (a) Nicotinic Receptor Binding Site Probed with Unnatural Amino-Acid Incorporation in Intact Cells. M. W. Nowak, P. C. Kearney, J. R. Sampson, M. E. Saks, C. G. Labarca, S. K. Silverman, W. Zhong, J. Thorson, J. N. Abelson, N. Davidson, P. G. Schultz, D. A. Dougherty, and H. A. Lester, *Science*, **1995**, 268, 439-442. (b) Is the Brain Ready for Physical Organic Chemistry? D. A. Dougherty, *J. Phys. Org. Chem.*, **1998**, 11, 334-340. (c) From Ab Initio Quantum Mechanics to Molecular Neurobiology: A Cation- π Binding Site in the Nicotinic Receptor. W. Zhong, J. P. Gallivan, Y. Zhang, L. Li, H. A. Lester, and D. A. Dougherty, *Proc. Natl. Acad. Sci. (USA)*, **1998**, 95, 12088-12093. (d) A Cation- π Binding Interaction with a Tyrosine in the Binding Site of the GABA_C Receptor. Sarah CR Lummis, Darren L Beene, Neil J. Harrison, Henry A. Lester, and Dennis A. Dougherty, *Chem. Biol.* **2005**, 12, 993-997. (e) A Cation- π Interaction between Extracellular TEA and an Aromatic Residue in Potassium Channels, C. A. Ahern, A. L. Eastwood, H. A. Lester and D. A. Dougherty and Richard Horn, *J. Gen. Phys.* **2006**, 128, 649-657. (f) Unnatural Amino Acid Mutagenesis of the GABA_A Receptor Binding Site Residues Reveals a Novel Cation- π Interaction Between GABA and b2 Tyr97. Padgett C.L., Hanek A.P., Lester H.A., Dougherty D.A. and Lummis S.C.R., *J. Neurosci.*, **2007**, 27, 886-892. (g) A Cation- π Interaction in The Binding Site of The Glycine Receptor Mediated by a Phenylalanine Residue, S. A. Pless, K. S. Millen, A. P. Hanek, J. W. Lynch, H. A. Lester, S. C.R. Lummis, and D. A. Dougherty, *J. Neurosci.*, **2008**, 28, 10937-10942. (h) Nicotine Binding to Brain Receptors Requires a Strong Cation- π Interaction X. Xiu*, N. L. Puskar*, J. A. P. Shanata, H. A. Lester, and D. A. Dougherty, *Nature*, **2009**, 458, 534-537. (i) A Cation- π Binding Interaction with a Tyrosine in the

Binding Site of the GABA_C Receptor. Sarah CR Lummis, Darren L Beene, Neil J. Harrison, Henry A. Lester, and Dennis A. Dougherty, *Chem. Biol.* **2005**, *12*, 993-997.

⁴ Another possible explanation for this reduced sensitivity is an aromatic-aromatic interaction or a π -polar interaction.

⁵ Quinone Methides, Rokita, S. E. John Wiley & Sons: **2009**, Hoboken, NJ

⁶ (a) Electrophilic Substituent Constants. Brown, H. C.; Okamoto, Y. *J. Am. Chem. Soc.* **1958**, *80*, 4979-4982. (b) Correlation of the STO-3G Calculated Substituent Effects on the Proton Affinity of Benzene with σ^+ Parameters. McKelvey, J. M.; Alexandratos, S.; Streitwieser, A.; Abboud, J.-L. M.; Hehre, W. J. *J. Am. Chem. Soc.* **1976**, *98*(1), 244-246. (c) Kinetic Solvent Effects on Proton and Hydrogen Atom Transfers from Phenols: Similarities and Differences. Nielsen, M. F.; Ingold, K. U. *J. Am. Chem. Soc.* **2006**, *128*, 1172-1182.

⁷ Pangborn, A. B.; Giardello, M. A.; Grubbs, R. H.; Rosen, R. K.; Timmers, F. J. *Organometallics* **1996**, *15*, 1518-1520.

⁸ Synthesis of a Chiral α -(Aminoxy)arylacetic Ester. II. A Route through a Chiral 2-Hydroxy-2-phenylacetic Acid Derivative. Iwagami, H.; Yatagai, M.; Nakazawa, M.; Orita, H.; Honda, Y.; Ohnuki, T.; Yukawa, T. *Bull. Chem. Soc. Japan* **1991**, *64*, 175-182. (b) α,α -Difluoroarylacetic acids: preparation from (diethylamino)sulfur trifluoride and α -oxoarylacetaes. Middleton, W. J.; Bingham, E. M. *J. Org. Chem.* **1990**, *45*(14), 2883-2887.

⁹ Still, W. C.; Kahn, M.; Mitra, A. *Journal of Organic Chemistry* **1978**, *43*(14), 2923

¹⁰ Borane Dimethyl Sulfide. Zaidlewicz, M.; Baum, O.; Srebnik, M. *e-EROS Encyclopedia of Reagents for Organic Synthesis* **2005** and references therein.

The Development of a New MALDI-TOF MS Method for the Analysis of Amino Acid-dCA Esters

The standing group protocol for assaying amino acid-dCA esters was electrospray MS. However, prior to assay, the esters were purified by HPLC using an ammonium acetate buffered phase, and the ammonium ions interfered with obtaining a good mass spectrum by electrospray. Therefore, a rigorous desalting protocol was needed prior to MS; the protocol took at least 4 days, which slowed progress, especially in cases where the esterification reaction was unreliable and needed to be run multiple times. In contrast, MALDI MS benefits from the addition of ammonium ions, which are often the ion source (ammonium is typically added to the sample prior to MALDI). I therefore worked with Mona Shahgholi to develop a MALDI-based protocol for analyzing these compounds, using the solvated fractions obtained directly from the HPLC. We screened several different matrices, concentrations, and ratios to develop the following protocol:

Note 1: the sample does NOT need to be desalted prior to MALDI; however, it should be desalted thereafter (removal of ammonium ions) by three cycles of dissolution/lyophilization using a 25 mM acetic acid solution. If ammonium ions remain, they could inhibit the subsequent enzymatic tRNA ligation.

Note 2: the reflector mode used in this protocol should allow for < 0.1% mass error. I have never seen it to give greater than 0.02% mass error. The error *increases* (along-the-baseline resolution gets worse) for more *concentrated* samples.

Preparation of Matrix Solutions:

- 1) 10 mg/mL 6-aza-2-thiothymine (ATT) in 1:1 water:acetonitrile
- 2) 10 mg/mL ammonium citrate (dianion) in 1:1 water:acetonitrile
- 3) 9:1 mixture of solutions 1:2 above
- 4) 50 μ M dCA-AA in water
 - a) for a ligation efficiency of 5-20 % (HPLC integration), the product fraction collected directly off the HPLC should work 'as is', without dilution (for higher ligation efficiencies, for starting materials, or for reactions run with more than 10 mg dCA, the collected fractions should be diluted accordingly)
 - b) as low as 5 μ M should still give good spectra; for solutions above 50 μ M, significant gas-phase dimerization can be observed, and the resolution along the baseline decreases
- 5) 9:1 mixture of solutions 3:4 above

Spot 0.3 μ L of solution 5 above onto the MALDI sample plates and allow to dry. (Note that this spot represents only 1.5 pmol = 1 ng dCA-AA, and we have shown that less than 0.1 ng still works—the sensitivity of the MALDI is very good.)

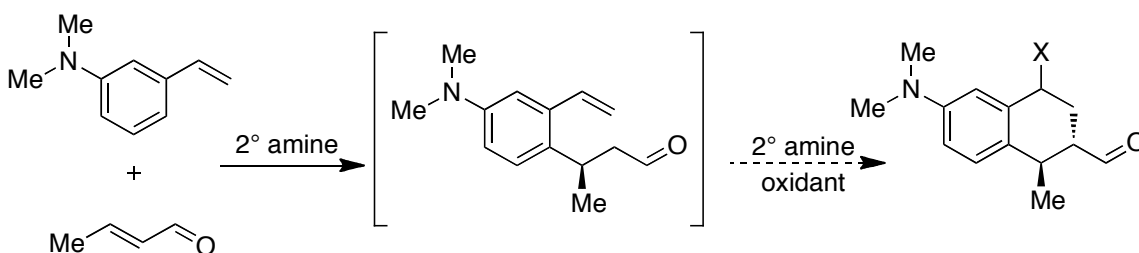
The method used is:

- Jeff Bics → Reflector 1500
- Two parameters may need to be adjusted:
 - Mass Range (500-1500 amu)
 - Laser Intensity (start around 2200, but if that fails to produce a good spectrum, adjust it up—I have needed to go as high as 3200 before)

Investigations into an Organocatalytic LUMO–SOMO Cascade

During my brief time in the MacMillan lab, my project was to explore the feasibility to a LUMO–SOMO (Friedel–Crafts–radical cyclization) organocatalysis cascade (Scheme A2.1). The conclusion is that such a sequence is quite doubtful: the oxidizing conditions needed for the SOMO reaction also oxidize the aniline substrate. Even if milder SOMO conditions could be developed, the oxidation potentials of enamines and anilines suggest that the electron-rich aniline would always be oxidized under conditions that are sufficient to oxidize the catalytic enamine intermediate. Furthermore, the aniline concentration in the reaction will always vastly exceed the enamine concentration, which will always be present only in catalytic amounts.

Scheme A2.1. Proposed one-pot organocatalytic cascade.



The best hope for this sort of cascade lies not in aniline substrates, but in less readily-oxidized aromatic heterocycles—such as furans—which can participate in the first step as activated potassium trifluoroborate salts,¹ then become significantly less readily-oxidized following the Friedel–Crafts (LUMO) step. In this case, the aromatic component is more likely to withstand the SOMO conditions.

References

-
- ¹ Organocatalytic Vinyl and Friedel-Crafts Alkylations with Trifluoroborate Salts. S. Lee, D. W. C. MacMillan. *J. Am. Chem. Soc.*, **2007**, *129*, 15438-15439.